Tracking Cosmic Dust with Extraterrestrial Helium and Neon in Deep-Sea Sediments

Thesis by
Ruolin Deng

In Partial Fulfillment of the Requirements for the
Degree of
PhD in Geology

Caltech

CALIFORNIA INSTITUTE OF TECHNOLOGY
Pasadena, California

2025
Defended July 23, 2025

Ruolin Deng
ORCID: https://orcid.org/0000-0001-5383-3039

ACKNOWLEDGEMENTS

First, I would like to express my deepest gratitude to my thesis advisor, Ken Farley, for his guidance, encouragement, patience, and unwavering support throughout my PhD journey. Ken introduced me to the world of noble gas geochemistry and cosmic dust and guided me through its complexities with knowledge, rigor, and enthusiasm. I am especially thankful for the freedom of exploration he encouraged, which led to some of the most rewarding discoveries of my doctoral work. I will always miss our lengthy discussions in his office, which were often punctuated by Cody's barks of agreement (or disagreement).

I am equally grateful to Paul Asimow, who advised one of my first-year propositions and chaired my thesis committee. His patience in explaining thermodynamics and igneous petrology has left a lasting impression. I also treasure the unforgettable graduation trip to Hawaii, where we witnessed the spectacular fountaining of Kīlauea.

My sincere thanks go to Joe Kirschvink, whose generosity in sharing his profound knowledge of magnetism and his ever-expanding curiosity about the world has deeply inspired me. I will fondly remember knocking on Joe's office door and spending an hour in lively conversation, sharing our wildest ideas and experimental designs.

I am indebted to François Tissot for many stimulating discussions on cosmochemistry and for allowing me to use his Isotoparium for trace metal analyses; to Konstantin Batygin, for his patient explanations of planetary dynamics and his guidance on building N-body simulations; to Dianne Newman for letting me use her geobiology lab, and to Korbi Thalhammer for helping me test if Shewanella eats magnetite in Dianne's lab; to Paula Antoshechkin, for teaching me about backend data structures in LEPR; and to Ren Marquez, who taught me everything I needed to know about clean lab work and assisted with trace metal analyses. I also benefited enormously from Frankie Pavia's mentorship in uranium and thorium isotope measurements, as well as from our conversations on oceanography and constant-flux proxies.

I am thankful to John Eiler for his incisive and constructive comments as a member of my thesis advisory committee, and to Jess Adkins and Jared Leadbetter for serving on my first-year qualification exam committee. Discussions with Don Burnett, George Rossman, Ted Present, Chi Ma, and Yunbin Guan have broadened my scientific perspective. I also wish to acknowledge Mike Lamb, Joann Stock, and Jean-Philippe Avouac for their service as Geology Option Representatives, and Alex Sessions for organizing the enrichment trip to New Zealand and co-leading the Hawaii graduation trip. Finally, my thanks go to Ed Stolper, who welcomed me into Caltech at the very beginning of this journey.

I owe special thanks to Jonathan Treffkorn, the best lab manager I could have imagined. Working alongside him taught me more about instrumentation than any manual ever could. His kindness, patience, and quiet wisdom have made an indelible mark. I will miss our coffee walks to Red Door and lunches outside.

I am grateful to Nathan Dalleska and Isaac Hilburn for training me in the mass spectrometry and paleomagnetics labs, and to the dedicated administrators at GPS, especially Julie Lee, for keeping everything in the division running so smoothly.

Beyond Caltech, I was fortunate to collaborate with many wonderful scientists. My heartfelt thanks to Alessandro Montanari and Rodolfo Coccioni for their warm hospitality during my fieldwork in Italy, and to Ross Mitchell (IGGCAS) for sharing his Scaglia Rossa samples that he sampled in Italy and his expertise in paleomagnetism and plate tectonics. I also appreciate Robert Anderson and Yao Qian (ANU) for providing Mediterranean sapropel samples and assisting with magnetic analyses, and Anthony Pivarunas (USGS) for accommodating my rock magnetism work. Discussions with Jasper Kok (UCLA) on atmospheric dust loading and climate modeling have been deeply valuable. I have benefited greatly with my conversations with Jordan Abell (Lehigh University) on noble gas geochemistry. I am grateful to Martin Fleischer (Columbia-LDEO) for sharing core-top samples, and to Zheng Gong, David Evans, and Phil McClausland (Yale) for helping locate Scaglia Rossa paleomagnetic cores. My thanks also to James Zachos (UCSC) for his help with stable isotope measurements on marine sediments.

My path into geoscience was sparked years ago by my middle school and high school geography teachers Yiping Chen, Jialing Shen, and Xiaopeng Tang. I am indebted to my undergraduate advisor Wei Tian and mentor Jianqing Ji at Peking University, and to my undergraduate thesis co-advisor Ian Campbell, as well as Hugh O'Neill and Anthony Burnham at ANU, for guiding my first steps into research.

To the members of the Farley Group, past and present: Jonathan Treffkorn, Carl Swindle, Ben Thyer, Hevelyn Monteiro, Frankie Pavia, Alessandra Flaherty, Jess Mueller, Iva Tomchovska, Jeff Osterhout, Daniel Halford, Kristen Der, and Shounak

Dutta, thank you for being not only wonderful colleagues but also close friends. I feel lucky to have shared so many days of both work, laughter, and donuts with you.

Besides the Farleyans, I am endlessly grateful to my friends who made life at Caltech unforgettable: Hao Zhang, Weiyi Liu, Junjie Dong, Adriana Paez, Krittanon "Pond" Sirorattanakul, Phelan Yu, Ren Marquez, Amanda Bednarick, Korbi Thalhammer, Surjyendu Bhattacharjee, Ojashvi Rautela, Shirui Peng, Justin Nghiem, Hannah Dion-Kirschner, Noam Lotem, Julie Inglis, Cheng Shen, Will Palfey, Emily Miaou, Xenia Boyes, Yuanyuan He, Haoyu Li, Xue Su, Juan David Hernandez, Yongzhao Guo, Guannan Dong, Renee Wang, Mike McKeon, Jordan Benjamin, Nadia Suryawinata, Sam Ponnada, Jack Wilding, Xun Wang, Jerry Wang, Shuo Cao, Binyang Sun, Lu Chen, Xinchu Wang, Yijian Zhou, Yuexin Li, Guanli Wang, Gabriella Fontaneta, Yutian Ke, and Xiongzi Ren. From dorm to national parks, from frisbee to kayaking, from omelets to hotpots, from basketball to badminton, thank you for the countless memories and adventures that sustained me through these years.

I also appreciate my friends at CGPU, who worked tirelessly toward building a more supportive and protective environment for the Caltech community.

Finally, my deepest love and gratitude go to my family and future family, who have stood by me unconditionally and supported every decision I've made. To my fiancée, Yangzhou Ou, thank you for sharing this incredible journey over the past decade with patience, support, and endless faith.

This thesis is dedicated to my father, who saw the start of it, but did not have the chance to see its completion.

ABSTRACT

Cosmic dust represents the dominant form of extraterrestrial material currently accreted by Earth, yet many fundamental aspects of its origin, composition, and impact remain poorly constrained. The past cosmic dust flux can be reconstructed by measuring extraterrestrial ^{3}He in deep-sea sediments, which is retained in cosmic dust for millions of years, even through diagenetic processes. While cosmic dust flux through most of the times in the last 100 Myr is relatively constant, several short-lived ^{3}He enhancement events have been identified and linked to asteroid disruptions in the asteroid belt. The cosmic dust sources of other similar events, however, remain uncertain. Moreover, the mineralogical carrier of solar wind helium and neon in marine sediments is still debated, and the broader influence of cosmic dust on terrestrial systems remains an open question. This thesis addresses these outstanding issues using noble gas geochemistry, trace metal analysis, paleomagnetism, stable isotope geochemistry, and dust dynamics modeling. Chapter II investigates the cosmic dust source and consequences of the K1 ^{3}He enhancement event in the Late Cretaceous. Chapter III explores the source of cosmic dust through time, including the potential role of the Moon. Chapter IV evaluates the climatic significance of enhanced cosmic dust flux during the Late Eocene. Together, these studies provide new insight into the source, dynamic evolution, composition, and terrestrial impact of cosmic dust.

TABLE OF CONTENTS

LIST OF ILLUSTRATIONS

LIST OF TABLES

Chapter 1

INTRODUCTION

There are micron-sized meteorites on the seafloor.

Almost 150 years ago, John Murray was the first human to describe some peculiar micro-spherules in dredged marine sediments during the famous HMS Challenger Expedition. He suspected their extraterrestrial origin because of the distant sample location from continental dust sources, and coined the term "cosmic dust" in the later published cruise report (Buchan et al., 1880).

In 1964, 90 years after the HMS Challenger Expedition, Craig Merrihue reported $^{3}He/^{4}He$ ratios in a piece of red clay from the Pacific that were almost two orders of magnitude higher than Earth's atmosphere. Linked to the enrichment of ^{3}He in meteorites, he correctly attributed the high $^{3}He/^{4}He$ ratios to the existence of extraterrestrial helium embedded in cosmic dust in marine sediments (Merrihue, 1964). His paper started an era of studying cosmic dust in marine sediments with noble gases, especially helium, as tracers.

Today, we have advanced so much with our knowledge of cosmic dust thanks not only to noble gases, but also space missions, radar technologies, micro-analysis techniques, and planetary dynamics modeling. It turns out that these sub-mm cosmic dust particles deliver the most extraterrestrial mass to Earth today, with a daily flux of 5–270 tons/day (Plane, 2012). Comets are likely the primary contributor to cosmic dust flux, supplying 80–95 % of the total dust in the zodiacal cloud (Nesvorný et al., 2010). Asteroids make up for the rest. Occasionally, a weird one is identified in the micrometeorites collected from Antarctica and Greenland (van Ginneken et al., 2024), like a lunar dust grain (Fernandes et al., 2025); or in the interplanetary dust particles captured with high-altitude aircraft (Brownlee, 1985), like presolar grains (Floss et al., 2006).

Cosmic dust can be thought of as micro-remnants of meteorites with similar mineralogy and major elements (Not to be mistaken with micrometeorites, which are a subset of cosmic dust larger than a few hundreds of µm), yet they can be vastly different with regard to dynamic evolution, accretion history, and chemical compositions. The differences almost all result from the minute size of cosmic dust.

Upon release from the parent body—whether an asteroid, a moon, or a comet—cosmic dust immediately feels solar radiation pressure due to its similar size to the wave-length of sunlight. Those smaller than ~2 µm are pushed out of the solar system (*i.e.*, β-meteoroids; Liou et al. (1995)). Those between 2 µm and ~200 µm will spiral into the Sun within 10^4–10^6 years because of the energy-dissipative Poynting-Robertson effect, which also comes from the strong interactions between cosmic dust and solar photons (Burns et al., 1979; Klačka et al., 2014). In this regard, cosmic dust differs from macroscopic fragments of celestial bodies, which will remain in their orbit for millions of years unless disrupted by resonance.

During its dynamic lifetime, a cosmic dust particle is also bombarded by the solar wind. The energy of a solar wind ion is on the order of 10^1 keV, which means the implantation depth of such ions in cosmic dust is only a few tens of nanometers (Ziegler et al., 2010). However, due to the large surface-area-to-volume ratio, surface-correlated implanted solar wind helium and neon end up dominating the whole helium and neon budget in a cosmic dust grain (Moreira, 2013). The typical helium and neon isotope compositions of cosmic dust (Nier et al., 1990; Nier et al., 1992; Pepin et al., 2001; Kehm et al., 2006), however, are heavier than the pure solar wind (Heber et al., 2009; Pepin et al., 2012). This selective depletion of lighter isotopes is proposed to result from their lower kinetic energy and hence shallower implantation depth (Grimberg et al., 2006), making them more easily lost during subsequent space weathering processes (Raquin et al., 2009; Moreira et al., 2016). As a result, implanted solar wind helium and neon (*i.e.*, "fractionated solar wind") typically have a ^{3}He/^{4}He of 2.8×10^{-4} and a ^{20}Ne/^{22}Ne of 11.9 (Nier et al., 1990; Nier et al., 1992; Pepin et al., 2001; Kehm et al., 2006), compared to a ^{3}He/^{4}He of 4.64×10^{-4} and a ^{20}Ne/^{22}Ne of ~14 in pure solar wind (Heber et al., 2009; Pepin et al., 2012).

As the orbit of cosmic dust decays, it eventually crosses Earth's semi-major axis of 1 AU. Some of the cosmic dust will be accreted by Earth, interrupting its journey to the Sun. By the time a cosmic dust grain evolves to Earth's vicinity, the Poynting-Robertson effect circularizes its orbit. As a result, cosmic dust derived from a comet with an eccentric orbit will have a similar impact velocity to cosmic dust derived from an asteroid with a much more circular orbit (Borin et al., 2017).

Again because of their small sizes, cosmic dust particles have a higher specific surface area and hence high radiation efficiency. This results in a lower peak temperature during drag heating as they collide with atmospheric molecules (Farley et al., 1997), which means cosmic dust grains are much more likely to bring their volatiles, including the shallowly implanted solar wind helium and neon, intact to Earth's surface. Sieving experiments have found that most helium is concentrated in cosmic dust smaller than ~35 µm (Mukhopadhyay et al., 2006; Brook et al., 2009; McGee et al., 2010), which is consistent with theory that larger cosmic dust grains more readily lose their volatiles during atmospheric entry heating. If solar wind helium and neon can be measured with confidence in deep-sea sediments, they are ultimately a tracer for fine extraterrestrial matter exclusively. This makes them different from refractory geochemical tracers, such as iridium and osmium, which track the mass flux of extraterrestrial material that includes meteoroids of all sizes (Peucker-Ehrenbrink et al., 2016). Such a characteristic (*i.e.*, being able to deliver volatiles to Earth's surface) has also led scientists to explore the possibility that cosmic dust delivers life-essential elements, which are usually volatile, to the early Earth (Walton et al., 2024).

Although cosmic dust is overwhelmed by the mass of marine sediments on the seafloor after falling through the atmosphere and water column, an extraterrestrial signal is easy to identify, especially for helium. Cosmic dust has a distinctively different helium isotope composition compared to terrigenous sediments (the other major contributor to helium in marine sediments Farley (2001)). Terrigenous sediments such as aeolian dust or Chinese loess, have $^3He/^4He$ ratios on the order of 10^{-8} (Marcantonio et al., 1998; Farley, 2001), four orders of magnitude lower than cosmic dust. The enrichment of ^4He relative to ^3He in terrestrial materials comes from the different production rates of the two isotopes. ^3He in sproduced on Earth in negligible amounts, except by a rare neutron capture reaction, $^7Li(n, \alpha)^3H(\beta^-)^3He$, that is only significant in lithium enriched minerals. On the other hand, ^4He is the product of all α-decay processes and has been produced since the formation of Earth. The $^3He/^4He$ production ratio in the crust has been estimated to be lower than 4×10^{-8} (Mamyrin et al., 1984).

Furthermore, the atmospheric contribution of ^3He to marine sediments is negligible. Belonging to the "rare gases", helium is a rare element on Earth, making up 5 ppm (parts per million) of Earth's atmosphere by volume (ppmv). This comes from the fact that helium is neither chemically nor gravitationally bound to the Earth, and is being continuously leaked to space. On top of that, ^3He is much more depleted that ^4He, for reasons described in the former paragraph. Earth's atmosphere has a $^3He/^4He$ ratio of 1.382×10^{-6} (Sano et al., 2013), bringing the mixing ratio of the rare isotope of a rare element, ^{3}He, down to ppt (parts per trillion) levels in the air. Thus, marine sediments are usually treated as a two-component mixture between cosmic dust and terrigenous sediments only (Farley, 2001). This is not the case for neon, which has an atmospheric abundance of 18 ppmv. Thus, marine sediments usually contain neon from three sources: cosmic dust, terrigenous sediments, and air (Chavrit et al., 2016). There are, however, rare cases where the neon budget in marine sediments is entirely dominated by an overwhelming contribution from cosmic dust, an example of which is reported in Chapter III.

Remarkably, once cosmic dust is deposited on the seafloor, it can retain the shallowly implanted solar wind helium (and neon) for millions of years (Patterson et al., 1998b). The retention mechanism and retentive carrier phase(s) are still unclear despite numerous studies (Ozima et al., 1984; Hiyagon, 1994; Mukhopadhyay et al., 2006). Nevertheless, while there exist multiple methods of constraining the present-day cosmic dust flux (Plane, 2012), this extraordinary retentivity means that extraterrestrial helium in ice cores and marine sediments are perhaps the best tracer for constraining cosmic dust flux in the past (McGee et al., 2013).

The fundamental equation that describes the relationship between the measured extraterrestrial ^{3}He concentration ([$^3\mathrm{He}_{\mathrm{ET}}$], in pcc/g, where pcc stands for 10^{-12} cubic centimeter) and the extraterrestrial ^{3}He flux (f_{He}, in pcc/cm^2/kyr) as a tracer for cosmic dust flux is:

$$[^3He_{ET}] = \frac{f_{He} \cdot R}{MAR} \tag{1.1}$$

where R is a dimensionless helium retention factor ranging from 0 and 1, and MAR stands for mass accumulation rate of sediments in g/cm^2/kyr (Farley, 1995). Knowing R is crucial for calculating the absolute f_{He}, but this factor is difficult to constrain. However, since helium can be retained in cosmic dust on the seafloor for millions of years, R can be reasonably assumed to be constant over short stretches of time (say, a few million years). When doing so, an implied $^3\mathrm{He}_{\mathrm{ET}}$ flux expressed as [$^3\mathrm{He}_{\mathrm{ET}}$]·MAR is defined to track relative changes in f_{He} without needing to know the absolute values, if MAR can be constrained independently (Farley et al., 1998). Alternatively, if f_{He} can be independently constrained to be constant, extraterrestrial ^{3}He can be used as a constant flux proxy to track changes in MAR (Marcantonio et al., 1995; Marcantonio et al., 1996; Marcantonio et al., 2001).

Based on ^{3}He records in deep-sea sediments, the cosmic dust flux history for the last 100 Myr is becoming increasingly complete (Farley, 1995; Farley et al., 1998; Mukhopadhyay et al., 2001; Farley et al., 2006; Farley et al., 2012). While cosmic dust flux remains relatively constant through most of the epochs from Late Cretaceous to today, occasionally there are intervals over which cosmic dust flux increasing by a factor of 5-10 for a span of 1-2 million years (Farley et al., 2006; Farley et al., 2012; Farley et al., 1998). These intervals correspond to periods when cosmic dust flux is briefly enhanced by excess dust flux, usually attributed to an event such as an asteroid collision or a comet shower. Thus, ^{3}He carried by cosmic dust in marine sediments also provides a way to assess the frequency of major cosmic dust production events in the Solar System.

There is, however, still much about cosmic dust that remains unknown despite decades of studies. For instance, some ^{3}He enhancement events have an unambiguous source for the excess cosmic dust, like the Late Miocene event associated with the Veritas asteroid family breakup event (Farley et al., 2006) and the Mid-Ordovician event associated with the L-chondrite parent body breakup event (Schmitz et al., 2019). Yet the cosmic dust sources of the other known events remain unknown or controversial (Farley et al., 1998; Kyte et al., 2004; Tagle et al., 2004; Tagle et al., 2007; Fritz et al., 2007; Boschi et al., 2017). Some of these difficulties result from the current lack of knowledge about the difference in chemistry between asteroids and comets. In addition, older events tend to have fewer and looser constraints (Farley et al., 2012).

The carrier phase(s) of extraterrestrial helium and neon in cosmic dust is another unsettled issue. While several reports confirmed the high concentration of extraterrestrial helium in magnetic separates of marine sediments (Merrihue, 1964; Ozima et al., 1984; Amari et al., 1988; Hiyagon, 1994; Mukhopadhyay et al., 2006), magnetite in cosmic dust is most likely formed from oxidizing Fe^{2+}-bearing minerals and/or Fe metal during atmospheric entry (Bradley, 2007). A primary, magnetic (or magnetite-related), and retentive carrier phase of solar wind helium and neon has not been identified, though several candidates have been proposed, including ilmenite, sulfide, and extraterrestrial silicates (Mukhopadhyay et al., 2001).

Lastly, being the dominant contributor of extraterrestrial mass to Earth, does cosmic dust flux have any impact on terrestrial systems? Some mechanisms have been explored, including changes in atmosphere chemistry from cosmic dust ablation and evaporation (Plane et al., 2017) and changes in the electrical conductance of the atmosphere (Ogurtsov et al., 2011). Climatic effects of cosmic dust have been inferred using various datasets. A 100-kyr cycle of cosmic dust flux was reported in Quaternary sediments, which apparently agrees with the 100-kyr Milankovitch eccentricity cycle, whose climatic effects in the late Pleistocene are well-known (Patterson et al., 1998a). The last major warmhouse-icehouse transition, at the Eocene-Oligocene boundary, also happened right after the Late Eocene ^{3}He enhancement event, suggesting a potential cosmic-dust-related mechanism to initiate this major cooling stage. However, the limited number of studies of this issue (Muller et al., 1995; Muller et al., 1997; Ogurtsov et al., 2011) have not made clear either the mechanism whereby cosmic dust might affect Earth's climate or the sensitivity of Earth's climate system to variations in cosmic dust flux.

My thesis aims to address some of the unknowns above, utilizing a diverse set of techniques and models including and going beyond noble gas geochemistry, with chapters arranged in a way that travels with a cosmic dust particle from source to sink.

I will start with Chapter II, which assesses the source of excess cosmic dust during K1, the largest ^{3}He enhancement event in the last 100 Myr (Farley et al., 2012; Montanari et al., 2023), with a combination of high-temporal resolution sampling, trace metal analyses, and dust dynamics modeling. I will also use paleomagnetism and stable isotopes to evaluate the statistical significance of the temporal coincidence between K1, the C33r-C33n geomagnetic reversal, and a modest δ^{13}C excursion known as the Early Campanian Event.

In Chapter III, I will use helium and neon in marine sediments of different ages to deduce the source of cosmic dust through time. We propose that the Moon might play a much more important role in cosmic dust delivery to Earth and preservation of the ^{3}He signal in marine sediments than previously expected.

In Chapter IV, I will evaluate the potential climatic effect of the Late Eocene ^{3}He enhancement event using helium isotopes, stable isotopes, and radiative forcing modeling.

References

Amari, Sachiko and Minoru Ozima (1988). "Extra-Terrestrial Noble Gases in Deep Sea Sediments". In: *Geochimica et Cosmochimica Acta* 52.5, pp. 1087–1095. ISSN: 0016-7037. DOI: 10.1016/0016-7037(88)90263-3.

Borin, P., G. Cremonese, F. Marzari, and A. Lucchetti (2017). “Asteroidal and Cometary Dust Flux in the Inner Solar System”. In: *Astronomy & Astrophysics* 605, A94. ISSN: 0004-6361, 1432-0746. DOI: 10.1051/0004-6361/201730617.

Boschi, Samuele, Birger Schmitz, Philipp R. Heck, Anders Cronholm, Céline Defouilloy, Noriko T. Kita, Simonetta Monechi, Alessandro Montanari, Surya S. Rout, and Fredrik Terfelt (2017). “Late Eocene 3He and Ir Anomalies Associated with Ordinary Chondritic Spinels”. In: *Geochimica et Cosmochimica Acta* 204, pp. 205–218. ISSN: 0016-7037. DOI: 10.1016/j.gca.2017.01.028.

Bradley, J. P. (2007). “1.26 - Interplanetary Dust Particles”. In: *Treatise on Geochemistry*. Ed. by Heinrich D. Holland and Karl K. Turekian. Oxford: Pergamon, pp. 1–24. ISBN: 978-0-08-043751-4. DOI: 10.1016/B0-08-043751-6/01152-X.

Brook, Edward J., Mark D. Kurz, and Joshua Curtice (2009). “Flux and Size Fractionation of 3He in Interplanetary Dust from Antarctic Ice Core Samples”. In: *Earth and Planetary Science Letters* 286.3, pp. 565–569. ISSN: 0012-821X. DOI: 10.1016/j.epsl.2009.07.024.

Brownlee, Donald E. (1985). “Cosmic Dust: Collection and Research”. In: *Annual Review of Earth and Planetary Sciences* 13.1, pp. 147–173. DOI: 10.1146/annurev.ea.13.050185.001051.

Buchan, Alexander, Thomas Henry Huxley, John Murray, George Strong Nares, Paul Pelseneer, C. Wyville Thomson, and Frank Tourle Thomson (1880). *Report on the scientific results of the voyage of H.M.S. Challenger during the years 1873-76 under the command of Captain George S. Nares ... and the late Captain Frank Tourle Thomson, R.N.* Neill. DOI: 10.5962/bhl.title.6513.

Burns, Joseph A., Philippe L. Lamy, and Steven Soter (1979). “Radiation Forces on Small Particles in the Solar System”. In: *Icarus* 40.1, pp. 1–48. ISSN: 0019-1035. DOI: 10.1016/0019-1035(79)90050-2.

Chavrit, Déborah, Manuel Moreira, and Frédéric Moynier (2016). “Estimation of the Extraterrestrial 3He and 20Ne Fluxes on Earth from He and Ne Systematics in Marine Sediments”. In: *Earth and Planetary Science Letters* 436, pp. 10–18. ISSN: 0012-821X. DOI: 10.1016/j.epsl.2015.12.030.

Farley, Kenneth A. (1995). “Cenozoic variations in the flux of interplanetary dust recorded by3He in a deep-sea sediment”. en. In: *Nature* 376.6536, pp. 153–156. ISSN: 0028-0836, 1476-4687. DOI: 10.1038/376153a0.

– (2001). “Extraterrestrial Helium in Seafloor Sediments: Identification, Characteristics, and Accretion Rate Over Geologic Time”. In: *Accretion of Extraterrestrial Matter Throughout Earth’s History*. Boston, MA: Springer US, pp. 179–204. DOI: 10.1007/978-1-4419-8694-8_11.

Farley, Kenneth A., S. G. Love, and Desmond B. Patterson (1997). "Atmospheric Entry Heating and Helium Retentivity of Interplanetary Dust Particles". In: *Geochimica et Cosmochimica Acta* 61.11, pp. 2309–2316. ISSN: 0016-7037. DOI: 10.1016/S0016-7037(97)00068-9.

Farley, Kenneth A., Alessandro Montanari, and Rodolfo Coccioni (2012). "A record of the extraterrestrial 3He flux through the Late Cretaceous". en. In: *Geochimica et Cosmochimica Acta* 84, pp. 314–328. ISSN: 00167037. DOI: 10.1016/j.gca.2012.01.015.

Farley, Kenneth A., Alessandro Montanari, E. M. Shoemaker, and C. S. Shoemaker (1998). "Geochemical Evidence for a Comet Shower in the Late Eocene". en. In: *Science* 280.5367, pp. 1250–1253. ISSN: 0036-8075, 1095-9203. DOI: 10.1126/science.280.5367.1250.

Farley, Kenneth A., David Vokrouhlický, William F. Bottke, and David Nesvorný (2006). "A late Miocene dust shower from the break-up of an asteroid in the main belt". en. In: *Nature* 439.7074, pp. 295–297. ISSN: 0028-0836, 1476-4687. DOI: 10.1038/nature04391.

Fernandes, D. and N. G. Rudraswami (2025). "An Unusual Lunar Origin and Chondritic Refractory Antarctic Micrometeorites". In: *Geoscience Frontiers* 16.2, p. 101975. ISSN: 1674-9871. DOI: 10.1016/j.gsf.2024.101975.

Floss, Christine, Frank J. Stadermann, John P. Bradley, Zu Rong Dai, Sasa Bajt, Giles Graham, and A. Scott Lea (2006). "Identification of Isotopically Primitive Interplanetary Dust Particles: A NanoSIMS Isotopic Imaging Study". In: *Geochimica et Cosmochimica Acta* 70.9, pp. 2371–2399. ISSN: 0016-7037. DOI: 10.1016/j.gca.2006.01.023.

Fritz, Jörg, Roald Tagle, and Natalia Artemieva (2007). "Lunar Helium-3 in Marine Sediments: Implications for a Late Eocene Asteroid Shower". In: *Icarus* 189.2, pp. 591–594. ISSN: 0019-1035. DOI: 10.1016/j.icarus.2007.03.026.

Grimberg, Ansgar, Heinrich Baur, Peter Bochsler, Fritz Bühler, Donald S. Burnett, Charles C. Hays, Veronika S. Heber, Amy J. G. Jurewicz, and Rainer Wieler (2006). "Solar Wind Neon from Genesis: Implications for the Lunar Noble Gas Record". In: *Science* 314.5802, pp. 1133–1135. DOI: 10.1126/science.1133568.

Heber, Veronika S., Rainer Wieler, Heinrich Baur, Chad Olinger, Tom A. Friedmann, and Donald S. Burnett (2009). "Noble Gas Composition of the Solar Wind as Collected by the Genesis Mission". In: *Geochimica et Cosmochimica Acta* 73.24, pp. 7414–7432. ISSN: 0016-7037. DOI: 10.1016/j.gca.2009.09.013.

Hiyagon, Hajime (1994). "Retention of Solar Helium and Neon in IDPs in Deep Sea Sediment". In: *Science* 263.5151, pp. 1257–1259. DOI: 10.1126/science.263.5151.1257.

Kehm, Karl, George J. Flynn, and Charles M. Hohenberg (2006). "Noble Gas Space Exposure Ages of Individual Interplanetary Dust Particles". In: *Meteoritics & Planetary Science* 41.8, pp. 1199–1217. ISSN: 1945-5100. DOI: 10.1111/j.1945-5100.2006.tb00516.x.

Klačka, J., J. Petržala, P. Pástor, and L. Kómar (2014). "The Poynting–Robertson Effect: A Critical Perspective". In: *Icarus* 232, pp. 249–262. ISSN: 0019-1035. DOI: 10.1016/j.icarus.2012.06.044.

Kyte, F. T., A. Shukolyukov, A. R. Hildebrand, G. W. Lugmair, and J. Hanova (2004). "Initial Cr-Isotopic and Iridium Measurements of Concentrates from Late Eocene Cpx-Spherule Deposits". In: p. 1824.

Liou, Jer-Chyi and Herbert A. Zook (1995). "An Asteroidal Dust Ring of Micron-Sized Particles Trapped in the 1:1 Mean Motion Resonance with Jupiter". en. In: *Icarus* 113.2, pp. 403–414. ISSN: 00191035. DOI: 10.1006/icar.1995.1030.

Mamyrin, Boris Aleksandrovich and Igor Tolstikhin (1984). *Helium isotopes in nature*. eng. Developments in geochemistry. Amsterdam New York New York, N.Y s.l: Elsevier. ISBN: 9781483289809.

Marcantonio, Franco, Robert F. Anderson, Sean Higgins, Martin Stute, Peter Schlosser, and Peter Kubik (2001). "Sediment Focusing in the Central Equatorial Pacific Ocean". In: *Paleoceanography* 16.3, pp. 260–267. ISSN: 1944-9186. DOI: 10.1029/2000PA000540.

Marcantonio, Franco, Robert F. Anderson, Martin Stute, Niraj Kumar, Peter Schlosser, and Alan Mix (1996). "Extraterrestrial 3He as a Tracer of Marine Sediment Transport and Accumulation". In: *Nature* 383.6602, pp. 705–707. ISSN: 1476-4687. DOI: 10.1038/383705a0.

Marcantonio, Franco, Sean Higgins, Robert F. Anderson, Martin Stute, Peter Schlosser, and E. Troy Rasbury (1998). "Terrigenous Helium in Deep-Sea Sediments". In: *Geochimica et Cosmochimica Acta* 62.9, pp. 1535–1543. ISSN: 0016-7037. DOI: 10.1016/S0016-7037(98)00091-X.

Marcantonio, Franco, Niraj Kumar, Martin Stute, Robert F. Anderson, Michele A. Seidl, Peter Schlosser, and Alan Mix (1995). "A Comparative Study of Accumulation Rates Derived by He and Th Isotope Analysis of Marine Sediments". In: *Earth and Planetary Science Letters* 133.3, pp. 549–555. ISSN: 0012-821X. DOI: 10.1016/0012-821X(95)00079-R.

McGee, David, Franco Marcantonio, Jerry F. McManus, and Gisela Winckler (2010). "The Response of Excess 230Th and Extraterrestrial 3He to Sediment Redistribution at the Blake Ridge, Western North Atlantic". In: *Earth and Planetary Science Letters* 299.1-2, pp. 138–149. ISSN: 0012821X. DOI: 10.1016/j.epsl.2010.08.029.

McGee, David and Sujoy Mukhopadhyay (2013). "Extraterrestrial He in Sediments: From Recorder of Asteroid Collisions to Timekeeper of Global Environmental Changes". In: *The Noble Gases as Geochemical Tracers*. Ed. by Pete Burnard. Berlin, Heidelberg: Springer, pp. 155–176. ISBN: 978-3-642-28836-4. DOI: 10.1007/978-3-642-28836-4_7.

Merrihue, Craig (1964). "Rare Gas Evidence for Cosmic Dust in Modern Pacific Red Clay". In: *Annals of the New York Academy of Sciences* 119.1, pp. 351–367. ISSN: 1749-6632. DOI: 10.1111/j.1749-6632.1965.tb47445.x.

Montanari, Alessandro, Kenneth A. Farley, Rodolfo Coccioni, N. Sabatino, D. Bice, M. Yesko, M. Sinnesael, and N. De Winter (2023). "Cosmogenic 3He anomaly K1 vs. the early Campanian isotopic event (ECE) as recorded in pelagic limestones of the Umbria-Marche succession (Italy)". en. In: *Geological Society of America Bulletin*. ISSN: 0016-7606, 1943-2674. DOI: 10.1130/B36952.1.

Moreira, Manuel (2013). "Noble Gas Constraints on the Origin and Evolution of Earth's Volatiles". In: *Geochemical Perspectives* 2.2, pp. 229–230. ISSN: 2223-7755.

Moreira, Manuel and Sébastien Charnoz (2016). "The Origin of the Neon Isotopes in Chondrites and on Earth". In: *Earth and Planetary Science Letters* 433, pp. 249–256. ISSN: 0012-821X. DOI: 10.1016/j.epsl.2015.11.002.

Mukhopadhyay, Sujoy and Kenneth A. Farley (2006). "New Insights into the Carrier Phase(s) of Extraterrestrial 3He in Geologically Old Sediments". In: *Geochimica et Cosmochimica Acta* 70.19, pp. 5061–5073. ISSN: 0016-7037. DOI: 10.1016/j.gca.2006.06.1566.

Mukhopadhyay, Sujoy, Kenneth A. Farley, and Alessandro Montanari (2001). "A 35 Myr Record of Helium in Pelagic Limestones from Italy: Implications for Interplanetary Dust Accretion from the Early Maastrichtian to the Middle Eocene". In: *Geochimica et Cosmochimica Acta* 65.4, pp. 653–669. ISSN: 0016-7037. DOI: 10.1016/S0016-7037(00)00555-X.

Muller, Richard A. and Gordon J. MacDonald (1995). "Glacial Cycles and Orbital Inclination". In: *Nature* 377.6545, pp. 107–108. ISSN: 1476-4687. DOI: 10.1038/377107b0.

– (1997). "Glacial Cycles and Astronomical Forcing". In: *Science* 277.5323, pp. 215–218. DOI: 10.1126/science.277.5323.215.

Nesvorný, David, Peter Jenniskens, Harold F. Levison, William F. Bottke, David Vokrouhlický, and Matthieu Gounelle (2010). "COMETARY ORIGIN OF THE ZODIACAL CLOUD AND CARBONACEOUS MICROMETEORITES. IMPLICATIONS FOR HOT DEBRIS DISKS". In: *The Astrophysical Journal* 713.2, p. 816. ISSN: 0004-637X. DOI: 10.1088/0004-637X/713/2/816.

Nier, Alfred O. and Dennis J. Schlutter (1990). "Helium and neon isotopes in stratospheric particles". en. In: *Meteoritics* 25.4, pp. 263–267. ISSN: 0026-1114. DOI: 10.1111/j.1945-5100.1990.tb00710.x.

Nier, Alfred O. and Dennis J. Schlutter (1992). "Extraction of Helium from Individual Interplanetary Dust Particles by Step-Heating". In: *Meteoritics* 27.2, pp. 166–173. ISSN: 1945-5100. DOI: 10.1111/j.1945-5100.1992.tb00744.x.

Ogurtsov, M. G. and O. M. Raspopov (2011). "Possible Impact of Interplanetary and Interstellar Dust Fluxes on the Earth's Climate". In: *Geomagnetism and Aeronomy* 51.2, pp. 275–283. ISSN: 1555-645X. DOI: 10.1134/S0016793211020137.

Ozima, Minoru, M. Takayanagi, S. Zashu, and Sachiko Amari (1984). "High 3He/4He Ratio in Ocean Sediments". In: *Nature* 311.5985, pp. 448–450. ISSN: 1476-4687. DOI: 10.1038/311448a0.

Patterson, Desmond B. and Kenneth A. Farley (1998a). "Extraterrestrial 3He in Seafloor Sediments: Evidence for Correlated 100 Kyr Periodicity in the Accretion Rate of Interplanetary Dust, Orbital Parameters, and Quaternary Climate". In: *Geochimica et Cosmochimica Acta* 62.23, pp. 3669–3682. ISSN: 0016-7037. DOI: 10.1016/S0016-7037(98)00263-4.

Patterson, Desmond B., Kenneth A. Farley, and Birger Schmitz (1998b). "Preservation of Extraterrestrial 3He in 480-Ma-old Marine Limestones". In: *Earth and Planetary Science Letters* 163.1, pp. 315–325. ISSN: 0012-821X. DOI: 10.1016/S0012-821X(98)00197-6.

Pepin, Robert O., R. L. Palma, and Dennis J. Schlutter (2001). "Noble Gases in Interplanetary Dust Particles, II: Excess Helium-3 in Cluster Particles and Modeling Constraints on Interplanetary Dust Particle Exposures to Cosmic-Ray Irradiation". In: *Meteoritics & Planetary Science* 36.11, pp. 1515–1534. ISSN: 1945-5100. DOI: 10.1111/j.1945-5100.2001.tb01843.x.

Pepin, Robert O., Dennis J. Schlutter, Richard H. Becker, and Daniel B. Reisenfeld (2012). "Helium, Neon, and Argon Composition of the Solar Wind as Recorded in Gold and Other Genesis Collector Materials". In: *Geochimica et Cosmochimica Acta* 89, pp. 62–80. ISSN: 0016-7037. DOI: 10.1016/j.gca.2012.04.024.

Peucker-Ehrenbrink, Bernhard, Greg Ravizza, and Gisela Winckler (2016). "Geochemical Tracers of Extraterrestrial Matter in Sediments". In: *Elements* 12.3, pp. 191–196. ISSN: 1811-5209. DOI: 10.2113/gselements.12.3.191.

Plane, John M. C. (2012). "Cosmic Dust in the Earth's Atmosphere". In: *Chemical Society Reviews* 41.19, pp. 6507–6518. DOI: 10.1039/C2CS35132C.

Plane, John M. C., George J. Flynn, Anni Määttänen, John E. Moores, Andrew R. Poppe, Juan Diego Carrillo-Sanchez, and Constantino Listowski (2017). "Impacts of Cosmic Dust on Planetary Atmospheres and Surfaces". In: *Space Science Reviews* 214.1, p. 23. ISSN: 1572-9672. DOI: 10.1007/s11214-017-0458-1.

Raquin, Aude and Manuel Moreira (2009). "Atmospheric 38Ar/36Ar in the Mantle: Implications for the Nature of the Terrestrial Parent Bodies". In: *Earth and Planetary Science Letters* 287.3, pp. 551–558. ISSN: 0012-821X. DOI: 10.1016/j.epsl.2009.09.003.

Sano, Yuji, Bernard Marty, and Pete Burnard (2013). “Noble Gases in the Atmosphere”. In: *The Noble Gases as Geochemical Tracers*. Ed. by Pete Burnard. Berlin, Heidelberg: Springer, pp. 17–31. ISBN: 978-3-642-28836-4. DOI: 10.1007/978-3-642-28836-4_2.

Schmitz, Birger, Kenneth A. Farley, Steven Goderis, Philipp R. Heck, Stig M. Bergström, Samuele Boschi, Philippe Claeys, Vinciane Debaille, Andrei Dronov, Matthias van Ginneken, David A.T. Harper, Faisal Iqbal, Johan Friberg, Shiyong Liao, Ellinor Martin, Matthias M. M. Meier, Bernhard Peucker-Ehrenbrink, Bastien Soens, Rainer Wieler, and Fredrik Terfelt (2019). “An Extraterrestrial Trigger for the Mid-Ordovician Ice Age: Dust from the Breakup of the L-chondrite Parent Body”. In: *Science Advances* 5.9, eaax4184. DOI: 10.1126/sciadv.aax4184.

Tagle, Roald and Philippe Claeys (2004). “Comet or Asteroid Shower in the Late Eocene?” In: *Science* 305.5683, pp. 492–492. DOI: 10.1126/science.1098481.

Tagle, Roald, T. Öhman, R. T. Schmitt, J. Erzinger, and Ph. Claeys (2007). “Traces of an H Chondrite in the Impact-Melt Rocks from the Lappajärvi Impact Structure, Finland”. In: *Meteoritics & Planetary Science* 42.10, pp. 1841–1854. ISSN: 1945-5100. DOI: 10.1111/j.1945-5100.2007.tb00542.x.

van Ginneken, Matthias, Penelope J. Wozniakiewicz, Donald E. Brownlee, Vinciane Debaille, Vincenzo Della Corte, Lucie Delauche, Jean Duprat, Cecile Engrand, Luigi Folco, Marc Fries, Jérôme Gattacceca, Matthew J. Genge, Steven Goderis, Matthieu Gounelle, Ralph P. Harvey, Guido Jonker, Lisa Krämer Ruggiu, Jon Larsen, James H. Lever, Takaaki Noguchi, Scott Peterson, Pierre Rochette, Julien Rojas, Alessandra Rotundi, N. G. Rudraswami, Martin D. Suttle, Susan Taylor, Flore Van Maldeghem, and Michael Zolensky (2024). “Micrometeorite Collections: A Review and Their Current Status”. In: *Philosophical Transactions of the Royal Society A: Mathematical, Physical and Engineering Sciences* 382.2273, p. 20230195. DOI: 10.1098/rsta.2023.0195.

Walton, Craig R., Jessica K. Rigley, Alexander Lipp, Robert Law, Martin D. Suttle, Maria Schönbächler, Mark Wyatt, and Oliver Shorttle (2024). “Cosmic Dust Fertilization of Glacial Prebiotic Chemistry on Early Earth”. In: *Nature Astronomy* 8.5, pp. 556–566. ISSN: 2397-3366. DOI: 10.1038/s41550-024-02212-z.

Ziegler, James F., M. D. Ziegler, and J.P. Biersack (2010). “SRIM – The stopping and range of ions in matter (2010)”. en. In: *Nuclear Instruments and Methods in Physics Research Section B: Beam Interactions with Materials and Atoms* 268.11–12, pp. 1818–1823. ISSN: 0168583X. DOI: 10.1016/j.nimb.2010.02.091.

Chapter 2

ASTEROIDS OR COMETS? SOURCE OF EXCESS COSMIC DUST DURING THE LATE CRETACEOUS K1 ^{3}HE ENHANCEMENT EVENT

2.1 Introduction

Cosmic dust consists of meteoroids smaller than ~2000 µm and is the most abundant extraterrestrial material falling on Earth (Peucker-Ehrenbrink et al., 2016). Asteroid and comets are the two main contributors to the current cosmic dust flux (*e.g.*, Kortenkamp et al. 1998; Nesvorný et al. 2010), whose relative contributions may have varied over the history of the Solar System, but in particular could be transiently perturbed by intense cosmic dust production events. These events include asteroid collisions in the main asteroid belt or an increased number of comets in the Solar System (*i.e.*, a comet shower). Studying the accretion history of cosmic dust thus provides crucial information about the history of the Solar System and the recurrence rate of dust-producing astronomical events.

Evaluations of the cosmic dust accretion rate in geological history are largely based on ^{3}He analysis in marine sediments (Farley, 1995; Farley et al., 2012; Mukhopadhyay et al., 2001; Patterson et al., 1998b). ^{3}He is a very sensitive indicator of cosmic dust due to its distinctive enrichment in ^{3}He and high ^{3}He/^{4}He compared to terrestrial materials, arising from implanted solar wind helium. For example, cosmic dust captured in the stratosphere has ^{3}He/^{4}He of ~200 R_A (Nier et al., 1990) (1 R_A = 1.382×10^{-6}, which is the ^{3}He/^{4}He of Earth's atmosphere; Burnard 2013), 4 orders of magnitude higher than that of average continental crust represented by Chinese loess (^{3}He/^{4}He = 0.014–0.028 R_A; Peucker-Ehrenbrink et al. 2001; Marcantonio et al. 1998). It is also exclusively a tracer of fine cosmic dust because infalling particles larger than a few tens of µm are intensely heated and degassed during atmospheric entry (Farley et al., 1997).

The sedimentary $^3He_{ET}$ (extraterrestrial ^{3}He) record of the last 100 Myr has been found to be relatively constant, suggesting a similarly constant cosmic dust flux and the usage of $^3He_{ET}$ as a constant flux proxy to obtain sedimentation rates (*e.g.*, Farley et al. 2003; Marcantonio et al. 1995). However, five episodes of elevated sedimentary $^3He_{ET}$ in the last 100 Myr have ~2-Myr durations and at least a 5-time

$^3He_{ET}$ enhancement that could not be explained by variations in the sedimentation rate, but must arise from enhanced dustiness in the Solar System (Farley, 1995; Farley et al., 2012; Farley et al., 1998; Farley et al., 2006; Mukhopadhyay et al., 2001). The sedimentary $^3He_{ET}$ record older than 100 Ma has not been reconstructed, but $^3He_{ET}$ analysis in Ordovician limestones shows that the cosmic dust flux may have increased by a hundredfold in at ~466 Ma (Patterson et al., 1998b; Schmitz et al., 2019).

One of the fundamental questions regarding these $^3He_{ET}$ events is the source of the excess cosmic dust, *i.e.*, the cosmic dust flux in excess of the pre-event background level. The Late Miocene $^3He_{ET}$ event that peaks at ~8.2 Ma (Farley et al., 2006) has been linked to formation of asteroid family 609 Veritas, independently dated to 8.3 ± 0.5 Ma by orbital backtracking (Nesvorny et al., 2003). Similarly, the Mid-Ordovician $^3He_{ET}$ event has been linked to the breakup of the ∼150-km L-chondrite parent body (Schmitz et al., 2019), based on evidence from ^{40}Ar-^{39}Ar ages of meteorites (*e.g.*, Haack et al. 1996) and elevated L-chondritic chromite abundance in Mid-Ordovician limestones (Schmitz et al., 2003). In contrast, the cause of the Late Eocene $^3He_{ET}$ event is debated. It was first attributed to a comet shower because its duration and temporal pattern resembles an independently-derived model of a comet shower caused by a nearby star perturbing the Oort Cloud (Farley et al., 1998). The simultaneous arrival of both cosmic dust and large near-Earth objects predicted by comet shower models (Hut et al., 1987; Nurmi et al., 2001) is also consistent with the occurrence of the two largest impact craters of the Cenozoic over a very short interval at the peak of the $^3He_{ET}$ event (Farley et al., 1998). Alternatively, an asteroidal origin of the Late Eocene $^3He_{ET}$ event has been proposed to explain the non-carbonaceous nature of one of the impactors, on the assumption that comets are compositionally similar to carbonaceous chondrites (Boschi et al., 2017; Fritz et al., 2007; Kyte et al., 2004; Schmitz et al., 2015; Tagle et al., 2004; Tagle et al., 2005). In the second interpretation the temporal evolution of the event, including the timing of the impacts, is not *a priori* predicted.

Few details are known regarding the recently reported three $^3He_{ET}$ events in the Cretaceous (informally called K1, K2, and K3). K2 (~85 Ma) and K3 (~91 Ma) have well-preserved sedimentary records, but their temporal patterns are distinct from the two Cenozoic events, for unknown reasons (Farley et al., 2012). K1 is the youngest (~80 Ma) and the most prominent Cretaceous $^3He_{ET}$ event, with a peak ^3He concentration 5–9 times the pre-event background and a duration of a few Myr (Farley et al., 2012; Montanari et al., 2023). It's temporal evolution bears similarities to the Cenozoic events, but the previously reported records in Bottaccione Gorge (Farley et al., 2012) and Furlo (Montanari et al., 2023), Italy are disturbed by faults, deformation, slumps, turbidites, and missing strata, which limits further interpretations.

The apparently instantaneous onset of K1 is coincident with the C33r-C33n geomagnetic reversal in the Bottaccione Gorge record, but the relative timing of these two events were not clear since both occur just above an interval of inferred missing section (Farley et al., 2012). A recent study of an undisturbed section at Apiro, Italy provides a more complete picture of K1 (Montanari et al., 2023), and demonstrates that not only does C33r-C33n occur near the peak of the ^{3}He event, but so too does a moderate carbon isotope excursion known as the early Campanian event (ECE;Sabatino et al. 2018). The co-occurrences raise the question of whether these disparate events could be related.

It has been proposed that a large extraterrestrial impact could trigger a geomagnetic reversal (Muller et al., 1986). The two are linked via an impact-induced transient ice age, which could rapidly change the Earth's moment of inertia by transferring a large mass of water from lower latitudes to polar regions. In this model, the different response times of mantle and core to the new moment of inertia would cause velocity shear in the outer core, which in turn could disturb the geodynamo and induce a geomagnetic excursion or even reversal. The Ivory Coast microtektite strewn field and the Australasian strewn field were once thought to be examples of this mechanism because of their stratigraphic proximity to geomagnetic reversals (*e.g.*, Glass et al. 1979), but both were later disproved with detailed stratigraphic analyses (Glass et al., 1991) and stable isotope records (Schneider et al., 1992). K1 is another potential example of an astronomical event triggering a geomagnetic reversal via climate change, but the sampling resolution in the previous study is inadequate to assess the possibility (Montanari et al., 2023).

Here we report new helium measurements from the minimally-disturbed Scaglia Rossa limestone section at Apiro. Combined with earlier data (Montanari et al., 2023), these measurements provide an apparently complete 6.5-Myr record that includes K1. We compare this record to other known ^{3}He events and evaluate the possible astronomical origin of the enhanced cosmic dust flux at this time. We also report high temporal resolution ($\sim$1 kyr) measurements of helium isotopes and trace metals over a short interval within the peak of K1, in an attempt to assess bolide

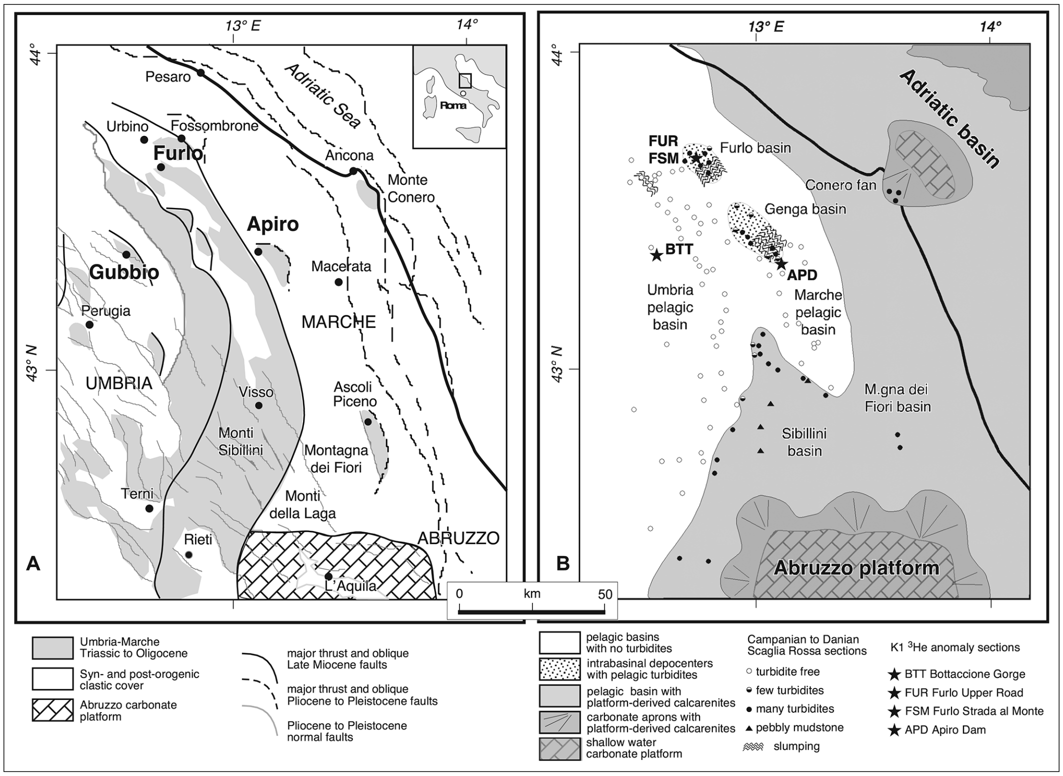

Figure 2.1: Geological Map of the Umbria-Marche sedimentary basin (Montanari et al., 2023)

impact signals.

2.2 Materials and Methods

Geological Background and Sampling

The Scaglia Rossa Formation consists of a 400-meter thick succession of pink to red deep-sea limestones and marls deposited in the Umbria-Marche paleobasin from the Turonian to early Eocene (Fig. 2.1) (Arthur et al., 1977). Turbidites, faults and slumps are common in the Scaglia Rossa as a result of seismic activity (Bice et al., 2007; Montanari et al., 1989; Tognaccini et al., 2019). This activity is the proposed cause of the disturbances that define the R2m layer in Bottaccione Gorge in which K1 occurs, and is likely responsible for faulting or slumping that excised the onset of the event (Bice et al., 2007; Farley et al., 2012).

The Apiro section (43°22'51.30"N; 13°09'18.13"E) is located some 45 km east of the Bottaccione Gorge and exposes a continuous succession of upper Santonian to Danian Scaglia Rossa limestones along the provincial road SP 26 that flanks the Castreccioni reservoir (Mitchell et al., 2021; Montanari et al., 2023). Detailed biostratigraphic and magnetostratigraphic characterization indicates that the section is complete and free of turbidites, slumps and faults, and spans magnetochron C33 (Mitchell et al., 2021).

We studied two types of samples from the Apiro section: discrete paleomagnetic core samples drilled parallel to bedding, and wafer slices of bedding-perpendicular cores acquired from block samples across the C33r-C33n chron boundary. The 28 discrete core samples were selected from an existing paleomagnetic core collection (Mitchell et al., 2021), with a specific focus on the onset of K1 between ~105 m and ~107 m in stratigraphic height. Each 2.5 cm diameter core corresponds to a time interval of ~2.5 kyr assuming a mean sedimentation rate of ~1 cm/kyr (Arthur et al., 1977). Only helium analyses were carried out on these samples. These samples complement a previously published dataset from the same area (Montanari et al., 2023). Together this suite of 122 samples spans 84.5 meters of section with sample spacing between 2 cm and 7.4 m.

The wafer samples prepared from three contiguous blocks of limestone that include the C33r-C33n boundary (Mitchell et al., 2021) were acquired to examine impact signals and the temporal relationship between K1 and the reversal at high resolutions. The blocks provide a continuous sedimentary record of 55 cm (~55 kyr), from 108.10 to 108.65 m in stratigraphic height (Mitchell et al., 2021). Cores were drilled from these blocks, then cut into 1-cm-thick wafers (each representing ~1 kyr). Paleomagnetic analyses, helium analyses, and trace metal analyses were carried out on these samples.

Paleomagnetism

Remanent magnetization measurements were made on a 2G DC-SQuID magnetometer with the RAPID setup (Kirschvink et al., 2008). Natural remanent magnetization was measured on all samples first, prior to a cryogenic demagnetization in liquid nitrogen in a magnetically-shielded room.

Alternating-field (AF) demagnetization was applied instead of thermal demagnetization so the demagnetized cores could be analyzed for helium later, without concern over helium loss at elevated temperatures. For each sample, 47 partial demagnetization steps were applied, ramping up from 0 to 80 mT with a step-size of 1–5 mT.

Magnetic components of each sample were computed based on principal component analysis (Kirschvink, 1980) with the software PaleoMag (Jones, 2002). By AF demagnetization, we observed a weaker component until 18 mT and a stronger component from 18 mT to 80 mT. Principal component analysis was performed on the stronger component to calculate the vector direction of the paleomagnetic field.

Helium Isotopes

Samples for helium isotope analysis were prepared following standard procedures (Farley et al., 2012) with a few modifications. Samples were crushed with a small jaw crusher (for the core slices, crushing occurred after magnetic analyses), then leached with 10 v/v% acetic acid to remove carbonate. Each sample was washed three times with deionized water, centrifuged, then decanted of the supernatant. The acid insoluble residue was dried for 3~4 days in a 40 ℃ oven to ensure complete dehydration. The mass fraction of this residue in the bulk sample was recorded as the non-carbonate fraction, or NCF. Because our decarbonation step is performed under conditions different from those usually used to quantify carbonate content (*e.g.*, Fu et al. 2020), NCF may differ slightly from (1 – carbonate-fraction).

We prepared multi-gram quantities of each sample in a single decarbonation step and homogenized the residue with mortar and pestle. This allowed multiple measurements to be made with just a single decarbonation. This approach differs from previous work (Farley et al., 2012) in which each replicate analysis was performed on a bulk aliquot independently decarbonated. For each measurement, a ~50-mg sub-sample of the acid insoluble residue was wrapped in tin foil, then degassed of helium in a double-walled vacuum furnace at ~1250 ℃. Evolved helium was purified by a series of getters, cryogenically concentrated on charcoal at 14 K, and then released at 34 K into a Thermo Helix SFT mass spectrometer.

^{3}He was measured on a pulse-counting electron multiplier while ^{4}He was simultaneously measured on a Faraday detector. The mass spectrometer was calibrated for sensitivity and pressure nonlinearity using a synthetic helium gas standard with a ^{3}He/^{4}He ratio of 2.05 R$_A$. We estimate the analytical precision on sediment measurements to be better than 2 % for each isotope based on replicate measurements of standards of comparable size. In all cases, the blank levels for both ^{3}He and ^{4}He were negligible (<0.5 %) compared to measured signals.

Variance between helium measurements is dominated by statistical sampling of rare IDPs enriched in ^{3}He, rather than by measurement precision (Farley et al., 1997). Following previous work (*e.g.*, Farley et al. 2012), to reduce statistical scatter, replicates were measured when an abnormally high ^{3}He concentration or ^{3}He/^{4}He ratio was measured compared to adjacent samples. A triplicate was analyzed whenever a duplicate did not replicate the first ^{3}He measurement. When a ^{3}He measurement was 40 % above the mean of its companion replicates, it was discarded as being a highflier. We have rejected just 2 measurements with this criterion, out of a total of 126 measurements. Including these two observations would make no difference to our conclusions.

Trace Metals

A separate set of cores was obtained from the limestone blocks for trace metal analyses. These were cut into 1-cm-thick cylindrical wafers with a table saw, then polished with sandpaper to remove the surface that had contact with the stainless steel blade with a diamond edge. The polished samples were ground into powders with an agate mortar and pestle.

Acid digestion of the powdered samples was carried out in PFA beakers in the class 1000 trace-metal clean lab at the Isotoparium (Caltech). About 50 mg of each powdered sample was treated with a sequence of acid digestions. Carbonate phases were removed with 2.3 mL of 1.5 M hydrochloric acid on a hot plate at 60 ℃ for 1 day, then dried down at 90 ℃. Silicates were digested with 2 mL of twice-distilled concentrated 2:1 HF-HNO3 mixture on a hot plate at 150 ℃ for 4 days, then dried down at 130 ℃. Fluoride precipitates were then dissolved with 1 mL of aqua regia on a hot plate at 110 ℃ for 3 days. In cases where there were visible fluorides remaining, additional digestion with concentrated nitric acid and/or inverse aqua regia was used.

Trace metal concentration measurements were carried out in standard mode on the Thermo Fisher iCAP RQ ICP-MS at the Isotoparium (Caltech). Periodic measurements of multi-element solution standards were used to correct for instrument drift and estimate reproducibility. The average procedural blank contribution was 4 % for Cr, 0.04 % for Co, and 0.3 % for Ni.

2.3 Results

The paleomagnetic cores we measured, together with the results of other paleomagnetic cores briefly presented previously (Montanari et al., 2023), are reported and described here in detail. The ^{3}He concentration in the bulk limestone ([^{3}He]) ranges from 0.039 pcc/g to 0.81 pcc/g (pcc: 10^{-12} cm^3 at STP), [^{4}He] ranges from 14 ncc/g to 64 ncc/g (ncc: 10^{-9} cm^3 at STP) and ^{3}He/^{4}He ranges from 1.1 R_A to 28 R_A (Fig. 2.2). An interval of elevated ^{3}He/^{4}He is evident between ~105 m and ~125 m, with a steep, 9-fold increase from 2.3 R_A to 21 R_A between 105 m and 107 m followed by

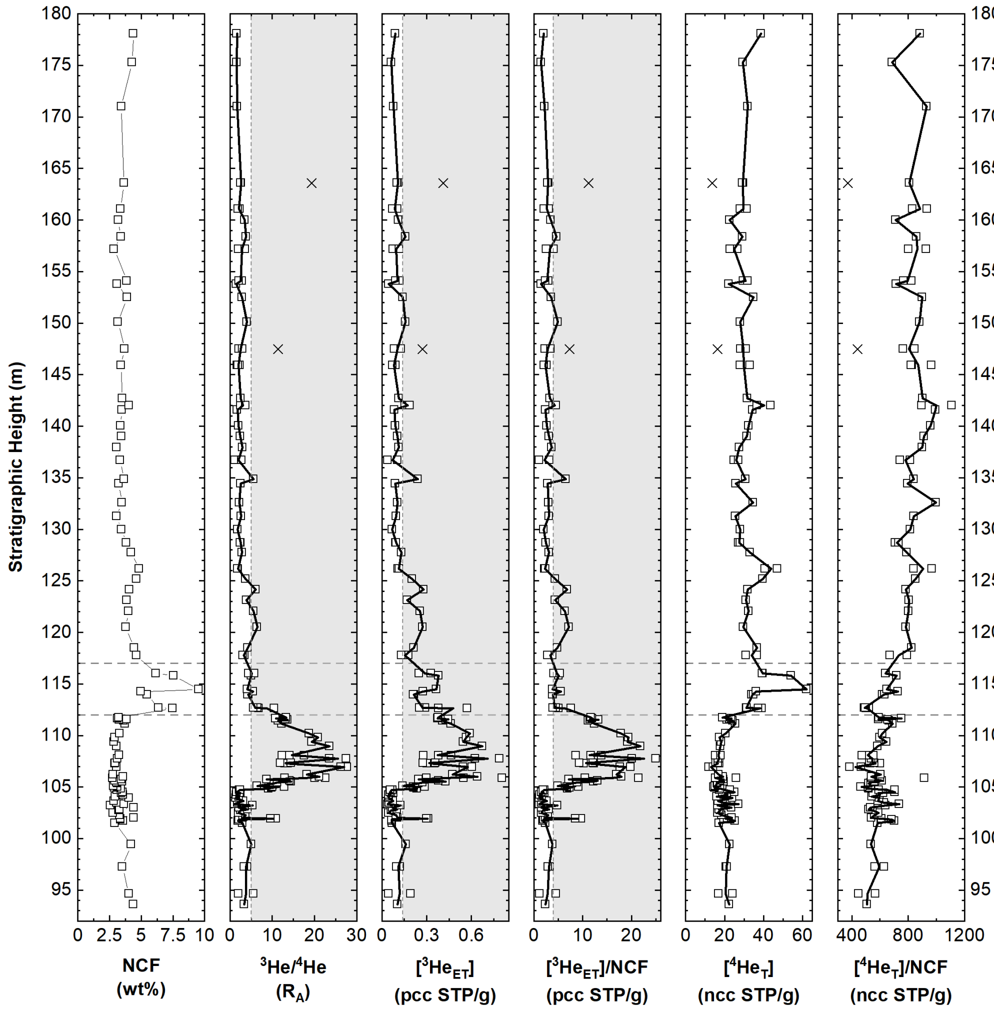

Figure 2.2: Non-carbonate fraction (NCF) and helium isotope data of the discrete core samples. Thick solid lines in the right 5 panels connects the average measurements of each sample. The shaded regions include all values that are 2σ above the pre-event background. The horizontal dashed lines bracket the interval with high NCF (see text). 2 measurements labelled as crosses were discarded as outliers (see text).

a gradual decline. This interval was previously associated with the K1 $^3He_{ET}$ event (Montanari et al., 2023).

Helium in deep-sea sediments is a two-component mixture of extraterrestrial helium in cosmic dust and terrestrial helium from terrigenous sediments and can be deconvoluted (Patterson et al., 1998a; Takayanagi et al., 1987) using known endmember ^{3}He/^{4}He ratios. Here we use cosmic dust captured in the stratosphere as the extraterrestrial endmember (174 R_A; Nier et al. 1990 and Chinese loess as the terrestrial endmember (0.014–0.028 R_A; Peucker-Ehrenbrink et al. 2001; Marcantonio et al. 1998). Deconvolution shows that in the paleomagnetic core suite >98 % of ^{3}He is extraterrestrial ($^3He_{ET}$), while 84–99 % of ^{4}He is terrestrial (^4He_T). The exact composition of the endmembers makes little or no difference to the endmember proportions obtained by deconvolution.

In the paleomagnetic core samples [$^3He_{ET}$] concentrations range from 0.038 to 0.81 pcc/g and define a similar pattern and span to ^{3}He/^{4}He, with a 10-fold increase between ~105 m and ~107 m. [^4He_T] ranging from 12 to 62 ncc/g does not correlate with [$^3He_{ET}$], but instead shows a gradual up-section increase from ~20 to ~30 ncc/g. A narrow interval of elevated [^4He_T] occurs between ~112 m and ~117 m, reaching the global maximum of 62 ncc/g at ~114.5 m.

We also report helium concentrations normalized to the non-carbonate fraction (NCF, *i.e.*, the fraction of sediment mass that survives our acetic acid leaching step), which can be used to correct for [$^3He_{ET}$] variations due to changes in the sedimentation rate, and reveal [$^3He_{ET}$] variations associated with changes in the $^3He_{ET}$ flux (*e.g.*, Farley et al. 2012). Similarly, since most of the material in the noncarbonate fraction is terrigenous matter, [^4He_T]/NCF is a measure of the ^{4}He concentration of the terrigenous component. Throughout the dataset, NCF ranges from 2.6 to 9.5 wt% (Fig. 2.2), with a mean of 3.7 ± 2.2 wt% (2 standard deviation). NCF is generally constant at ~3.5 wt% except in the interval between ~112 m and ~117 m, in which NCF is up to 9.5 wt% (Fig. 2.2). This is the same interval noted above to have elevated ^4He_T. [$^3He_{ET}$]/NCF ranges from 1.1 to 28 pcc/g, while [^4He_T]/NCF ranges from 370 to 1100 ncc/g (Fig. 2.2). A 9-fold rise in [$^3He_{ET}$]/NCF is observed between ~105 m and ~107 m, then it decreases to the pre-event level at ~125 m. [^4He_T]/NCF increases gradually up-section from ~500 to ~900 ncc/g. Unlike [^4He_T], the [^4He_T]/NCF profile is featureless from ~112 m to ~117 m, indicating that [^4He_T] and NCF are strongly correlated.

To quantify the span of the K1 $^3He_{ET}$ event, we define an elevated value to be one that is > 2 standard deviations above pre-event levels, where the latter is defined as the mean of 23 samples between 93.6 m and 104.7 m. The sample at 101.92 m was excluded because it was > 3σ higher than the mean of the 24 samples and thus considered as statistically different from the mean. The pre-event ^{3}He/^{4}He ratio is calculated to be 2.7 ± 2.2 R_A, and the elevated interval spans 104.8 m to 124.2 m in stratigraphic height. Similarly, [$^3He_{ET}$] and [$^3He_{ET}$]/NCF both define an elevated interval from 104.8 m to 125.2 m, relative to the pre-event [$^3He_{ET}$] of 0.078 ± 0.062

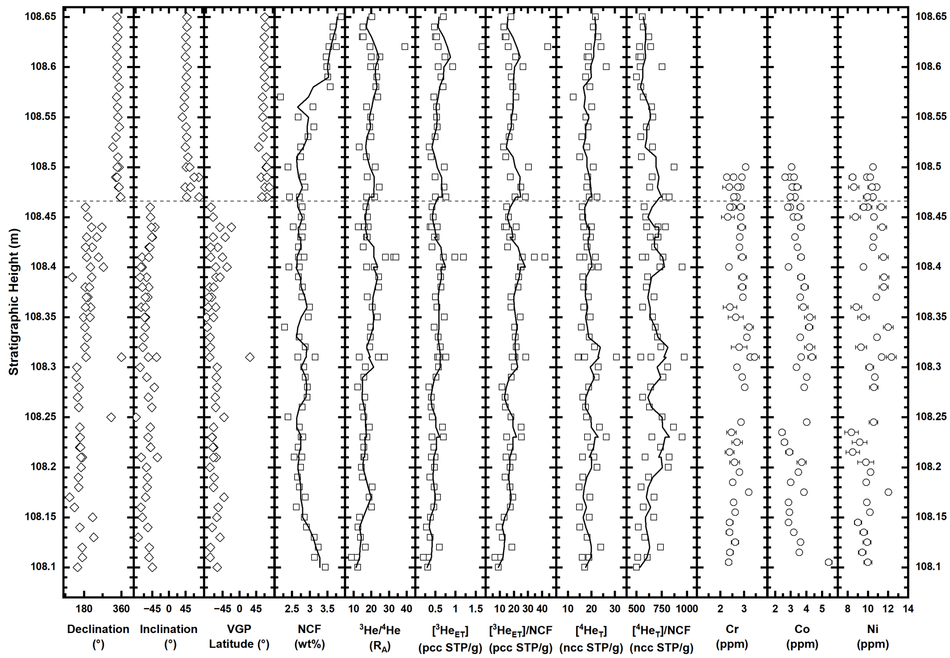

Figure 2.3: Paleomagnetic, NCF, helium isotope, and trace metal data of the continuous core slices. The dashed line at 108.46 m denotes the shift from reversed polarity to normal polarity, which is identified as the C33r-C33n geomagnetic reversal boundary. Solid lines are 3-point running mean. Error bars the last three panels are 2σ uncertainties estimated based on reproducibility of standard solutions with known concentrations.

pcc/g and to the pre-event [$^3He_{ET}$]/NCF of 2.25 ± 1.76 pcc/g.

In the wafer samples, our paleomagnetic analyses found a reversal in both declination and inclination at 108.46 m (Fig. 2.3). This is within 15 cm of the previously recognized position of the C33r-C33n reversal (Mitchell et al., 2021). The directional change is sharp, with clear reversed polarity at 108.46 m and normal at 108.47 m. Maximum angular deviation (MAD), which describes the directional scatter of the remanent magnetic vectors, shows an increase from ~5° between 108.10 m and 108.25 m to ~16° right at the reversal boundary, then a decrease to ~3° above the reversal.

For the wafer samples, NCF and helium data vary modestly in this 55 cm interval (Fig. 2.3) and are consistent with adjacent samples from the paleomagnetic cores. NCF decreases from ~3.5 wt% at 108.10 m to ~2.8 wt% at 108.16 m, stays flat across the reversal, then starts to increase at 108.60 m until it reaches ~3.6 wt% at 108.65 m. The ^{3}He/^{4}He ratio increases from ~10 R_A at 108.10 m to ~20 R_A at 108.16 m, then fluctuates around an average value of 19 R_A (Fig. 2.3). Deconvolution shows that >99 % of ^{3}He is extraterrestrial, while 78–95 % of ^{4}He is terrestrial. [$^3He_{ET}$] has a similar trend to ^{3}He/^{4}He, while [^4He_T] shows a much flatter profile around its mean. [$^3He_{ET}$]/NCF and [^4He_T]/NCF show a similar trend to [$^3He_{ET}$] and [^4He_T], respectively.

We report Cr concentrations between 2.27 and 3.46 ppm (mean: 2.73 ± 0.58 ppm), Co between 2.45 and 5.43 ppm (mean: 3.44 ± 1.10 ppm), and Ni between 8.38 and 12.3 ppm (mean:10.21 ± 1.98 ppm) (Fig. 2.3). No obvious trend or peaks in these quantities are observed across the interval.

2.4 Temporal Evolution of K1

The Apiro section,being apparently free of faults, slumps, turbidites, and hiatuses (Mitchell et al., 2021), provides us with an apparently complete temporal record of K1. We developed a new age model because the existing age model for this interval in Apiro uses a constant sedimentation rate of 1.25 cm/kyr in magnetochron C33n and 0.95 cm/kyr in magnetochron C33r (Mitchell et al., 2021). Given our focus on the interval near the chron boundary, this step function would produce a pattern dominated by the coincidental location of the age tie point. In addition, the age model is too coarse to capture short-term fluctuations in sedimentation rate that may affect the helium record.

Our new age model uses non-carbonate fraction (NCF) in each sample as a constant sedimentation flux proxy, specifically assuming that the concentration of terrigenous detritus that makes up the non-carbonate fraction can be used as a constant flux proxy to track variations in carbonate sedimentation rate in these very carbonate rich sediments. In this new model, increases in NCF are interpreted to indicate a reduction in carbonate sedimentation rate (or carbonate dissolution), while decreases in NCF are attributed to enhanced carbonate sedimentation rate.

We first calculate the average sedimentation rates between geomagnetic reversal boundaries C33n-C32r.2r (74.20 Ma), C33r-C33n (79.90 Ma), and C34n-C33r (83.65 Ma) identified in Apiro (Mitchell et al., 2021) with updated ages (Gradstein, 2020). This leads to a sedimentation rate of 1.34 cm/kyr in magnetochron C33n and 0.84 cm/kyr in magnetochron C33r. Since most of our record is within C33n and the C34n-C33r boundary is not well constrained in Apiro (Mitchell et al., 2021), we use 1.34 cm/kyr as the average sedimentation rate for the entire ~85-meter studied section.

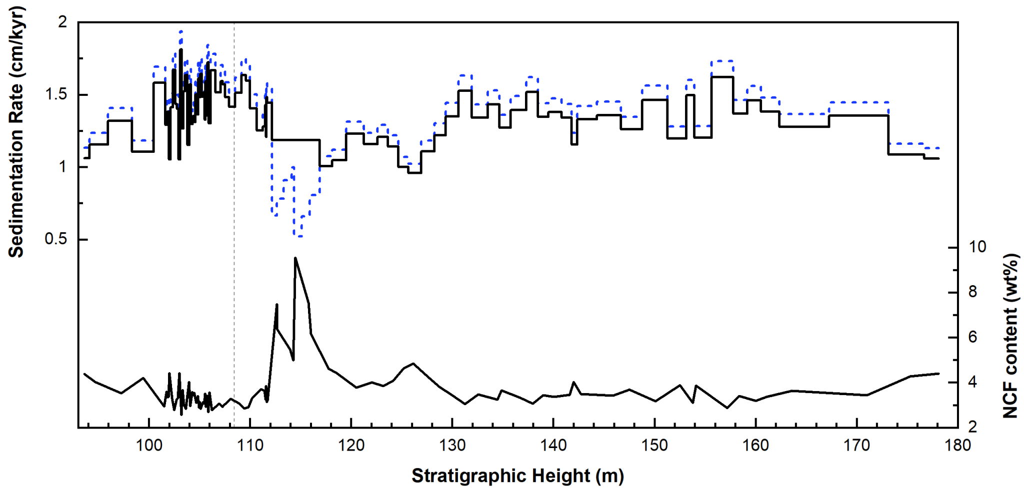

Figure 2.4: The age model built for this study and the NCF of each sample. Blue dashed line is the age model when normalized to the average NCF of all discrete core samples (3.7 wt%). Black solid line in the upper panel is the age model when normalized to the average NCF of all discrete core samples excluding the 7 samples with abnormally high NCF within 112 m and 117 m (3.5 wt%). Black solid line in the lower panel is the measured NCF of each discrete core sample. Vertical dashed line shows the C33r-C33n geomagnetic reversal boundary.

An NCF-normalized sedimentation rate of each sample is then calculated by dividing this average sedimentation rate by the normalized NCF of that sample. The latter is defined as the measured NCF of each sample normalized to the average NCF over the whole record. Here, instead of using an average NCF of 3.7 wt%, we use a revised average NCF of 3.5 wt%, excluding the 7 samples with abnormally high NCF contents between 112 m and 117 m. As discussed, we attribute the high NCF in this interval to an actual increase in non-carbonate sediment input associated with regional tectonic activities, instead of a change in carbonate sedimentation rate. Since the NCF between 112 m and 117 m potentially has contributions from excess non-carbonate flux and may not serve as a constant flux proxy for this interval, we assume the sedimentation rate to be constant within this 5-m interval, and use the average NCF of the two samples bracketing these 7 samples as the average NCF across this interval.

Finally, the time between two adjacent samples is the product of their stratigraphic separation and the average NCF-normalized sedimentation rate of the two samples, and the age of each sample is calculated by anchoring the age model at the C33r-C33n boundary (79.90 Ma; Gradstein 2020 at 108.46 m. The sedimentation rates determined this way fluctuate around the constant sedimentation rate of 1.34 cm/kyr by about ± 30 % (Fig. 2.4).

With the new age model, we show that K1 spans ~1.7 Ma from ~80.2 Ma to ~78.5 Ma (Fig. 2.5), in Mid-Campanian time. The elevated ^{3}He interval shows an asymmetrical evolution with a rapid rise and gradual decline. Within ~0.14 Myr, $[^{3}He_{ET}]$, $^{3}He/^{4}He$ and $[^{3}He_{ET}]$/NCF rise by a factor of 9 to 10. This rapid rise is followed by a peak interval of ~0.14 Myr and characterized by several local maxima and minima. Finally, the decay period lasts ~1.4 Myr from ~79.9 Ma until ~78.5 Ma.

K1 has been previously reported in Bottaccione Gorge (Farley et al., 2012) and Furlo (Montanari et al., 2023) in the same sedimentary basin as Apiro. In Fig. 2.5, we attempt to align the Bottacione record with the Apiro record by pinning the first occurrence positions of the index fossil *Contusotruncana plummerae* and the last sample in both sections with low $[^{3}He_{ET}]$/NCF values prior to the onset of K1. In so doing it becomes clear that the Bottacione section is in fact missing most of the K1 peak, an interval of at least 1 Myr. This is compatible with the estimated ~1.6-Myr (~18-m) section missing at Bottaccione Gorge (Farley et al., 2012), and also explains why the relative increase in ^{3}He at Bottacione is only half of that at Apiro. The Furlo record (Fig. 2.5) shows a more prolonged increase in $[^{3}He_{ET}]$/NCF from background to peak, spanning ~0.8 Myr from ~80.5 Ma to ~79.7 Ma. The peak at ~79.7 Ma is ~15 times higher than the pre-event background mean, which then gradually decays away in over 2.5 Myr. However, comparing the Furlo record and the Apiro record is not straightforward due to the frequent disturbance of turbidite layers and faults in the former (Fig. 2.5; Montanari et al. 2023). These comparisons illustrate the uniqueness of the minimally-disturbed Apiro record, based on which we can interpret the fine details of K1.

Fluctuations in $[^{3}He_{ET}]$, $^{3}He/^{4}He$ and $[^{3}He_{ET}]$/NCF occur within the peak period of K1. At 79.98 Ma and 79.92 Ma, $[^{3}He_{ET}]$, $^{3}He/^{4}He$ and $[^{3}He_{ET}]$/NCF drop by almost 50 %, but are still 4–5 times higher than pre-event background. The minimum at 79.98 Ma is defined by 2 samples, while the minimum at 79.92 Ma and the local maximum at 79.95 Ma contain only 1 sample. To evaluate whether the fluctuations within the peak of K1 are statistical and associated with the small number of cosmic dust grains in the samples, we ran a Monte Carlo simulation to estimate the probability of randomly generating the observed peak-to-trough differences. In each simulation, $[^{3}He_{ET}]$, $^{3}He/^{4}He$ and $[^{3}He_{ET}]$/NCF values are

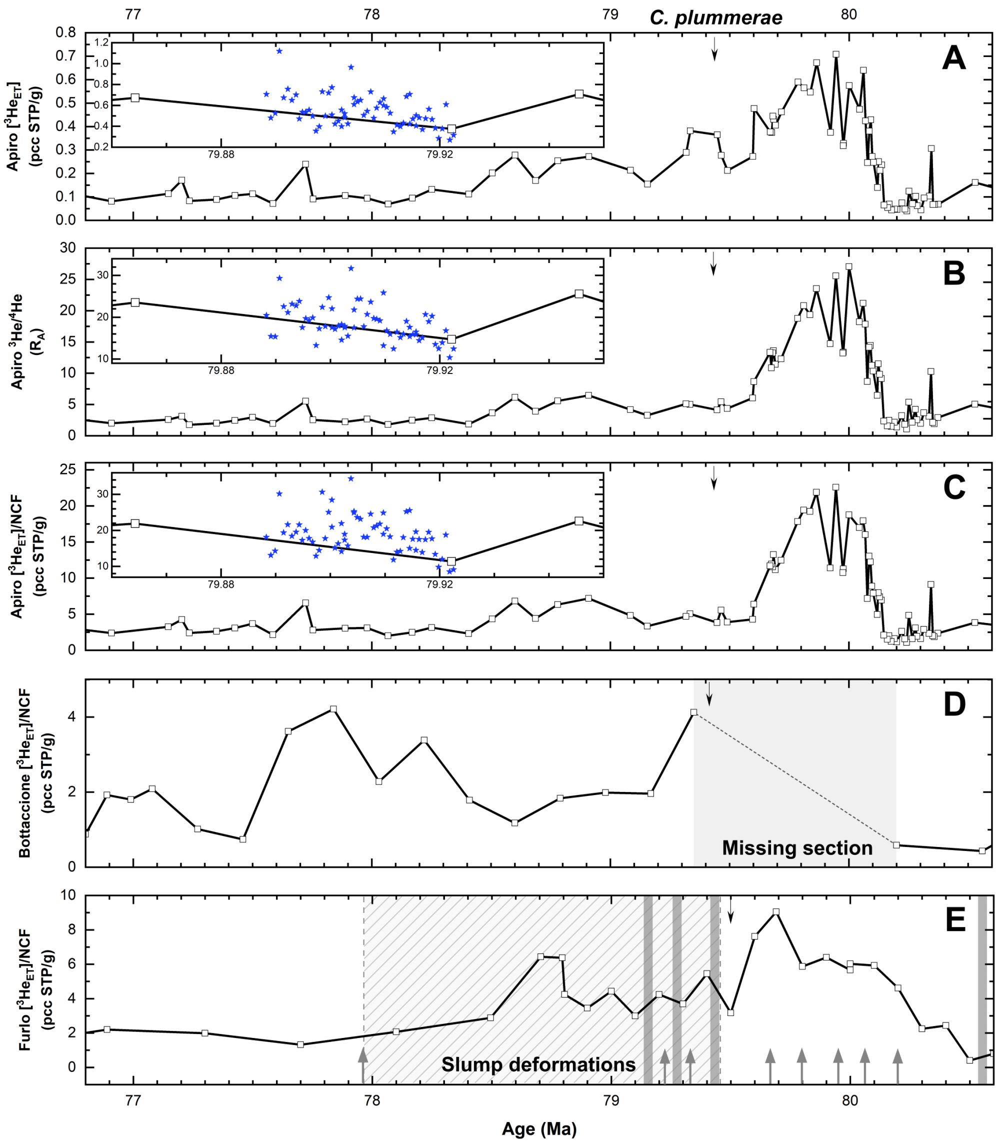

Figure 2.5: Temporal record of K1 in (A)–(C) Apiro (this study), (D) Bottaccione Gorge (Farley et al., 2012), and (E) Furlo (Montanari et al., 2023). Average of each sample is plotted as squares. Black arrows pointing down indicate the first occurrence of *C. plummerae*. In (A), (B) and (C), squares are data from paleomagnetic core samples. In the insets, filled stars are individual measurements of each wafer sample. In (D), the dotted line connects two data points with potential missing section in-between the shaded area. The temporal difference between these two data points should not be taken as being accurate, since the true temporal difference between these two data points is unknown and can be as long as 1.6 Myr (Farley et al., 2012). In (E), grey arrows pointing up indicate occurrence of turbidites, dark grey bars indicate faults, and the striped region indicates the interval with slump deformations (Montanari et al., 2023)

.

generated for 2 samples (assuming they are adjacent in stratigraphic position), each with 2 replicates, to mimic the helium measurements in practice. The values are generated according to the mean and variance of the continuous core slice samples, *i.e.*, treating the ~40-kyr continuous record as one single sample. We note that this is likely overestimating the true statistical variance, as the continuous core samples do not all have the same [$^3He_{ET}$], $^3He/^4He$ or [$^3He_{ET}$]/NCF (Fig. 2.3). As a result, the Monte Carlo simulation provides an upper-limit estimate of the probability.

The number of cases generating at least the minimum peak-to-trough difference (Δ) in [$^3He_{ET}$], $^3He/^4He$ and [$^3He_{ET}$]/NCF within the peak of K1 are counted. Specifically, the observed minimum Δ([$^3He_{ET}$]) = 0.25 pcc/g, minimum Δ($^3He/^4He$) = 9 R_A, and minimum Δ([$^3He_{ET}$]/NCF) = 8 pcc/g. In n=10^6 simulations, the probability of randomly generating the minimum Δ is 9.5 % for [$^3He_{ET}$], 7.2 % for $^3He/^4He$, and 11 % for [$^3He_{ET}$]/NCF, indicating that the fluctuations in [$^3He_{ET}$], $^3He/^4He$ and [$^3He_{ET}$]/NCF during the peak of K1 are not strongly statistically significant (Fig. 2.6). In practice, $^3He/^4He$ measurements of continuous core slice samples agree within 16 %, while [$^3He_{ET}$] and [$^3He_{ET}$]/NCF measurements agree within 25 %. If these are taken as the reproducibility of helium measurements, and only simulations with replicates that agree within the reproducibility are counted, then the probability of the fluctuations being random decreases to 1.6 % for [$^3He_{ET}$], 0.6 % for $^3He/^4He$, and 2.1 % for [$^3He_{ET}$]/NCF. Invariance in the NCF and [^4He_T]/NCF profiles across this interval suggest that these local extrema are not likely due to varying sedimentation rates (Fig. 2.2), but instead reflect short term changes in the $^3He_{ET}$ flux.

The prolonged decay of K1 starts from the last maximum in [$^3He_{ET}$], $^3He/^4He$ and [$^3He_{ET}$]/NCF at 79.86 Ma and reaches the pre-event background at ~78.5 Ma. Despite their general similarity in temporal evolution, a brief deviation between [$^3He_{ET}$] on the one hand vs. $^3He/^4He$ and [$^3He_{ET}$]/NCF on the other is observed between 79.1 Ma and 79.6 Ma. While [$^3He_{ET}$] shows a continuous decline through this interval, $^3He/^4He$ and [$^3He_{ET}$]/NCF experience a step-function decrease at 79.6 Ma towards a ~0.6-Myr local minimum. This interval corresponds precisely with the period of enhanced NCF between 112 and 117 m (Fig. 2.2), which we attribute to a temporarily enhanced non-carbonate flux associated with regional seismic activities, without substantially changing the overall sedimentation rate. Such an interpretation is based on the observation of frequent turbidites at Furlo in this interval (Fig. 2.5), mobilized by earthquakes (Bice et al., 2007). Unlike Furlo, which is an intrabasinal

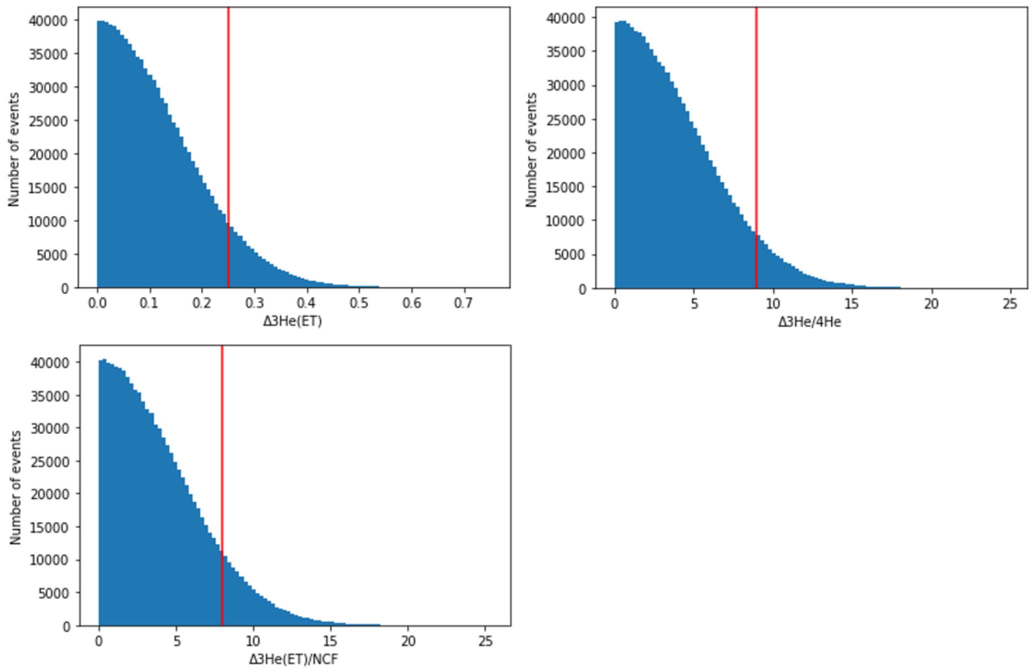

Figure 2.6: Results of the Monte Carlo simulations. [^{3}He$_{ET}$], ^{3}He/^{4}He and [^{3}He$_{ET}$]/NCF values are randomly generated for pairs of samples, each with two replicates, according to the mean and variance of the continuous core slice samples (Materials and Methods). Red solid lines show the values of the smallest peak-to-trough difference (Δ) in [^{3}He$_{ET}$], ^{3}He/^{4}He and [^{3}He$_{ET}$]/NCF during the peak of K1. There are a total of n = 10^6 simulations in each panel.

depocenters formed by local subsidence from faulting (Montanari et al., 1989; Tognaccini et al., 2019), Bottaccione Gorge and Apiro are from pelagic basins surrounding these subsided depocenters and mostly free of turbidites (Farley et al., 2012; Mitchell et al., 2021; Montanari et al., 2023). Nevertheless, the disturbed R2m member of Scaglia Rossa limestone at Bottacione (Farley et al., 2012) and the associated loss of section corresponding to the peak of the K1 event (Fig. 2.5) suggest that the seismic activities could have affected Bottaccione Gorge (and Apiro) in other forms.

The seismicity-mobilized turbidites in the vicinity of Apiro may have led to lateral transport and redeposition of reworked sediments, especially the fine-grained fraction that makes up most of the non-carbonate and carries most of the ^{4}He$_T$ and ^{3}He$_{ET}$. Redeposition of older (pre K1) fine grained sediments could lead to an increase in NCF by a factor of 2–3, but a decrease in [^{3}He$_{ET}$]/NCF and ^{3}He/^{4}He. The effect on [^{3}He$_{ET}$] would be less noticeable, because the change in the total sedimentation rate (carbonate + non-carbonate) is small. This pattern is exactly what we observe in the 112 to 117 m interval, supporting our interpretations. Other records of K1 from outside of the Umbria Marche basin could be studied to verify this hypothesis. In such a scenario the best indicator of the $^3He_{ET}$ flux is provided by [$^3He_{ET}$], which describes a slow steady decline over 1.5 Ma from the peak at 79.86 Ma (Fig. 2.5).

2.5 Comparison with Cenozoic ^{3}He Events

The temporal profile of K1 is similar to those of the two Cenozoic $^3He_{ET}$ events, and thus it is worth calculating the apparent $^3He_{ET}$ flux (f_{He}^{app}) during these three events for comparison. f_{He}^{app} is defined as the product of the true $^3He_{ET}$ flux f_{He} and the helium retentivity parameter$R$, which in return equals to [$^3He_{ET}$]$\cdot\alpha$ where α is the mass accumulation rate (Farley, 1995). R ranges between 0 (all helium lost) and 1 (all helium retained), and can be reasonably assumed to be invariant within the timespan of a few million years and in sedimentary rocks with similar post-deposition conditions (Peucker-Ehrenbrink et al., 2001). With this assumption, f_{He}^{app} can be used to track changes in f_{He} despite the difficulty in constraining the true values of f_{He} and R. For each sample, α is calculated as the product of the instantaneous sedimentation rate (Fig. 2.4) and the average density of 2.1 g/cm^3 of the core samples.

For convenience in comparing K1 with the Cenozoic $^3He_{ET}$ events (Farley et al., 1998; Farley et al., 2006), time relative to the peak (defined as time = 0) is shown on the abscissa instead of absolute age in Fig. 2.7. It is difficult to define the exact position of the peak of K1 because of multiple local maxima, and we arbitrarily select the first local maximum as time = 0. All three events have asymmetrical f_{He}^{app} evolution records, characterized by a rapid onset to the peak and a more gradual decay over a period of 1.5 Myr to 2 Myr. These temporal patterns are attributed to prolonged production of excess cosmic dust in the Solar system, with a short-term build-up and a long-term decay (Farley et al., 1998; Farley et al., 2006).

On the other hand, the details of the f_{He}^{app} records vary, such as the structure of the peak interval in the ^{3}He evolution records, and the rise times (Fig. 2.7). Among all three events, the Late Eocene $^3He_{ET}$ event has the longest rise time (~0.5 Myr), while the Late Miocene $^3He_{ET}$ event has the shortest (~0.03 Myr). K1 has an intermediate rise time of ~0.14 Myr when the first local maximum is chosen as time = 0 (Fig. 2.7), which can be as long as ~0.28 Myr when the last local maximum (79.86 Ma) is chosen instead. The origin of excess cosmic dust can potentially be

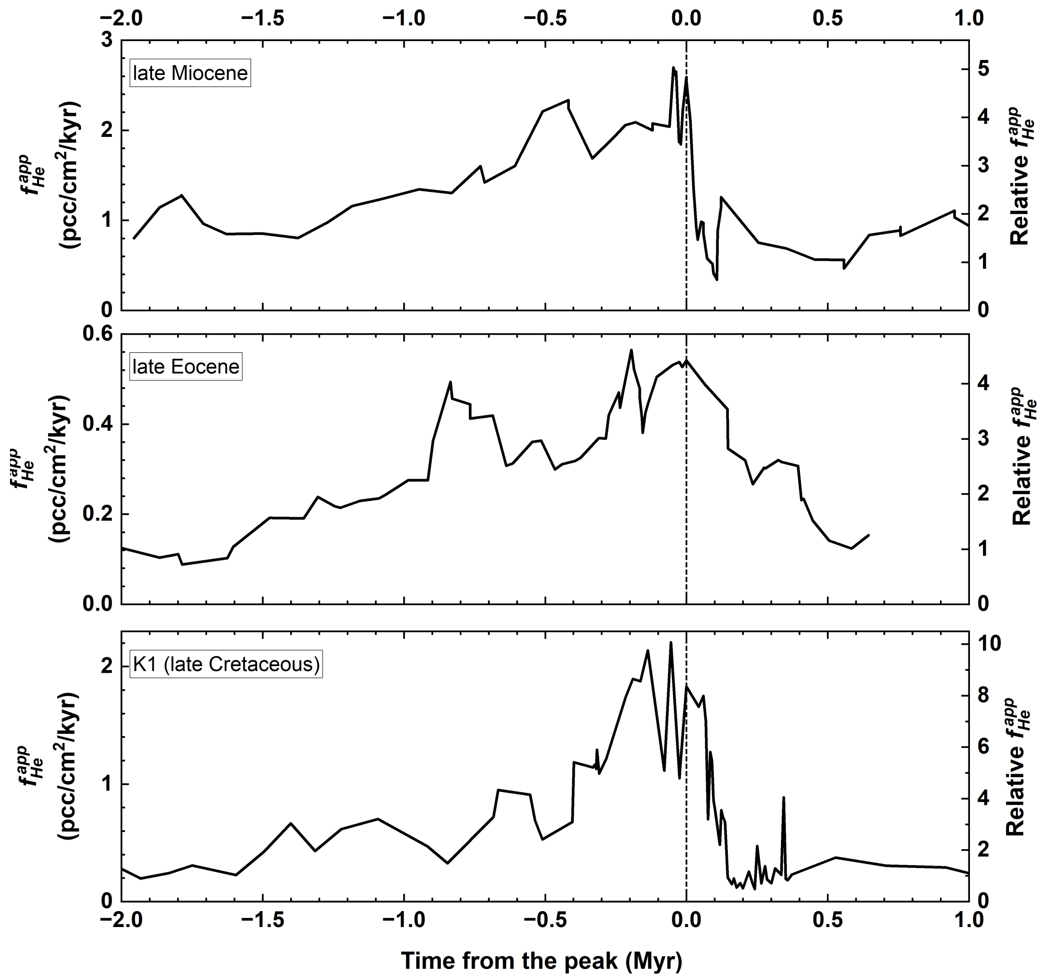

Figure 2.7: Apparent $^3He_{ET}$ fluxes calculated for the Late Miocene event, the Late Eocene event, and the Late Cretaceous K1 event. Relative flux is the computed $^3He_{ET}$ flux normalized to the pre-event background flux. All of these events are anchored together at their peak value, which is denoted by the vertical dashed line, for comparison of their shapes and durations.

established from the rise time of the event (Farley et al., 1998; Farley et al., 2006) as will be further discussed in the next section.

Comparing the magnitudes of the three events, the peak absolute f_{He}^{app} of K1 is ~2 pcc/cm^2/kyr, while the Late Miocene $^3He_{ET}$ event has an absolute f_{He}^{app} of 2.7 pcc/cm^2/kyr and the Late Eocene $^3He_{ET}$ event 0.56 pcc/cm^2/kyr (Fig. 2.7). However, absolute f_{He}^{app} must be interpreted with great care since the helium retentivity parameter R, despite being assumed to be constant for each event, could be different across these events. On the other hand, the maximum relative increase in f_{He}^{app} from background during the two Cenozoic ^{3}He enhancement events is ~5 fold, about half that of K1 (Fig. 2.7). Areas under the relative f_{He}^{app} curves give the total relative f_{He}^{app} through each event and show that during K1, Earth accreted ~2–3 times more $^3He_{ET}$ than during the two Cenozoic $^3He_{ET}$ events. K2 (86 Ma) and K3 (91 Ma) are also smaller than K1 using the same metric (Farley et al., 2012). If background f_{He} is constant for all events and that f_{He} scales with cosmic dust flux, K1 is undoubtedly the largest cosmic dust enhancement event in the last 100 Myr.

2.6 Origin of K1

Multiple lines of evidence could help us identify the source of excess cosmic dust during a $^3He_{ET}$ event, such as the temporal evolution of the ^{3}He flux (*e.g.*, Farley et al. 2012; Farley et al. 1998; Farley et al. 2006; Patterson et al. 1998a), reconstructed asteroid family formation ages (*e.g.*, Brož et al. 2013; Milani et al. 2017; Spoto et al. 2015), elemental/mineralogical/chemical tracers that point to specific extraterrestrial sources (*e.g.*, Boschi et al. 2017; Kyte et al. 2004; Schmitz 2013; Schmitz et al. 2015; Tagle et al. 2005), meteorite ages (Schmitz et al., 2019; Schmitz et al., 2003), associated terrestrial impacts (Schmieder et al., 2020), etc. Here, we attempt to identify the source of the excess cosmic dust during K1.

The temporal evolution of a $^3He_{ET}$ event reflects the dynamic evolution of excess cosmic dust in the size range ~2 µm and ~50 µm because the coarser is subject to substantial helium loss during atmospheric entry heating (Farley et al., 1997), while the finer will leave the Solar System on hyperbolic orbits due to the dominance of solar radiation pressure over other forces in this size range (Liou et al., 1995). Upon release from the parent body, orbits of cosmic dust between 2-50 µm will first expand due to radiation pressure compensating for part of gravity (Liou et al., 1995), then decay towards the sun on a timescale of 10^4-10^6 yr under the Poynting-Robertson effect (P-R effect; Burns et al. 1979). The time it takes for a cosmic dust particle to travel from its solar-radiation-modified orbit to the location of accretion is called the P-R time, or t_{PR}. During the dynamic evolution, cosmic dust is rapidly saturated by implanted solar wind helium (Raquin et al., 2009). As we will discuss below, these processes apply to both cosmic dust released in an asteroid collision and from comets, but with different outcomes (*e.g.*, Jackson et al. 1992; Heck et al. 2008).

Asteroid Collision

In an asteroid collision, excess cosmic dust ("asteroidal dust") of different sizes is produced during the initial collision and subsequent collisions between co-orbiting fragments. We applied a dust dynamics model to track t_{PR} of cosmic dust, from their orbit modified by solar radiation pressure to Earth's orbit at 1 AU.

Upon release from its parent body, the new semimajor axis (α_{new}) and eccentricity (e_{new}) of a cosmic dust particle under solar radiation pressure are given by (Liou et al., 1995):

$$\begin{cases} \alpha_{\text{new}} = \alpha_{\text{pb}} \left(\dfrac{1-\beta}{1-2\alpha_{\text{pb}}\beta/r_{\text{in}}} \right) \\ e_{\text{new}} = \left(1 - \dfrac{\left(1-\frac{2\alpha_{\text{pb}}\beta}{r_{\text{in}}}\right)(1-e_{\text{pb}}^2)}{(1-\beta)^2} \right)^{0.5} \end{cases} \tag{2.1}$$

where α_{pb} (in AU, astronomical unit) and e_{pb} are the semimajor axis and eccentricity of the parent body, r_{in} (in AU) is the heliocentric distance at which the cosmic dust leaves the parent body, which varies between the perihelion distance and the aphelion distance. β is the ratio of radiation pressure to solar gravity and can be approximated for cosmic dust larger than ~1 µm in diameter by (Grün et al., 2012):

$$\beta = \frac{1150}{\rho D} \tag{2.2}$$

where ρ is cosmic dust density in kg/m^3 and D is particle diameter in µm. From the new orbit, cosmic dust then decays towards the sun under the Poynting-Robertson effect (Burns et al., 1979):

$$\begin{cases} \dfrac{d\alpha}{dt} = -6.24 \times 10^{-4} \cdot \dfrac{\beta}{\alpha} \dfrac{(2+3e^2)}{(1-e^2)^{1.5}} \\ \dfrac{de}{dt} = -2.5 \times 6.24 \times 10^{-4} \cdot \dfrac{\beta}{\alpha^2} \dfrac{e}{(1-e^2)^{0.5}} \end{cases} \tag{2.3}$$

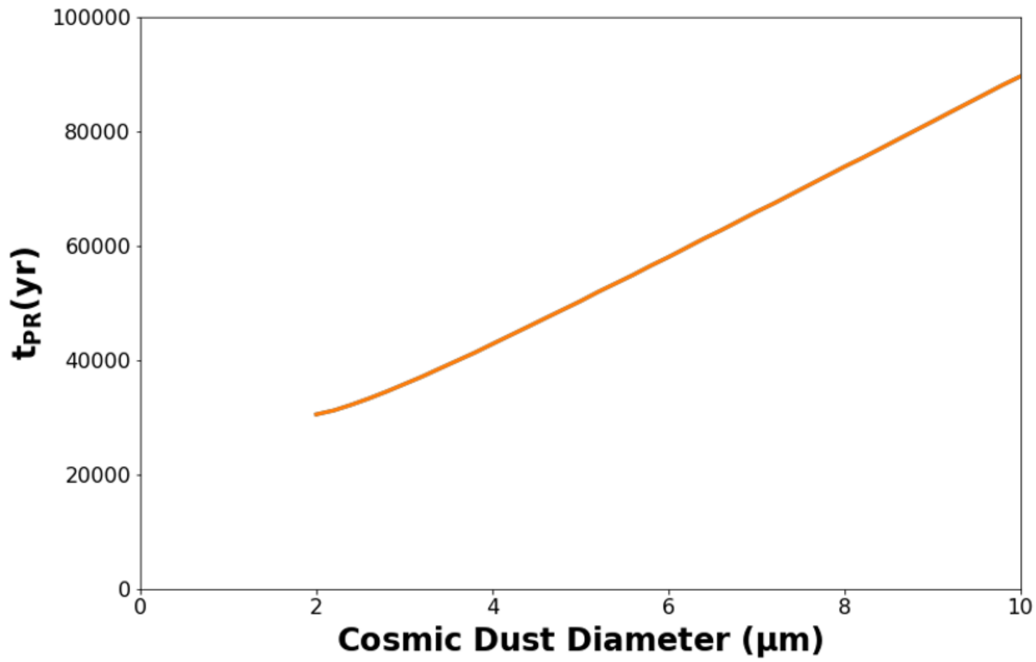

Figure 2.8: P-R time (t_{PR}) of cosmic dust particles travelling from 3.2 AU to 1 AU, assuming initially circular orbits and a density of 2500 kg/m^3. Cosmic dust particles below the cutoff diameter of 2 µm are β-meteoroids with hyperbolic orbits, so they are omitted in this calculation.

where t is in years, α is the semimajor axis of the cosmic dust orbit at each time step in AU, and e is the eccentricity of the cosmic dust orbit at each step. Eqn. (1)–(3) are valid for cosmic dust particles larger than ~1 µm (Grün et al., 2012). For each cosmic dust, with a given density and diameter, its orbital decay under the Poynting-Robertson effect is numerically tracked with these equations at time step dt = 100 yr until α reaches 1 AU. Each cosmic dust is released at both the perihelion and the aphelion to yield the range of possible outcomes.

Our model shows that, in each collision, smaller dust particles almost always arrive earlier than larger ones, if they are of the same density (Fig. 2.8). The rise time (Δt_{PR}; Materials and Methods) of a $^3He_{ET}$ event could thus reflect the difference in t_{PR} between the smaller asteroidal dust particles that arrive earliest at 1 AU and the larger, more slowly migrating particles that carry most $^3He_{ET}$ to Earth's surface, assuming no contamination from secondary collisions (see discussions below).

Using the rise times of known $^3He_{ET}$ events tied to asteroid collisions, plus the physical and orbital properties of the associated asteroid families, our model constrains the density and size of asteroidal dust produced in asteroid collisions and allows us to evaluate the likelihood of K1 being of asteroid origin.

Both the Late Miocene $^3He_{ET}$ event and the Mid-Ordovician $^3He_{ET}$ event have been strongly tied to asteroid collisions: The former is linked to the formation of asteroid family 609 Veritas at 3.17 AU and has a well-constrained rise time of 30 kyr (Farley et al., 2006); while the latter is linked to the breakup of the L-chondrite parent body (Schmitz et al., 2019) that was recently associated with asteroid family 404 Massalia at 2.41 AU (Marsset et al., 2024), but with a loosely constrained rise time of 25–60 kyr depending on the age model (Liao et al., 2020). Veritas is a Ch-type asteroid has a well-established connection with CM chondrites (DeMeo et al., 2022). If asteroidal dust produced in the 609 Veritas formation is of a CM chondrite bulk density (1880–2470 kg/m^3; Consolmagno et al. 2008; Macke et al. 2011), Δt_{PR} of the Late Miocene $^3He_{ET}$ event is constrained by the first arrival of dust of 2.3–2.9 µm and the last arrival of dust of 6.3–8.6 µm that carries the most ^{3}He. Similarly, adopting an L-chondrite bulk density of (3200–3520 kg/m^3; Consolmagno et al. 2008), Δt_{PR} of the Mid-Ordovician $^3He_{ET}$ event is defined by the first arrival of 2.0-µm dust and the last arrival of dust of 6.3–13.8 µm, depending on the age model (Schmitz et al., 2019). The consistency between these two size constraints despite the location and taxonomy of the parent body asteroids indicates that there could be a common size distribution of ^{3}He-carrying dust produced in asteroid collisions that is not sensitive to density. These results are also consistent with an independent model of helium loss during atmospheric entry, which indicates that delivery of the most surface-area correlated ^{3}He occurs for dust particles of ~7 µm for the size, velocity, and angular distribution of cosmic dust currently accreting to Earth (Farley et al., 1997).

Applying the same model to the hypothetical main-belt asteroid parent body (semi-major axis α_{pb} = 2.2–3.5 AU) that is disrupted to create K1 with the observed rise time (Δt_{PR} = 0.14–0.28 Myr), the diameter-density (D-ρ) combinations of asteroidal dust carrying the most ^{3}He must fall in the region bounded by the "max α_{pb} = 3.5 AU, min Δt_{PR} = 0.14 Myr" line and the "min α_{pb} = 2.2 AU, max Δt_{PR} = 0.28 Myr" line (Fig. 2.9). If the size distribution constrained above (D = 6.3–13.8 µm) also applies to the asteroidal dust associated with K1, D-ρ must fall within the wedged area that satisfies all three constraints (Fig. 2.9). This sets a minimum dust density of ~3100 kg/m^3, which means only asteroid parent bodies of high-density carbonaceous chondrites, ordinary chondrites, and iron meteorites can potentially be the source of excess asteroidal dust during K1 (Fig. 2.9).

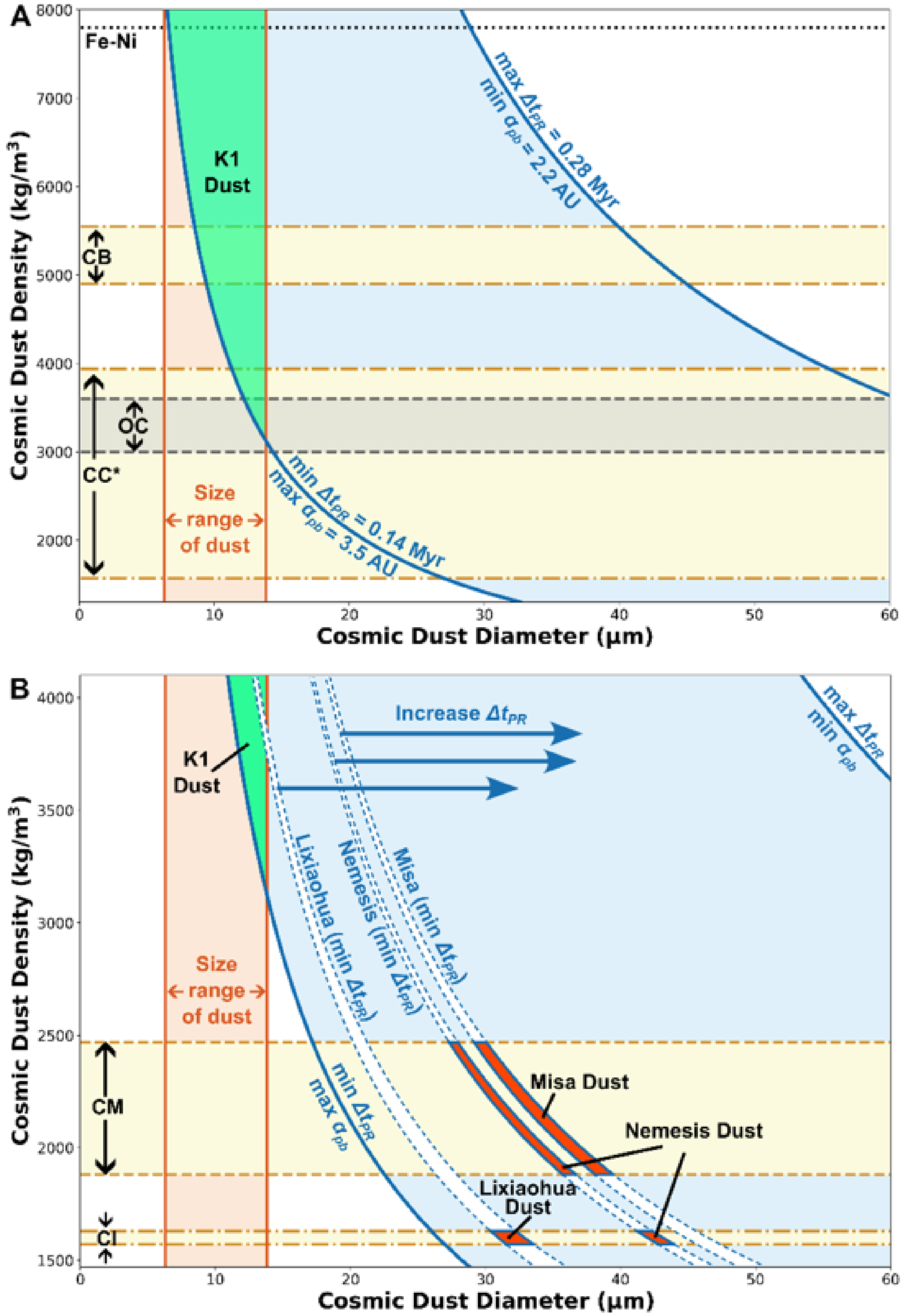

A
Fe-Ni
K1 Dust
max Δt_PR = 0.28 Myr
min α_pb = 2.2 AU
CB
OC
CC*
Size range of dust
min Δt_PR = 0.14 Myr
max α_pb = 3.5 AU
Cosmic Dust Density (kg/m³)
Cosmic Dust Diameter (µm)
B
Increase Δt_PR
max Δt_PR
min α_pb
K1 Dust
Lixiaohua (min Δt_PR)
Nemesis (min Δt_PR)
Misa (min Δt_PR)
Size range of dust
CM
min Δt_PR
max α_pb
Misa Dust
Nemesis Dust
Lixiaohua Dust
CI
Cosmic Dust Density (kg/m³)
Cosmic Dust Diameter (µm)

Figure 2.9: Diameter-Density (D-ρ) relationship of cosmic dust carrying the most $^3He_{ET}$ released from an asteroid collision. (A) The vertical bar bounded by orange solid lines correspond to the diameter constraint of cosmic dust (D = 6.2–13.8 μm) from the Late Miocene $^3He_{ET}$ event and the Mid-Ordovician $^3He_{ET}$ event. The blue region bounded by the "max α_{pb} = 3.5 AU/min Δt_{PR} = 0.14 Myr" and "max α_{pb} = 2.2 AU/min Δt_{PR} = 0.28 Myr" covers all the possible cosmic dust D-ρ combinations that can meet the parent body location constraint (α_{pb} = 2.2–3.5 AU) and the K1 rise time constraint (Δt_{PR} =0.14–0.28 Myr). The green wedged area labeled "K1 dust" corresponds to the cosmic dust that can fulfill all three constraints. Typical ranges of density of meteorites are labeled as horizontal bars. OC: Ordinary chondrites. CC*: Carbonaceous chondrites excluding CB chondrites. CB: CB chondrites. Fe-Ni: Fe-Ni alloys that corresponds to iron meteorites. (B) The narrow zones within each pair of dashed blues curves correspond to the D-ρ combinations of cosmic dust released from the asteroid families potentially associated with K1 (504 Nemesis, 510 Misa and 613 Lixiaohua), given their orbital parameters and min Δt_{PR} = 0.14 Myr. The red areas correspond to the most likely cosmic dust D-ρ combinations based on the density of meteorites (Macke et al., 2011) that potentially originated from these asteroid families, none of which overlaps with the green wedged area. Increasing Δt_{PR} will shift the zones and red areas further to the right. CM: CM chondrites. CI: CI chondrites.

However, when we narrow down the list of asteroid families potentially supplying the excess asteroidal dust during K1 by age and estimated size of disrupted parent body, we don't found any that can meet all three constraints. As discussed above, the K1-associated asteroid collision accreted to Earth at least twice as much dust as the 609 Veritas formation event (Fig. 2.7). If the amount of accreted cosmic dust scales with parent body size, the hypothetical K1 parent body would have a diameter at least 1.25 times greater than that of 609 Veritas (~112 km; Michel et al. 2011), or ~140 km. Of all the known main-belt asteroid families with ages potentially overlapping with K1, 504 Nemesis (150 ± 80 Ma; Carruba et al. 2019), 510 Misa (320 ± 260 Ma; Spoto et al. 2015), and 613 Lixiaohua (150 ± 50 Ma; Brož et al. 2013) are the only ones with parent bodies that are potentially large enough (Brož et al., 2013). Asteroid Misa as a Cg-type asteroid (Bus, 2002) is linked to CM chondrites (Kwon et al., 2022) with an average bulk density of 1880–2470 kg/m^3, while asteroid Lixiaohua (T-tpe; De Prá et al. 2020) is associated with CI chondrites (DeMeo et al., 2022) with an average bulk density of 1570–1630 kg/m^3

(Consolmagno et al., 2008), and asteroid Nemesis (C-type; Bus 2002) is tied to either CI or CM chondrites (Amano et al., 2023; DeMeo et al., 2022). These densities are certainly too low to qualify these asteroid families as potential sources of excess asteroidal dust during K1 (Fig. 2.9). Unless these asteroid families could produce dust substantially heavier (> 3800 kg/m^3; Fig. 2.9) than their meteorite resemblance, our model results strongly disfavor an asteroidal origin of K1.

Nevertheless, within this hypothesis, the multiple maxima during the peak of K1 may be explained by disruptions of large asteroid fragments following the first collision. This could be a general process in asteroid collisions. The Late Miocene ^{3}He event also appears to have a double maximum (Fig. 2.7), although its statistical significance has not been determined. The prolonged decay of K1 also requires continuous production of excess asteroidal dust, potentially from subsequent collisions and comminution of asteroid fragments. We note that secondary collisions are not considered in our model, which we think is a reasonable assumption for the size range of cosmic dust (< 50 µm) and the stage of the event we apply it to. Models show that cosmic dust particles smaller than ~500 µm have collisional lifetime longer than their t_{PR} (Wyatt et al., 1999), which means these dust particles will most likely survive their orbital decay without experiencing any secondary collision. Direct observation of the zodiacal cloud also shows that the size distribution of cosmic dust accreted by Earth peaks at ~200 µm (Love et al., 1993), likely a result of the practical threshold size above which the larger fragments are broken up through collisions during their transport to Earth.

Comet Shower

Comets release dust when they are close enough to the sun to sustain sublimation of volatiles, thus being a plausible source of excess cosmic dust during a $^3He_{ET}$ event. However, it is unlikely that a single comet can be the cause of K1, since even long-period comets have a lifetime of only ~600 kyr (Weissman, 1990). Such a lifetime is too short to explain the ~2 Myr duration of K1. On the other hand, perturbation of the Oort Cloud by a passing star can send a large number of Oort Cloud objects into the inner Solar System and result in a dust-producing comet shower lasting a few Myr (*e.g.*, Dybczyński 2005; Heisler et al. 1987; Hut et al. 1987). Such comet showers happen every 10^7–10^8 years depending on their magnitude (Heisler et al., 1987; Hut et al., 1987).

Micron-sized cosmic dust released by active comets ("cometary dust") is, like

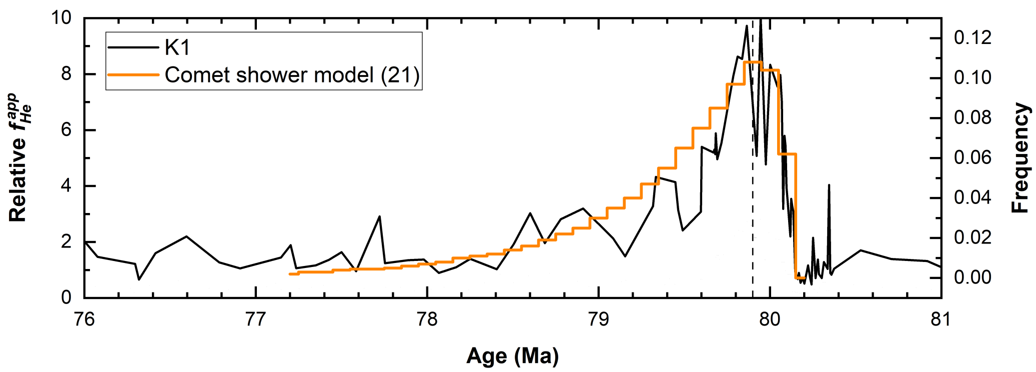

Figure 2.10: Comparing the comet perihelion passage model (orange; Hut et al. 1987) with relative f_{He}^{app} during K1 (black). The black dashed line shows the C33r-C33n geomagnetic reversal boundary.

asteroidal dust, subject to solar radiation and P-R effect (Jackson et al., 1992). But unlike in an asteroid collision, comets remain active in dust-production throughout their journey in the Solar System until they break up, escape the Solar System, or their volatiles are completely depleted. Thus, cometary dust arriving on Earth is not expected to be size sorted with time. Earth's accretion record of cometary dust (and in turn, of $^3He_{ET}$) during a comet shower should instead follow the evolution of active comets in the Solar System, with more dust produced when there are more active comets (Farley et al., 1998).

Models show that after a passing star perturbs the Oort Cloud, the frequency of perihelion passages of comets and the number of active comets build up to maximum in ~0.2-1 Myr and gradually decays in the next ~2-4 Myr (*e.g.*, Dybczyński 2005; Hut et al. 1987). When compared with K1, the modeled evolution of frequency of perihelion passages of comets agrees very well with the Apiro ^{3}He record in shape and duration (Fig. 2.10). The independency between model results and observed ^{3}He record thus strongly supports a comet shower origin for K1. It also motivates the search for another ^{3}He record of K1 beyond the Umbria-Marche basin to further evaluate the decay period of K1, which is potentially complicated by the regional tectonic activities described above. The multiple maxima during the peak of K1 is not directly predicted by the model, but they could result from short-term fluctuations in the enhanced comet population in the inner Solar System during the comet shower or possibly individual comets shedding dust to orbits especially favorable for Earth's capture.

The observation of K1 is also compatible with independently estimated recurrence rates of comet showers. Although the proportion of cometary dust in the zodiacal cloud is still debated (*e.g.*, Kortenkamp et al. 1998; Nesvorný et al. 2010), we can conservatively estimate the maximum cometary dust abundance to have increased by at least an order of magnitude during K1, since maximum $^3He_{ET}$ is ~10 times above the background (Fig. 2.5). If cometary dust production scales with the number of active comets, it requires the putative comet shower associated with K1 to enhance the comet population in the Solar System by 10 fold. It has been estimated that every ~100 Myr, a close passing star can trigger a strong comet shower with a maximum shower intensity more than 10 times that of the background (Heisler et al., 1987), consistent with the observation of only one event in the last 100 Myr with the magnitude of K1.

Terrestrial impact probability scales with the number of active comets in the inner Solar System in a comet shower (Nurmi et al., 2001), which implies the simultaneous arrival of most excess cometary dust particles and impactors. A critical argument in favor of a comet shower origin for the Late Eocene $^3He_{ET}$ event is the occurrence of two well-dated terrestrial impact craters within the peak of the event (Farley et al., 1998). If cosmic dust production correlates with the number of active comets, we might expect there to be around twice this number of impacts during K1 (Fig. 2.7). Instead, there is only one small impact structure, Zeleny Gai (3.5 km), dated with high uncertainty (± 20 Ma) to occur within the span of K1 (Schmieder et al., 2020). From Poisson statistics the likelihood of having one impact when 4 are expected is about 7 %. Given that 80 Ma impact craters are harder to detect in the geologic record than 36 Ma impact craters, this probability does not strongly argue against a comet shower origin for K1. Our alternative approach for detecting a large impact found no Cr, Co, or Ni peak in the 20 kyr studied interval. This observation argues against an impactor larger than ~5 km in diameter (Fig. 2.3) in this short interval, assuming a chondritic composition of the impactor (Tagle et al., 2008).

In summary, the Apiro ^3He record of K1 and the independent model of comet showers agree well with each other, and the observed frequency of K1-scale cosmic dust enhancement events is consistent with estimated recurrence rate of K1-scale comet showers, favoring a cometary origin of K1. On the other hand, our asteroid dust dynamics model shows that K1 is unlikely to originate from a main-belt asteroid collision unless very special conditions are met. We thus tentatively conclude that the largest comet shower in the last 100 Myr is the dust source of K1. Studies on impact tracers like tektites, impact spherules, and highly siderophile elements

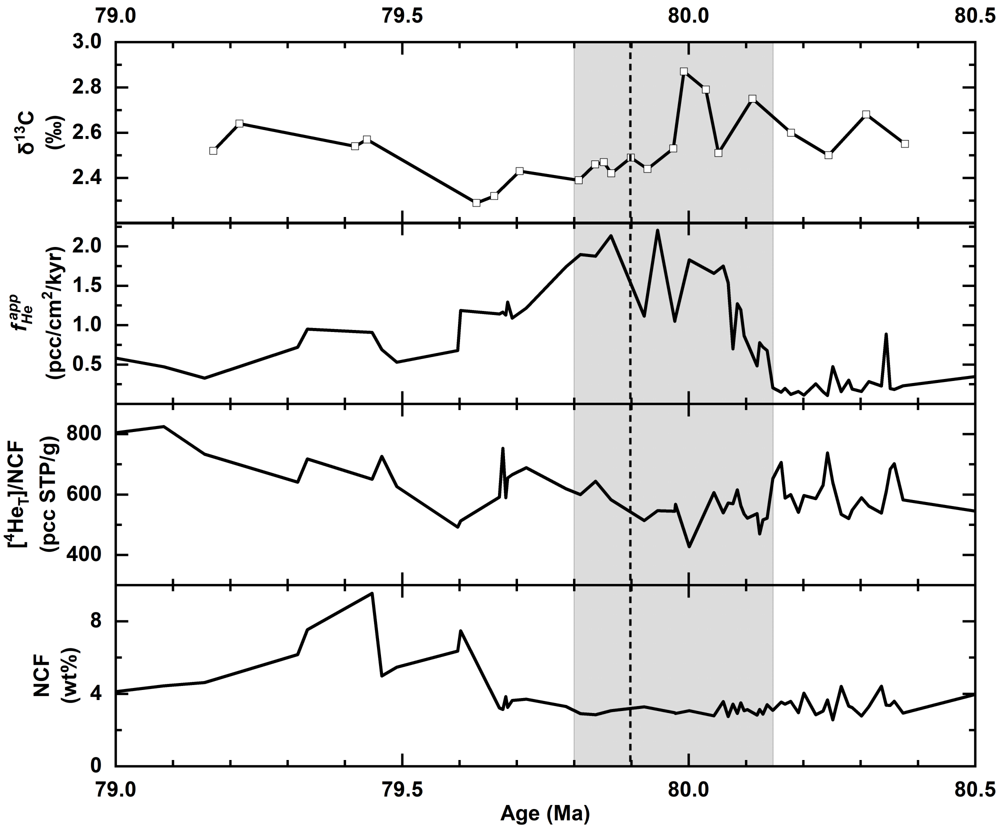

Figure 2.11: Temporal relationship among K1, C33r-C33n geomagnetic reversal, and ECE. Dashed line: C33r-C33n geomagnetic reversal. Shaded area: ECE (Montanari et al., 2023).

could contribute to the evaluation of both the existence of impact events and our conclusion.

2.7 K1, C33r-C33n, and ECE

The Apiro record confirms that the C33r-C33n geomagnetic reversal coincides with the peak of K1 (Fig. 2.2), as does the negative carbon isotope excursion that defines the early Campanian event (ECE) (Fig. 2.11; Montanari et al. 2023; Sabatino et al. 2018). In this section, we first show that their co-occurrence is not statistically favored, then discuss potential relationships among these three events.

The probability of at least one geomagnetic reversal happening within the 0.14-Myr interval of maximum $^{3}He_{ET}$ concentration in K1, *i.e.*, between the first local maximum and the third local maximum (Fig. 2.11), can be estimated with Poisson probability:

$$
\begin{aligned}
P &= \sum_{k=1}^{\infty} \frac{(r \cdot t)^k}{k!} \cdot e^{-(r \cdot t)} \\
&= 1 - P(k = 0) \\
&= 1 - \frac{(r \cdot t)^0}{0!} \cdot e^{-(r \cdot t)}
\end{aligned}
$$

In this case, k is the expected number of geomagnetic reversals in $t = 0.14$ Myr, and r is the recurrence rate of geomagnetic reversals determined within a time window. Here, the calculated probability depends on the selected time window since r is variable with time (Ogg, 2020), and especially depends on whether or not the Cretaceous Normal Superchron (CNS) is included in the window (Fig. 2.12). In the first case, with CNS included, the probability first increases with width of time window before it plateaus at ~6 % out to 80 Myr, then continues to increase towards 25 %. In the second case, the calculated probability shows a similar trend except that it plateaus at ~11 % out to 50 Ma. The plateau in each scenario indicates the range of suitable time window width for assessing the probability, within which the recurrence rate of geomagnetic reversal is not changing significantly. The probability of randomly generating at least one geomagnetic reversal within the peak of K1 is thus ~6 % (CNS included) to ~11 % (CNS excluded) (Fig. 2.12).

Similarly, we can estimate the probability of having at least one carbon isotope excursion like the ECE within $t = 0.14$ Myr, assuming such excursions happen with random intervals. There are 5 identified carbon isotope excursion events that are similar in magnitude to ECE within the Campanian (t~11.4 Myr; Sabatino et al. 2018), which gives a recurrence rate r of ~0.4 Myr^{-1} and a probability of ~6 %. Thus, a geomagnetic reversal or an ECE-like event at the peak of K1 are both statistically unlikely, but not enormously so. The probability of both a geomagnetic reversal and a carbon isotope excursion within the ~0.14-Myr peak of K1 is only ~0.3 % to ~0.7 % if all three are statistically independent.

If these events are correlated, what could be the mechanism? The terrestrial magnetosphere can only shield Earth from cosmic dust particles smaller than ~0.1 µm (Juhász et al., 2001) so the weakening of Earth's magnetic field prior to and during a geomagnetic reversal will not affect the flux of ^{3}He-carrying cosmic dust (> ~2 µm) into Earth's atmosphere. The flat NCF profile across the onset and peak of K1 (Fig. 2.11) also indicates that ECE is not associated with a noticeable change in the sedimentation environment that could have affected the delivery of cosmic dust

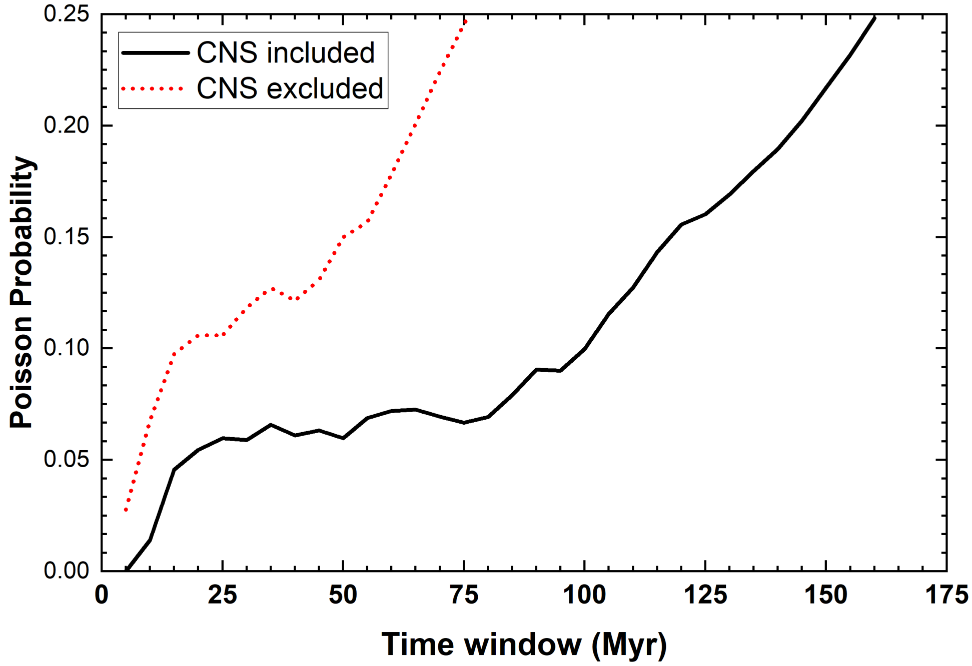

Figure 2.12: Poisson Probability of at least one geomagnetic reversal happening within the peak of K1. The x-axis is the width of time window over which the recurrence rate of geomagnetic reversals is calculated. Black solid lines are calculated based on symmetric time windows across C33r-C33n at 79.90 Ma, with Cretaceous Long Superchron (CNS) included. Red dotted lines are calculated with time windows fixed on the older boundary at C33n-C34r at 82.875 Ma, excluding CNS.

particles to the seafloor. Thus, it is implausible that the production and accretion of cosmic dust is controlled by the C33r-C33n geomagnetic reversal or ECE in the Earth system.

Alternatively, the accretion of excess extraterrestrial material can potentially induce either a prolonged cooling via radiative effects of cosmic dust in the atmosphere (*e.g.*, Schmitz et al. 2019) or a transient "impact winter" via a massive impactor (*e.g.*, Vellekoop et al. 2014). Furthermore, it has been proposed that if such a sudden climatic change could result in a rapid ice cap growth and global sea level fall, it could potentially trigger a geomagnetic excursion or reversal within 10^3–10^4 yr of the climatic event (*i.e.*, the Muller-Morris model; Muller et al. 1986).

Is the co-occurrence among these events compatible with the Muller-Morris model? Maximum angular deviation (MAD) of remanent magnetic vectors starts to increase from ~20 cm below the geomagnetic reversal until it reaches a maximum of ~16° at the boundary, after which it decreases and stabilizes at ~3° (Fig. 2.2). MAD positively correlates with the stability of the remanent magnetic signal, which reflects the strengths of the paleo-geomagnetic field. Thus, the weakening of the geomagnetic field has started ~13 kyr prior to the geomagnetic reversal at 79.90 Ma, which is compatible with the response time of the geodynamo to the transient ice age in the Muller-Morris model. However, the ECE negative carbon isotope excursion starts at ~80 Ma, which predates C33r-C33n by ~10^5 yr (Fig. 2.11). $^3He/^4He$, [$^3He_{ET}$], and [$^3He_{ET}$]/NCF in the wafer samples between 108.10 m and 108.46 m (*i.e.*, below and older than C33r-C33n geomagnetic reversal) are relatively constant with relative standard deviations under 35 ‰, not suggestive of any substantial change in cosmic dust flux that could have induced a transient climate change in the 10^3–10^4 yr interval before the C33r-C33n boundary (Fig. 2.2). [^4He_T]/NCF and NCF also do not correlate with the carbon isotope excursion during the ECE (Fig. 2.11), indicating no change in sedimentation conditions. Furthermore, the Muller-Morris model requires a large impactor to induce the climate change. Zeleny Gai is the only impact crater dated to within the range of K1 (Schmieder et al., 2020), but it might be too small to trigger a geomagnetic reversal since much larger impact craters like Chicxulub (~200 km) are not associated with any geomagnetic reversal (Gradstein, 2020). Our trace metal analyses also rule out the existence of achondritic impactor > ~5 km in diameter within ~0.02 Myr prior to C33r-C33n (Fig. 2.2).

Alternatively, if the actual response time of the geodynamo to the climatic change were on the order of 10^5 yr rather than 10^3–10^4, one could posit that the ECE caused the reversal, and the ECE was caused by the cosmic dust flux enhancement. This possibility is consistent with the start of the negative carbon isotope excursion at ~80.0 Ma (Fig. 2.11). This also corresponds to the start of the peak of K1 when cosmic dust flux is the highest, which potentially has the most prominent climatic effect (Schmitz et al., 2019). Although a rigorous mechanism is unknown, this provides a coherent link among the three co-occurring events.

The geomagnetic field is fundamental to Earth's habitability, shielding the atmosphere from solar wind erosion and protecting life from cosmic radiation. Understanding the mechanisms and causes behind geomagnetic reversals is therefore crucial, especially given the temporary weakening of the geomagnetic field during such events (Valet et al., 2005) and the potential consequences for the biosphere. Potentially correlated with the ECE and the C33r-C33n geomagnetic reversal, K1 thus provides a compelling case for further investigation into the interactions among cosmic dust, Earth's climate, and the geodynamo.

References

Amano, Kana, Moe Matsuoka, Tomoki Nakamura, Eiichi Kagawa, Yuri Fujioka, Sandra M. Potin, Takahiro Hiroi, Eri Tatsumi, Ralph E. Milliken, Eric Quirico, Pierre Beck, Rosario Brunetto, Masayuki Uesugi, Yoshio Takahashi, Takahiro Kawai, Shohei Yamashita, Yuma Enokido, Taiga Wada, Yoshihiro Furukawa, Michael E. Zolensky, Driss Takir, Deborah L. Domingue, Camilo Jaramillo-Correa, Faith Vilas, Amanda R. Hendrix, Mizuha Kikuiri, Tomoyo Morita, Hisayoshi Yurimoto, Takaaki Noguchi, Ryuji Okazaki, Hikaru Yabuta, Hiroshi Naraoka, Kanako Sakamoto, Shogo Tachibana, Toru Yada, Masahiro Nishimura, Aiko Nakato, Akiko Miyazaki, Kasumi Yogata, Masanao Abe, Tatsuaki Okada, Tomohiro Usui, Makoto Yoshikawa, Takanao Saiki, Satoshi Tanaka, Fuyuto Terui, Satoru Nakazawa, Sei-ichiro Watanabe, and Yuichi Tsuda (2023). "Reassigning CI chondrite parent bodies based on reflectance spectroscopy of samples from carbonaceous asteroid Ryugu and meteorites". en. In: *Science Advances* 9.49, eadi3789. ISSN: 2375-2548. DOI: 10.1126/sciadv.adi3789.

Arthur, Michael A. and Alfred G. Fischer (1977). "Upper Cretaceous–Paleocene magnetic stratigraphy at Gubbio, Italy I. Lithostratigraphy and sedimentology". en. In: *Geological Society of America Bulletin* 88.3, p. 367. ISSN: 0016-7606. DOI: 10.1130/0016-7606(1977)88<367:UCMSAG>2.0.CO;2.

Bice, D. M., Alessandro Montanari, and G. Rusciadelli (2007). "Earthquake-induced turbidites triggered by sea level oscillations in the Upper Cretaceous and Paleocene of Italy". en. In: *Terra Nova* 19.6, pp. 387–392. ISSN: 0954-4879, 1365-3121. DOI: 10.1111/j.1365-3121.2007.00752.x.

Boschi, Samuele, Birger Schmitz, Philipp R. Heck, Anders Cronholm, Céline Defouilloy, Noriko T. Kita, Simonetta Monechi, Alessandro Montanari, Surya S. Rout, and Fredrik Terfelt (2017). "Late Eocene 3He and Ir anomalies associated with ordinary chondritic spinels". en. In: *Geochimica et Cosmochimica Acta* 204, pp. 205–218. ISSN: 00167037. DOI: 10.1016/j.gca.2017.01.028.

Brož, M., A. Morbidelli, W. F. Bottke, J. Rozehnal, D. Vokrouhlický, and D. Nesvorný (2013). "Constraining the cometary flux through the asteroid belt during the late heavy bombardment". In: *Astronomy & Astrophysics* 551, A117. ISSN: 0004-6361, 1432-0746. DOI: 10.1051/0004-6361/201219296.

Burnard, Pete (2013). *The noble gases as geochemical tracers*. eng. Advances in isotope geochemistry. Heidelberg New York: Springer. ISBN: 9783642288364.

Burns, Joseph A., Philippe L. Lamy, and Steven Soter (1979). "Radiation forces on small particles in the solar system". en. In: *Icarus* 40.1, pp. 1–48. ISSN: 00191035. DOI: 10.1016/0019-1035(79)90050-2.

Bus, S (2002). "Phase II of the Small Main-Belt Asteroid Spectroscopic Survey A Feature-Based Taxonomy". en. In: *Icarus* 158.1, pp. 146–177. ISSN: 00191035. DOI: 10.1006/icar.2002.6856.

Carruba, V. and W. Barletta (2019). "The influence of Ceres on the dynamical evolution of the Zdenekhorsky/Nemesis asteroid family". en. In: *Planetary and Space Science* 165, pp. 10–18. ISSN: 00320633. DOI: 10.1016/j.pss.2018.12.006.

Consolmagno, G.J., D.T. Britt, and R.J. Macke (2008). "The significance of meteorite density and porosity". en. In: *Geochemistry* 68.1, pp. 1–29. ISSN: 00092819. DOI: 10.1016/j.chemer.2008.01.003.

De Prá, M.N., J. Licandro, N. Pinilla-Alonso, V. Lorenzi, E. Rondón, J. Carvano, D. Morate, and J. De León (2020). "The spectroscopic properties of the Lixiaohua family, cradle of Main Belt Comets". en. In: *Icarus* 338, p. 113473. ISSN: 00191035. DOI: 10.1016/j.icarus.2019.113473.

DeMeo, Francesca E., Brian J. Burt, Michaël Marsset, David Polishook, Thomas H. Burbine, Benoît Carry, Richard P. Binzel, Pierre Vernazza, Vishnu Reddy, Michelle Tang, Cristina A. Thomas, Andrew S. Rivkin, Nicholas A. Moskovitz, Stephen M. Slivan, and Schelte J. Bus (2022). "Connecting asteroids and meteorites with visible and near-infrared spectroscopy". en. In: *Icarus* 380, p. 114971. ISSN: 00191035. DOI: 10.1016/j.icarus.2022.114971.

Dybczyński, P. A. (2005). "Simulating observable comets: II. Simultaneous stellar and galactic action". In: *Astronomy & Astrophysics* 441.2, pp. 783–790. ISSN: 0004-6361, 1432-0746. DOI: 10.1051/0004-6361:20053327.

Farley, Kenneth A. (1995). "Cenozoic variations in the flux of interplanetary dust recorded by3He in a deep-sea sediment". en. In: *Nature* 376.6536, pp. 153–156. ISSN: 0028-0836, 1476-4687. DOI: 10.1038/376153a0.

Farley, Kenneth A. and S. F. Eltgroth (2003). "An alternative age model for the Paleocene–Eocene thermal maximum using extraterrestrial 3He". en. In: *Earth and Planetary Science Letters* 208.3–4, pp. 135–148. ISSN: 0012821X. DOI: 10.1016/S0012-821X(03)00017-7.

Farley, Kenneth A., S. G. Love, and Desmond B. Patterson (1997). "Atmospheric entry heating and helium retentivity of interplanetary dust particles". en. In: *Geochimica et Cosmochimica Acta* 61.11, pp. 2309–2316. ISSN: 00167037. DOI: 10.1016/S0016-7037(97)00068-9.

Farley, Kenneth A., Alessandro Montanari, and Rodolfo Coccioni (2012). "A record of the extraterrestrial 3He flux through the Late Cretaceous". en. In: *Geochimica et Cosmochimica Acta* 84, pp. 314–328. ISSN: 00167037. DOI: 10.1016/j.gca.2012.01.015.

Farley, Kenneth A., Alessandro Montanari, E. M. Shoemaker, and C. S. Shoemaker (1998). "Geochemical Evidence for a Comet Shower in the Late Eocene". en. In: *Science* 280.5367, pp. 1250–1253. ISSN: 0036-8075, 1095-9203. DOI: 10.1126/science.280.5367.1250.

Farley, Kenneth A., David Vokrouhlický, William F. Bottke, and David Nesvorný (2006). "A late Miocene dust shower from the break-up of an asteroid in the main belt". en. In: *Nature* 439.7074, pp. 295–297. ISSN: 0028-0836, 1476-4687. DOI: 10.1038/nature04391.

Fritz, J., Roald Tagle, and N. Artemieva (2007). "Lunar helium-3 in marine sediments: Implications for a late Eocene asteroid shower". en. In: *Icarus* 189.2, pp. 591–594. ISSN: 00191035. DOI: 10.1016/j.icarus.2007.03.026.

Fu, Hanjing, Xing Jian, Wei Zhang, and Fei Shang (2020). "A comparative study of methods for determining carbonate content in marine and terrestrial sediments". en. In: *Marine and Petroleum Geology* 116, p. 104337. ISSN: 02648172. DOI: 10.1016/j.marpetgeo.2020.104337.

Glass, Billy P., Dennis V. Kent, David A. Schneider, and L. Tauxe (1991). "Ivory Coast microtektite strewn field: description and relation to the Jaramillo geomagnetic event". en. In: *Earth and Planetary Science Letters* 107.1, pp. 182–196. ISSN: 0012821X. DOI: 10.1016/0012-821X(91)90054-L.

Glass, Billy P., M. Swincki, and P. Zwart (1979). "Australasian, Ivory Coast and North American tektite strewnfields-Size, mass and correlation with geomagnetic reversals and other earth events." In.

Gradstein, Felix M. (2020). *Geologic Time Scale 2020*. eng. San Diego: Elsevier. ISBN: 9780128243619.

Grün, Eberhard, B. A. Gustafson, S. Dermott, and H. Fechtig (2012). *Interplanetary Dust*. Springer Science & Business Media.

Haack, Henning, Paolo Farinella, Edward R.D. Scott, and Klaus Keil (1996). "Meteoritic, Asteroidal, and Theoretical Constraints on the 500 Ma Disruption of theLChondrite Parent Body". en. In: *Icarus* 119.1, pp. 182–191. ISSN: 00191035. DOI: 10.1006/icar.1996.0010.

Heck, Philipp R., Birger Schmitz, Heinrich Baur, and Rainer Wieler (2008). "Noble Gases in Fossil Micrometeorites and Meteorites from 470 Myr Old Sediments from Southern Sweden, and New Evidence for the L-chondrite Parent Body Breakup Event". In: *Meteoritics & Planetary Science* 43.3, pp. 517–528. ISSN: 1945-5100. DOI: 10.1111/j.1945-5100.2008.tb00669.x.

Heisler, Julia, Scott Tremaine, and Charles Alcock (1987). "The frequency and intensity of comet showers from the Oort cloud". en. In: *Icarus* 70.2, pp. 269–288. ISSN: 00191035. DOI: 10.1016/0019-1035(87)90135-7.

Hut, Piet, Walter Alvarez, William P. Elder, Thor Hansen, Erle G. Kauffman, Gerta Keller, Eugene M. Shoemaker, and Paul R. Weissman (1987). "Comet showers as a cause of mass extinctions". en. In: *Nature* 329.6135, pp. 118–126. ISSN: 0028-0836, 1476-4687. DOI: 10.1038/329118a0.

Jackson, A. A. and Herbert A. Zook (1992). "Orbital evolution of dust particles from comets and asteroids". en. In: *Icarus* 97.1, pp. 70–84. ISSN: 00191035. DOI: 10.1016/0019-1035(92)90057-E.

Jones, Craig H. (2002). "User-driven integrated software lives: "Paleomag" paleomagnetics analysis on the Macintosh". en. In: *Computers & Geosciences* 28.10, pp. 1145–1151. ISSN: 00983004. DOI: 10.1016/S0098-3004(02)00032-8.

Juhász, Antal and Mihály Horányi (2001). "Magnetospheric Effects on the Cosmic Dust Input into the Earth's Atmosphere". en. In: *Accretion of Extraterrestrial Matter Throughout Earth's History*. Ed. by Bernhard Peucker-Ehrenbrink and Birger Schmitz. Boston, MA: Springer US, pp. 93–106. ISBN: 9781461346685. DOI: 10.1007/978-1-4419-8694-8_6.

Kirschvink, Joseph L. (1980). "The least-squares line and plane and the analysis of palaeomagnetic data". en. In: *Geophysical Journal International* 62.3, pp. 699–718. ISSN: 0956-540X, 1365-246X. DOI: 10.1111/j.1365-246X.1980.tb02601.x.

Kirschvink, Joseph L., Robert E. Kopp, Timothy D. Raub, Christopher T. Baumgartner, and John W. Holt (2008). "Rapid, precise, and high-sensitivity acquisition of paleomagnetic and rock-magnetic data: Development of a low-noise automatic sample changing system for superconducting rock magnetometers". en. In: *Geochemistry, Geophysics, Geosystems* 9.5, 2007GC001856. ISSN: 1525-2027, 1525-2027. DOI: 10.1029/2007GC001856.

Kortenkamp, Stephen J and Stanley F Dermott (1998). "Accretion of Interplanetary Dust Particles by the Earth". en. In: *Icarus* 135.2, pp. 469–495. ISSN: 00191035. DOI: 10.1006/icar.1998.5994.

Kwon, Yuna G., Sunao Hasegawa, Sonia Fornasier, Masateru Ishiguro, and Jessica Agarwal (2022). "Probing the surface environment of large T-type asteroids". In: 666, A173. ISSN: 0004-6361, 1432-0746. DOI: 10.1051/0004-6361/202243816.

Kyte, F., A. Shukolyukov, A. Hildebrand, G. Lugmair, and J. Hanova (2004). "Initial Cr-isotopic and iridium measurements of concentrates from late Eocene CPX-Spherule deposits". In.

Liao, ShiYong, Magdalena H. Huyskens, Qing-Zhu Yin, and Birger Schmitz (2020). "Absolute dating of the L-chondrite parent body breakup with high-precision U–Pb zircon geochronology from Ordovician limestone". en. In: *Earth and Planetary Science Letters* 547, p. 116442. ISSN: 0012821X. DOI: 10.1016/j.epsl.2020.116442.

Liou, Jer-Chyi and Herbert A. Zook (1995). “An Asteroidal Dust Ring of Micron-Sized Particles Trapped in the 1:1 Mean Motion Resonance with Jupiter”. en. In: *Icarus* 113.2, pp. 403–414. ISSN: 00191035. DOI: 10.1006/icar.1995.1030.

Love, S. G. and Donald E. Brownlee (1993). “A Direct Measurement of the Terrestrial Mass Accretion Rate of Cosmic Dust”. en. In: *Science* 262.5133, pp. 550–553. ISSN: 0036-8075, 1095-9203. DOI: 10.1126/science.262.5133.550.

Macke, Robert J., Guy J. Consolmagno, and Daniel T. Britt (2011). “Density, porosity, and magnetic susceptibility of carbonaceous chondrites”. en. In: 46, pp. 1842–1862. ISSN: 1086-9379, 1945-5100. DOI: 10.1111/j.1945-5100.2011.01298.x.

Marcantonio, Franco, Sean Higgins, Robert F. Anderson, Martin Stute, Peter Schlosser, and E.Troy Rasbury (1998). “Terrigenous helium in deep-sea sediments”. en. In: *Geochimica et Cosmochimica Acta* 62.9, pp. 1535–1543. ISSN: 00167037. DOI: 10.1016/S0016-7037(98)00091-X.

Marcantonio, Franco, Niraj Kumar, Martin Stute, Robert F. Anderson, Michele A. Seidl, Peter Schlosser, and Alan Mix (1995). “A comparative study of accumulation rates derived by He and Th isotope analysis of marine sediments”. en. In: *Earth and Planetary Science Letters* 133.3–4, pp. 549–555. ISSN: 0012821X. DOI: 10.1016/0012-821X(95)00079-R.

Marsset, M., P. Vernazza, M. Brož, C. A. Thomas, F. E. DeMeo, B. Burt, R. P. Binzel, V. Reddy, A. McGraw, C. Avdellidou, B. Carry, S. Slivan, and D. Polishook (2024). “The Massalia asteroid family as the origin of ordinary L chondrites”. en. In: *Nature* 634.8034, pp. 561–565. ISSN: 0028-0836, 1476-4687. DOI: 10.1038/s41586-024-08007-6.

Michel, Patrick, Martin Jutzi, Derek C. Richardson, and Willy Benz (2011). “The Asteroid Veritas: An intruder in a family named after it?” en. In: *Icarus* 211.1, pp. 535–545. ISSN: 00191035. DOI: 10.1016/j.icarus.2010.10.012.

Milani, Andrea, Zoran Knežević, Federica Spoto, Alberto Cellino, Bojan Novaković, and Georgios Tsirvoulis (2017). “On the ages of resonant, eroded and fossil asteroid families”. en. In: *Icarus* 288, pp. 240–264. ISSN: 00191035. DOI: 10.1016/j.icarus.2016.12.030.

Mitchell, Ross N., Christopher J. Thissen, David A. D. Evans, Sarah P. Slotznick, Rodolfo Coccioni, Toshitsugu Yamazaki, and Joseph L. Kirschvink (2021). “A Late Cretaceous true polar wander oscillation”. en. In: *Nature Communications* 12.1, p. 3629. ISSN: 2041-1723. DOI: 10.1038/s41467-021-23803-8.

Montanari, Alessandro, L.S. Chan, and W. Alvarez (1989). “Synsedimentary Tectonics in the Late Cretaceous-Early Tertiary Pelagic Basin of the Northern Apennines, Italy”. In: *Controls on Carbonate Platforms and Basin Development*. SEPM (Society for Sedimentary Geology).

Montanari, Alessandro, Kenneth A. Farley, Rodolfo Coccioni, N. Sabatino, D. Bice, M. Yesko, M. Sinnesael, and N. De Winter (2023). "Cosmogenic 3He anomaly K1 vs. the early Campanian isotopic event (ECE) as recorded in pelagic limestones of the Umbria-Marche succession (Italy)". en. In: *Geological Society of America Bulletin*. ISSN: 0016-7606, 1943-2674. DOI: 10.1130/B36952.1.

Mukhopadhyay, Sujoy, Kenneth A. Farley, and Alessandro Montanari (2001). "A 35 Myr record of helium in pelagic limestones from Italy: implications for interplanetary dust accretion from the early Maastrichtian to the middle Eocene". en. In: *Geochimica et Cosmochimica Acta* 65.4, pp. 653–669. ISSN: 00167037. DOI: 10.1016/S0016-7037(00)00555-X.

Muller, Richard A. and Donald E. Morris (1986). "Geomagnetic reversals from impacts on the Earth". en. In: *Geophysical Research Letters* 13.11, pp. 1177–1180. ISSN: 0094-8276, 1944-8007. DOI: 10.1029/GL013i011p01177.

Nesvorny, David, William F. Bottke, Harold F. Levison, and Luke Dones (2003). "Recent Origin of the Solar System Dust Bands". en. In: *The Astrophysical Journal* 591.1, pp. 486–497. ISSN: 0004-637X, 1538-4357. DOI: 10.1086/374807.

Nesvorný, David, Peter Jenniskens, Harold F. Levison, William F. Bottke, David Vokrouhlický, and Matthieu Gounelle (2010). "COMETARY ORIGIN OF THE ZODIACAL CLOUD AND CARBONACEOUS MICROMETEORITES. IMPLICATIONS FOR HOT DEBRIS DISKS". In: *The Astrophysical Journal* 713.2, pp. 816–836. ISSN: 0004-637X, 1538-4357. DOI: 10.1088/0004-637X/713/2/816.

Nier, Alfred O. and Dennis J. Schlutter (1990). "Helium and neon isotopes in stratospheric particles". en. In: *Meteoritics* 25.4, pp. 263–267. ISSN: 0026-1114. DOI: 10.1111/j.1945-5100.1990.tb00710.x.

Nurmi, P., M. J. Valtonen, and J. Q. Zheng (2001). "Periodic variation of Oort Cloud flux and cometary impacts on the Earth and Jupiter". en. In: *Monthly Notices of the Royal Astronomical Society* 327.4, pp. 1367–1376. ISSN: 0035-8711, 1365-2966. DOI: 10.1046/j.1365-8711.2001.04854.x.

Ogg, J. G. (2020). "Chapter 5 - Geomagnetic Polarity Time Scale". In: *Geologic Time Scale 2020*. Ed. by Felix M. Gradstein, James G. Ogg, Mark D. Schmitz, and Gabi M. Ogg. Elsevier, pp. 159–192. ISBN: 978-0-12-824360-2. DOI: 10.1016/B978-0-12-824360-2.00005-X.

Patterson, Desmond B. and Kenneth A. Farley (1998a). "Extraterrestrial 3He in seafloor sediments: evidence for correlated 100 kyr periodicity in the accretion rate of interplanetary dust, orbital parameters, and Quaternary climate". en. In: *Geochimica et Cosmochimica Acta* 62.23–24, pp. 3669–3682. ISSN: 00167037. DOI: 10.1016/S0016-7037(98)00263-4.

Patterson, Desmond B., Kenneth A. Farley, and Birger Schmitz (1998b). "Preservation of extraterrestrial 3He in 480-Ma-old marine limestones". en. In: *Earth* *and Planetary Science Letters* 163.1–4, pp. 315–325. ISSN: 0012821X. DOI: 10.1016/S0012-821X(98)00197-6.

Peucker-Ehrenbrink, B., Greg Ravizza, and Gisela Winckler (2016). "Geochemical Tracers of Extraterrestrial Matter in Sediments". en. In: *Elements* 12.3, pp. 191–196. ISSN: 1811-5209, 1811-5217. DOI: 10.2113/gselements.12.3.191.

Peucker-Ehrenbrink, B. and Birger Schmitz (2001). *Accretion of extraterrestrial matter throughout Earth's history*. eng. New York: Springer Science+Business Media, LLC. ISBN: 9781441986948.

Raquin, Aude and Manuel Moreira (2009). "Atmospheric 38Ar/36Ar in the mantle: Implications for the nature of the terrestrial parent bodies". en. In: *Earth and Planetary Science Letters* 287.3–4, pp. 551–558. ISSN: 0012821X. DOI: 10.1016/j.epsl.2009.09.003.

Sabatino, Nadia, Stephen R. Meyers, Silke Voigt, Rodolfo Coccioni, and Mario Sprovieri (2018). "A new high-resolution carbon-isotope stratigraphy for the Campanian (Bottaccione section): Its implications for global correlation, ocean circulation, and astrochronology". en. In: *Palaeogeography, Palaeoclimatology, Palaeoecology* 489, pp. 29–39. ISSN: 00310182. DOI: 10.1016/j.palaeo.2017.08.026.

Schmieder, Martin and David A. Kring (2020). "Earth's Impact Events Through Geologic Time: A List of Recommended Ages for Terrestrial Impact Structures and Deposits". en. In: *Astrobiology* 20.1, pp. 91–141. ISSN: 1531-1074, 1557-8070. DOI: 10.1089/ast.2019.2085.

Schmitz, Birger (2013). "Extraterrestrial spinels and the astronomical perspective on Earth's geological record and evolution of life". en. In: *Geochemistry* 73.2, pp. 117–145. ISSN: 00092819. DOI: 10.1016/j.chemer.2013.04.002.

Schmitz, Birger, Samuele Boschi, Anders Cronholm, Philipp R. Heck, Simonetta Monechi, Alessandro Montanari, and Fredrik Terfelt (2015). "Fragments of Late Eocene Earth-impacting asteroids linked to disturbance of asteroid belt". en. In: *Earth and Planetary Science Letters* 425, pp. 77–83. ISSN: 0012821X. DOI: 10.1016/j.epsl.2015.05.041.

Schmitz, Birger, Kenneth A. Farley, Steven Goderis, Philipp R. Heck, Stig M. Bergström, Samuele Boschi, Philippe Claeys, Vinciane Debaille, Andrei Dronov, Matthias Van Ginneken, David A.T. Harper, Faisal Iqbal, Johan Friberg, Shiyong Liao, Ellinor Martin, Matthias M. M. Meier, B. Peucker-Ehrenbrink, Bastien Soens, Rainer Wieler, and Fredrik Terfelt (2019). "An extraterrestrial trigger for the mid-Ordovician ice age: Dust from the breakup of the L-chondrite parent body". en. In: *Science Advances* 5.9, eaax4184. ISSN: 2375-2548. DOI: 10.1126/sciadv.aax4184.

Schmitz, Birger, Therese Häggström, and Mario Tassinari (2003). "Sediment-Dispersed Extraterrestrial Chromite Traces a Major Asteroid Disruption Event".

en. In: *Science* 300.5621, pp. 961–964. ISSN: 0036-8075, 1095-9203. DOI: 10.1126/science.1082182.

Schneider, David A., Dennis V. Kent, and Gilberto A. Mello (1992). "A detailed chronology of the Australasian impact event, the Brunhes-Matuyama geomagnetic polarity reversal, and global climate change". en. In: *Earth and Planetary Science Letters* 111.2–4, pp. 395–405. ISSN: 0012821X. DOI: 10.1016/0012-821X(92)90192-X.

Spoto, Federica, Andrea Milani, and Zoran Knežević (2015). "Asteroid family ages". en. In: *Icarus* 257, pp. 275–289. ISSN: 00191035. DOI: 10.1016/j.icarus.2015.04.041.

Tagle, Roald and Jana Berlin (2008). "A database of chondrite analyses including platinum group elements, Ni, Co, Au, and Cr: Implications for the identification of chondritic projectiles". en. In: *Meteoritics & Planetary Science* 43.3, pp. 541–559. ISSN: 1086-9379, 1945-5100. DOI: 10.1111/j.1945-5100.2008.tb00671.x.

Tagle, Roald and Philippe Claeys (2004). "Comet or Asteroid Shower in the Late Eocene?" en. In: *Science* 305.5683, pp. 492–492. ISSN: 0036-8075, 1095-9203. DOI: 10.1126/science.1098481.

– (2005). "An ordinary chondrite impactor for the Popigai crater, Siberia". en. In: *Geochimica et Cosmochimica Acta* 69.11, pp. 2877–2889. ISSN: 00167037. DOI: 10.1016/j.gca.2004.11.024.

Takayanagi, M. and Minoru Ozima (1987). "Temporal variation of3 He/4 He ratio recorded in deep-sea sediment cores". en. In: *Journal of Geophysical Research: Solid Earth* 92.B12, pp. 12531–12538. ISSN: 0148-0227. DOI: 10.1029/JB092iB12p12531.

Tognaccini, S., E. Tavarnelli, and Alessandro Montanari (2019). "Synsedimentary deformation in Upper Cretaceous–Lower Paleogene limestones within a thrust anticline of the Umbria-Marche Apennines, Italy". en. In: *250 Million Years of Earth History in Central Italy: Celebrating 25 Years of the Geological Observatory of Coldigioco*. Ed. by Christian Koeberl and David M. Bice. Geological Society of America, pp. 213–228. ISBN: 9780813725420. DOI: 10.1130/2019.2542(11).

Valet, Jean-Pierre, Laure Meynadier, and Yohan Guyodo (2005). "Geomagnetic dipole strength and reversal rate over the past two million years". en. In: *Nature* 435.7043, pp. 802–805. ISSN: 1476-4687. DOI: 10.1038/nature03674.

Vellekoop, Johan, Appy Sluijs, Jan Smit, Stefan Schouten, Johan W. H. Weijers, Jaap S. Sinninghe Damsté, and Henk Brinkhuis (2014). "Rapid short-term cooling following the Chicxulub impact at the Cretaceous–Paleogene boundary". en. In: *Proceedings of the National Academy of Sciences* 111.21, pp. 7537–7541. ISSN: 0027-8424, 1091-6490. DOI: 10.1073/pnas.1319253111.

Weissman, Paul R. (1990). "The Oort cloud". en. In: *Nature* 344.6269, pp. 825–830. ISSN: 0028-0836, 1476-4687. DOI: 10.1038/344825a0.

Wyatt, M. C., S. F. Dermott, C. M. Telesco, R. S. Fisher, K. Grogan, E. K. Holmes, and R. K. Pina (1999). "How Observations of Circumstellar Disk Asymmetries Can Reveal Hidden Planets: Pericenter Glow and Its Application to the HR 4796 Disk". en. In: *The Astrophysical Journal* 527.2, pp. 918–944. ISSN: 0004-637X, 1538-4357. DOI: 10.1086/308093.

Chapter 3

ASTEROIDS & MOON: A COSMIC DUST AMPLIFIER

3.1 Introduction

Helium is the only noble gas that is not gravitationally bound to Earth, which makes it extremely depleted in terrestrial materials compared to cosmic dust that is saturated with implanted solar wind helium (Peucker-Ehrenbrink et al., 2016). As a result, identifying extraterrestrial helium (He_{ET}) carried by cosmic dust in marine sediments has been the easiest and most straightforward (Merrihue, 1964; Krylov et al., 1973; Ozima et al., 1984; Amari et al., 1985; Takayanagi et al., 1987). In contrast, not only are the heavier noble gases bound by Earth's gravity, but the elemental composition of noble gases in cosmic dust also shows a pattern of decreasing abundance with atomic number, with helium being 3–4 orders of magnitude more enriched than xenon (Hudson et al., 1981; Kehm et al., 2009). Because of this, krypton and xenon (and sometimes argon) in marine sediments are always dominated by the terrestrial signal carried by terrigenous sediments or air, even in magnetic separates of marine sediments where extraterrestrial material is concentrated (Merrihue, 1964; Fukumoto et al., 1986; Amari et al., 1988). Extraterrestrial neon (Ne_{ET}) is observed only in marine sediments with high $^3He/^4He$ ratios (and thus a high abundance of extraterrestrial material) (Fukumoto et al., 1986; Matsuda et al., 1990; Darrah et al., 2012; Chavrit et al., 2016) and in the magnetic separates of marine sediments (Fukumoto et al., 1986; Amari et al., 1988; Matsuda et al., 1990; Nier et al., 1990b; Hiyagon, 1994). A maximum $^{20}Ne/^{22}Ne$ of ~12.5 has been reported in marine sediments or their magnetic separates (Hiyagon, 1994; Darrah et al., 2012). This is consistent with neon isotopes measured in individual interplanetary dust particles (IDPs) captured in the stratosphere (Nier et al., 1990a; Nier et al., 1992; Pepin et al., 2000; Kehm et al., 2006), which directly sample the cosmic dust flux. Thus, both He_{ET} and Ne_{ET} in marine sediments have been confirmed to be carried by cosmic dust irradiated by the solar wind.

While both helium and neon isotopes in marine sediments agree with those in IDPs, some marine sediments between 3 Ma and 39 Ma from the tropical Indian Ocean (Core 757B; Chavrit et al. 2016) have a $^3He/^{22}Ne$ that cannot be explained by mixing between air, terrigenous sediments, and IDPs (Fig. 3.1). An extraterrestrial endmember with a higher $^3He/^{22}Ne$ than that of IDPs is required. To explain this apparent paradox, it has been proposed that the IDPs captured in the stratosphere sample only the coarse fraction of cosmic dust (Chavrit et al., 2016). Since the peak temperature that a cosmic dust particle experiences during atmospheric entry heating is a function of size when other physical and orbital parameters are fixed, larger particles are expected to heat up more (Love et al., 1991). On the other hand, helium has a higher diffusivity than neon, as measured in magnetic separates of marine sediments at a given temperature (Matsuda et al., 1990; Hiyagon, 1994). As a result, elemental fractionation between helium and neon in cosmic dust is expected to be greater in coarser grains, which experience more diffusive loss of helium than neon and therefore have a lower $^3He/^{22}Ne$ than marine sediments, assuming the latter collect cosmic dust of all sizes (Chavrit et al., 2016). A similar interpretation has been offered when deep-sea magnetic fines (DSMF; Brownlee 1985) were reported to have higher $^3He/^{20}Ne$ (and also $^3He/^{22}Ne$; Fig. 3.1) than IDPs (Darrah et al., 2012). Interestingly, lunar regolith ilmenite has a $^3He/^{22}Ne$ high enough to explain the values observed in marine sediments from Core 757B (Chavrit et al. 2016; Fig. 3.1). Rather than arguing for the actual presence of lunar regolith ilmenite in these sediments, lunar regolith ilmenite has been interpreted as more representative of the average $^3He/^{22}Ne$ of cosmic dust in marine sediments due to its high helium retentivity (Chavrit et al., 2016). The high $^3He/^{22}Ne$ of DSMF does not contradict this interpretation (Fig. 3.1).

However, not all magnetic separates of marine sediments agree with DSMF in $^3He/^{22}Ne$. These magnetic separates extracted from different marine sediments, in different laboratories, and with different techniques (Fukumoto et al., 1986; Amari et al., 1988; Matsuda et al., 1990; Nier et al., 1990b; Hiyagon, 1994; Darrah et al., 2012) show a range of $^3He/^{22}Ne$ between 0.16 and 1.3, and $^{20}Ne/^{22}Ne$ between 11.1 and 12.5. They fall within a triangular area bounded by IDPs, lunar regolith ilmenite, and air/terrigenous sediments (Fig. 3.1). These results indicate that magnetic fines and their parent bulk marine sediments contain extraterrestrial components with both high and low $^3He/^{22}Ne$. Thus, the slope of the mixing line that passes through most of the Core 757B sediments and air/terrigenous sediment, which is equivalent to the $^{20}Ne/^3He$ of the extraterrestrial endmember in these sediments, essentially reflects the mixing ratio between the high-$^3He/^{22}Ne$ (low-$^{20}Ne/^3He$) and low-$^3He/^{22}Ne$ (high-$^{20}Ne/^3He$) extraterrestrial components. Implanted solar wind neon in solids has a $^{20}Ne/^{22}Ne$ of ~12.5 (Black, 1972; Moreira, 2013). Assuming that the extraterrestrial endmember in Core 757B samples has a similar $^{20}Ne/^{22}Ne$,

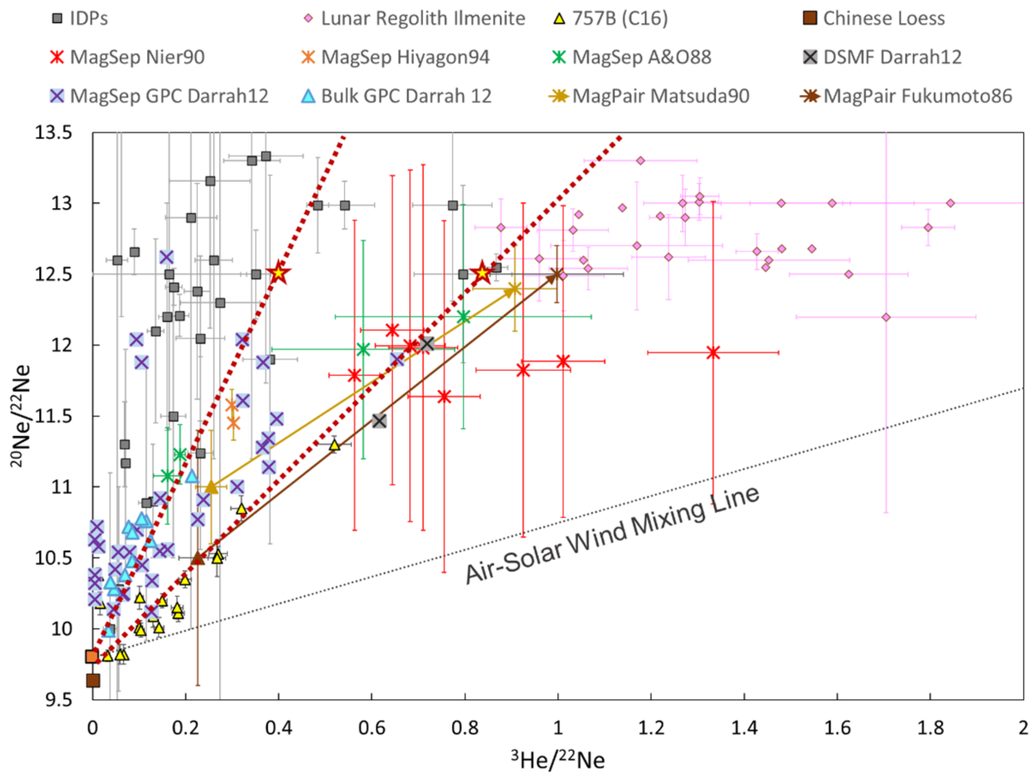

Figure 3.1: Compilation of published $^{20}Ne/^{22}Ne$ and $^{3}He/^{22}Ne$ data from interplanetary dust particles (IDPs), lunar regolith ilmenite, marine sediments and magnetic separates of marine sediments. The orange square shows the composition of Earth's atmosphere. The "Air-Solar Wind Mixing Line" connects Earth's atmosphere and solar wind (Heber et al., 2009). Chinese loess is plotted as a representative for terrigenous sediments. The two red dotted lines are the individual mixing lines that go through LL-44 GPC-3 samples (Darrah et al., 2012) and Core 757B samples (Chavrit et al., 2016), respectively. The yellow stars with red boundary are the extrapolated extraterrestrial endmember at $^{20}Ne/^{22}Ne$ of 12.5 (See main text). Error bars show 1 σ uncertainty. Data points with no error bar have no uncertainty reported. MagSep: magnetic separates. DSMF: deep sea magnetic fines (Brownlee, 1985). MagPair: a pair of bulk marine sediment and its magnetic separate, with the arrow pointing at the magnetic separate. Data sources: IDPs - Nier et al. (1990a), Pepin et al. (2000), and Kehm et al. (2006). Lunar Regolith Ilmenite - Eberhardt et al. (1972), Wieler et al. (1983), Heber et al. (2003), and Curran et al. (2020). 757B (C16) - Chavrit et al. (2016). Chinese loess – unpublished data. Nier90 - Nier et al. (1990b). Hiyagon94 - Hiyagon (1994). A&O88 - Amari et al. (1988). Darrah12 - Darrah et al. (2012). Matsuda90 - Matsuda et al. (1990). Fukumoto86 - Fukumoto et al. (1986).

this corresponds to a $^{3}He/^{22}Ne$ of ~0.9 and a $^{20}Ne/^{3}He$ of ~3 for this endmember (Fig. 3.1). This endmember composition falls between IDPs and lunar regolith ilmenite with respect to $^{3}He/^{22}Ne$, showing an intermediate composition due to the mixing of different extraterrestrial components. If IDPs are partially degassed and lunar regolith ilmenite represents undegassed cosmic dust, this endmember composition essentially reflects the average extent of degassing of cosmic dust in Core 757B sediments.

This endmember He/Ne composition is likely heterogeneous among marine sediments. A different extraterrestrial endmember composition can be similarly constrained for marine sediments between 19 Ma and 70 Ma in a pelagic red clay core (LL-44 GPC-3) from the North Pacific (Darrah et al., 2012). Assuming the same $^{20}Ne/^{22}Ne$ of 12.5 for the extraterrestrial endmember, the mixing line through the LL-44 GPC-3 samples extrapolates to a $^{3}He/^{22}Ne$ of ~0.4, with a $^{20}Ne/^{3}He$ of ~7 (Fig. 3.1). This potentially reflects a greater proportion of partially degassed cosmic dust grains in LL-44 GPC-3 samples compared to those from Core 757B. The heterogeneity in extraterrestrial endmember He/Ne is also suggested by the scatter in $^{3}He/^{22}Ne$ observed in magnetic separates of marine sediments. However, since the corresponding bulk marine sediment for each magnetic separate was rarely measured, we cannot determine whether the apparent range of $^{3}He/^{22}Ne$ reflects genuine heterogeneity in bulk marine sediments or uncertainty in the extraction of extraterrestrial components during magnetic separation.

There is only one piece of nominally 0-Ma, "modern," marine sediment from the South Pacific that has been independently measured by two groups (Fukumoto et al., 1986; Matsuda et al., 1990). Their corresponding magnetic separates have He/Ne ratios consistent with lunar regolith ilmenite (Fig. 3.1), indicating the presence of the high-$^{3}He/^{22}Ne$ extraterrestrial component in modern marine sediments. However, regarding the 0-Ma **bulk** marine sediment, one reported He/Ne value agrees with the Core 757B samples, while the other aligns more closely with LL-44 GPC-3 samples (Fig. 3.1). Due to the large error bars on these measurements, it is not possible to distinguish between the two scenarios or to constrain the He/Ne ratio of the extraterrestrial endmember in modern marine sediments.

Motivated by the discussions above, we conducted a systematic and comprehensive survey of the spatial and temporal patterns of He/Ne in marine sediments. The samples we selected cover a broad range of locations and ages, from core-top marine sediment samples that are nominally 0 Ma to drill core samples as old as

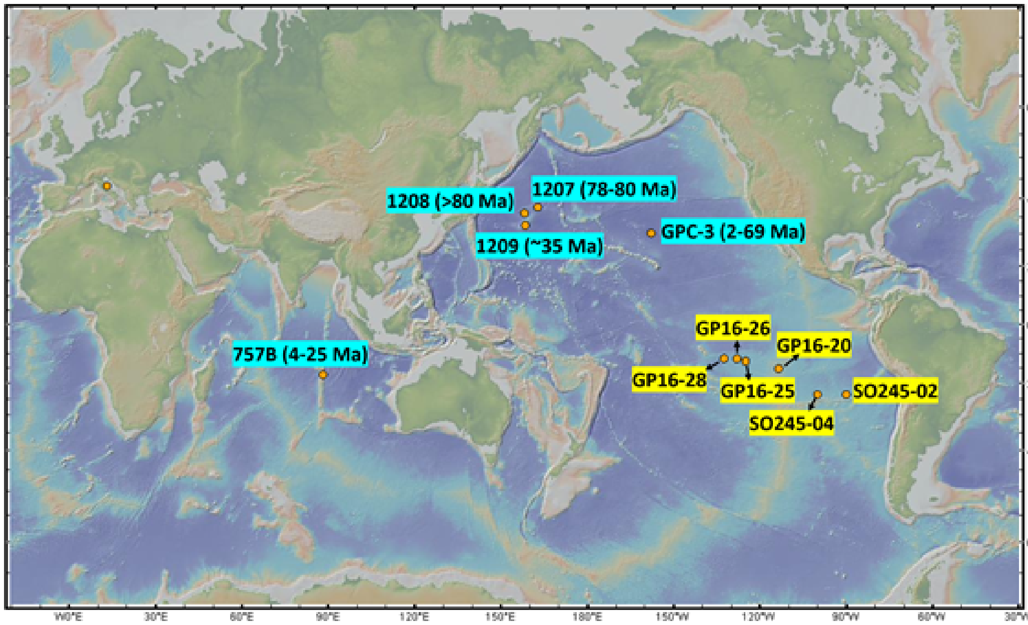

Figure 3.2: Map of sample locations. Modern sediments (nominally 0 Ma) are highlighted in yellow. Ancient sediments and their age range are highlighted in blue. The points correspond to their present-day location, instead of the location at the time of sediment deposition.

~85 Ma (Fig. 3.2). We intentionally selected deep-sea sediments with elevated ^{3}He/^{4}He ratios when possible, as these indicate enrichment in cosmic dust and a higher likelihood of a non–air-like neon isotope signature (Chavrit et al., 2016).

3.2 Materials and Methods

The samples we selected include six core-top marine sediment samples from the South Pacific Ocean on the GEOTRACES GP16 transect and the UltraPac expedition SO245 (nominally 0 Ma, "modern" sediments); eight pelagic red clay samples from the LL-44 GPC-3 core in the north-central Pacific Ocean (2 Ma to 69 Ma); three pelagic carbonate samples from IODP Hole 121-757B (4 Ma to 25 Ma); and forty-one pelagic carbonate samples from ODP Leg 198 in the North Pacific Ocean, including thirty-six from Site 1207 (78 Ma to 80 Ma), two from Site 1208 (~83 Ma), and three from Site 1209 (~35 Ma). Elevated ^{3}He/^{4}He ratios (>~10 R_A) in GP16 and SO245 samples (Pavia et al., 2024), LL-44 GPC-3 samples (Farley, 1995; Darrah et al., 2012), and Core 757B samples (Farley et al., 2006; Chavrit et al., 2016) have been reported previously and thus guided our selection. Site 1207 and Site 1208 samples span the Campanian stage of the Late Cretaceous and were initially measured in a search for the K1 event (Chapter II). Site 1209 samples span the Late Eocene and were initially measured in a search for the Late Eocene ^{3}He enhancement event (Farley et al. 1998; also Chapter IV). The $^{3}He/^{4}He$ ratios of Site 1207, Site 1208, and Site 1209 samples were determined for the first time in this work and were found to be > 10 R_A, and thus selected for helium and neon measurements.

Samples were prepared following the same procedure described in Chapter II. For He-only measurements (Sites 1207, 1208, and 1209), 2–10 mg of the acetic-acid-insoluble residue was wrapped in tin foil, then degassed of helium in a graphite liner in a double-walled vacuum furnace at ~1250 °C. Evolved helium was purified with a series of getters, cryogenically concentrated on charcoal at 14 K, and then released at 34 K into a Thermo Helix SFT mass spectrometer. ^{3}He was measured on a pulse-counting electron multiplier while ^{4}He was measured simultaneously on a Faraday detector.

For He+Ne measurements, 10–50 mg of the acid-insoluble residue was wrapped in tin foil before loading into the autosampler. The autosampler was then heated with a heater belt at ~150 °C for ~24 h to degas adsorbed atmospheric gases from the samples and line. We measured the desorbed gas from a batch of 12 samples at multiple times during the autosampler bake-out. Helium was at blank level, while neon was atmospheric, indicating no detectable loss of extraterrestrial helium or neon. We used a molybdenum liner instead of a graphite liner owing to its lower neon background. A 50:50 mixture of lithium metaborate and lithium tetraborate was loaded in the liner to help melt the samples at lower temperature; the mixed lithium borate flux melted at ~800 °C. We performed two temperature-release steps for each sample: a low-temperature step (< 400 °C) and a high-temperature step (~1100 °C). Both helium and neon were purified over the same series of getters. After neon was cryogenically concentrated on charcoal at 24 K, vapor-phase helium was expanded into a Thermo Helix-MC-Plus10K mass spectrometer and analyzed. Residual helium in the line was then pumped away, after which neon was released at 68 K into a Thermo Helix SFT mass spectrometer. On the Helix MC, we used magnetic-field hopping to sequentially measure $^{3}He^{+}$ on a pulse-counting electron multiplier and $^{4}He^{+}$ on a Faraday detector. For neon measurements on the Helix SFT, $^{20}Ne^{+}$, $^{21}Ne^{+}$, and $^{22}Ne^{+}$ were all measured on the pulse-counting electron multiplier. $^{20}(HF)^{+}$ and $^{40}Ar^{2+}$ cannot be resolved from $^{20}Ne^{+}$ on the Helix SFT. We measured $^{20}Ne^{+}$ at the magnetic field where contributions from $^{20}(HF)^{+}$ and $^{40}Ar^{2+}$ were minimized, and we used blanks (line blanks and hot blanks) to correct for HF^{+}

and $^{40}Ar^{2+}$ interferences in each air-standard or sample measurement. We also used blanks to correct for $^{44}(CO_2)^{2+}$ interference with $^{22}Ne^{+}$. In addition, we monitored $^{45}(CO_2)^{2+}$ on the pulse-counting electron multiplier to assess the background CO_2 level. Thus, for each measurement, we sequentially measured $^{20}Ne^{+}$, $^{21}Ne^{+}$, $^{22}Ne^{+}$, and $^{45}(CO_2)^{2+}$ with beam hopping by changing the accelerating voltage.

The mass spectrometers were calibrated for sensitivity using a synthetic gas standard with a $^{3}He/^{4}He$ ratio of 2.05 R_A and atmospheric Ne isotope ratios. For helium measurements, both ^{3}He and ^{4}He blanks are negligible ($\ll$ 1%) compared to sample signals; therefore, no blank correction was applied. Reported uncertainties are estimated from the reproducibility of replicate measurements of the air standard. For neon measurements, $^{44}(CO_2)^{2+}$ was found to be constant to ±10–20 % within each batch (~5 days). It contributes < 10 % of the total sample signal at most low-temperature steps (in a few gas-poor samples, the contribution can exceed 20 %) and < 5% at most high-temperature steps. We used the reproducibility of replicate measurements of air standards of different split sizes that matched to the total neon signal at each temperature step to calculate measurement uncertainties, assuming this captures uncertainty from all sources. All uncertainties reported here are 1 σ.

3.3 Results

The samples we measured have $^{3}He/^{4}He$ ratios between 6 R_A (R_A: $^{3}He/^{4}He$ of Earth's atmosphere, where 1 R_A = 1.382×10^{-6}; Sano et al. 2013) and 201 R_A (Fig. 3.3). In specific, GP16 samples range between 168 R_A and 183 R_A, SO245 sample range between 65 R_A and 86 R_A, LL-44 GPC-3 sample range between 6.3 R_A and 127 R_A, Core 757B samples range between 12 R_A and 29 R_A, Site 1207 samples range between 111 R_A and 201 R_A, Site 1208 samples range between 17 R_A and 70 R_A, Site 1209 samples range between 31 R_A and 100 R_A. Two major helium contributors to deep-sea sediments are terrigenous sediments with a $^{3}He/^{4}He$ of 0.01–0.03 R_A (Takayanagi et al., 1987; Marcantonio et al., 1998; Farley, 2001) and solar wind helium carried by cosmic dust with a $^{3}He/^{4}He$ of 100–300 R_A (Nier et al., 1990a; Nier et al., 1992; Pepin et al., 2000; Kehm et al., 2006). Using a two-component mixing model (Takayanagi et al., 1987; Patterson et al., 1998a), we found more than 99.5 % of the ^{3}He in all of the samples to be extraterrestrial. This value is not sensitive to the choice of endmember $^{3}He/^{4}He$. Notably, some of the samples from cruise GP16 and late Cretaceous samples from Site 1207 have $^{3}He/^{4}He$ >150 R_A, which suggests almost pure solar wind helium is present.

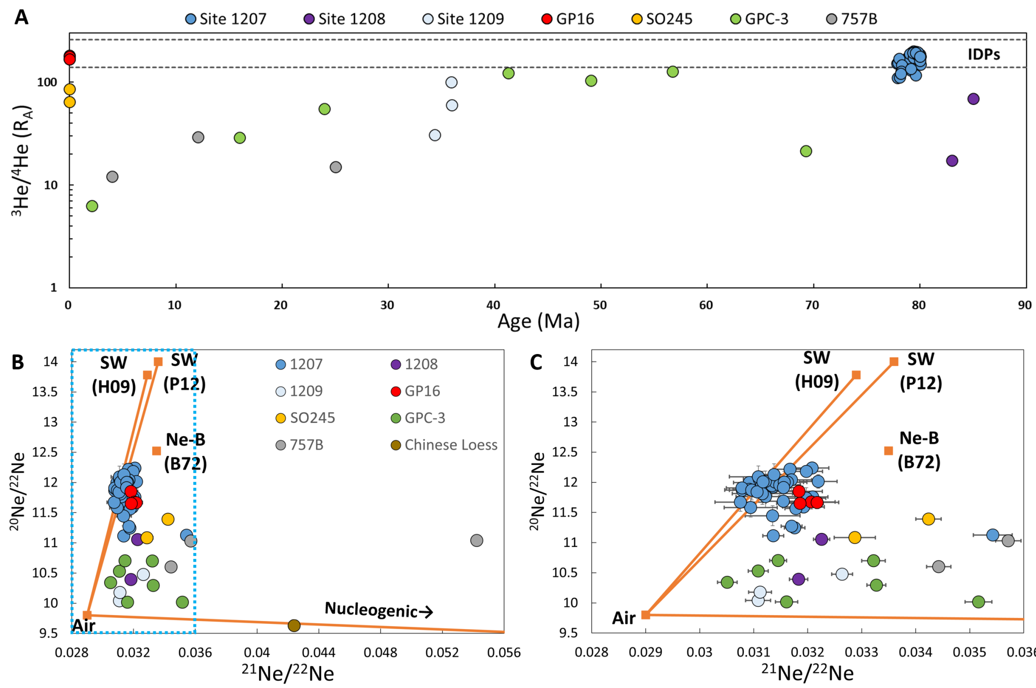

Figure 3.3: Helium and neon isotope results. (A) ^{3}He/^{4}He results. The region labeled as "IDPs" indicate the average ^{3}He/^{4}He of 200 ± 60 R_A calculated fromNier et al. (1990a), Nier et al. (1992), Pepin et al. (2000), and Kehm et al. (2006). (B) & (C) Neon isotope results. The blue frame in (B) indicates the location of (C). Two solar wind (SW) compositions are from Heber et al. (2009) and Pepin et al. (2012). Ne-B is the average neon composition measured in gas-rich meteorites (Black, 1972), which has been interpreted as being the fractionated solar wind neon composition in solids irradiated by solar wind. Chinese loess (unpublished data) is plotted as a representative composition for terrigenous sediments.

Site 1207 samples were originally measured in search for another sedimentary record for the K1 ^{3}He enhancement event at ~80 Ma (Farley et al. 2012; Montanari et al. 2023; Chapter II). This event was only identified in the Scaglia Rossa limestone formation in the Umbria-Marche basin in central Italy (Farley et al. 2012; Montanari et al. 2023; Chapter II). Our Site 1207 samples are constrained to be around 80 Ma by biostratigraphy (Bralower et al., 2006). Within the span of our samples, we have found a maximum factor-of-10 difference between implied $^{3}He_{ET}$ flux maximum at ~79.6 Ma and post-event background implied $^{3}He_{ET}$ flux at ~78.2 Ma (Fig. 3.4), agreeing with magnitude, age, and duration of K1 (Chapter II). Implied $^{3}He_{ET}$ flux and ^{3}He/^{4}He from helium-only measurements and He+Ne measurements agree with each other, showing the robustness of both methods (Fig. 3.4). We potentially missed the rise of K1 in our Site 1207 record, since the lowest sample in the sequence has an implied $^{3}He_{ET}$ flux higher than post-event background. Nevertheless, Site

1207 samples have provided a new sedimentary record for K1 outside the Umbria-Marche basin, confirming that K1 is a global ^{3}He enhancement event.

Our samples have ^{20}Ne/^{22}Ne ratios between 10.0 and 12.2, and ^{21}Ne/^{22}Ne between 0.031 and 0.054 (Fig. 3.3). In specific, GP16 samples have ^{20}Ne/^{22}Ne between 11.7 and 11.8, and ^{21}Ne/^{22}Ne of 0.032. SO245 samples have ^{20}Ne/^{22}Ne between 11.1 and 11.4, and ^{21}Ne/^{22}Ne between 0.033 and 0.034. LL-44 GPC-3 samples have ^{20}Ne/^{22}Ne between 10.0 and 10.7, and ^{21}Ne/^{22}Ne between 0.031 and 0.035. Core 757B samples have ^{20}Ne/^{22}Ne between 10.6 and 11.0, and ^{21}Ne/^{22}Ne between 0.034 and 0.054. Site 1207 samples have ^{20}Ne/^{22}Ne between 11.1 and 12.2, and ^{21}Ne/^{22}Ne between 0.031 and 0.035. Site 1208 samples have ^{20}Ne/^{22}Ne between 10.4 and 11.1, and ^{21}Ne/^{22}Ne of 0.032. Site 1209 samples have ^{20}Ne/^{22}Ne between 10.0 and 10.5, and ^{21}Ne/^{22}Ne between 0.031 and 0.033.

The neon characteristics of our samples can be described by mixing of three components: solar wind neon carried by cosmic dust, Earth's atmosphere, and a nucleogenic component enriched in ^{21}Ne that could be of terrigenous origin (Fig. 3.3). Since the production rate of nucleogenic ^{21}Ne is almost an order of magnitude higher than nucleogenic ^{20}Ne and ^{22}Ne in most minerals (Yatsevich et al., 1997), the slope of the air-nucleogenic mixing line in Fig. 3.3 is not sensitive to the choice of host mineral. Chinese loess, which we measured as a representative composition of terrigenous sediments (Farley, 2001), plots on the air-nucleogenic mixing line, confirming the possible contribution of the latter to the deep-sea sediments (Fig. 3.3).

Of all the samples, GP16 and Site 1207 samples (except one replicate) plot close to the Air-SW mixing line, indicating limited nucleogenic neon. The replicate with a high ^{21}Ne/^{22}Ne likely contains some terrigenous dust with nucleogenic ^{21}Ne. The ^{20}Ne/^{22}Ne of samples from Site 1207 and GP16 plot close to the average of individual cosmic dust particles (~12.5; Nier et al. 1990a; Nier et al. 1992; Pepin et al. 2000; Kehm et al. 2006), showing limited contributions from atmospheric neon. Within the Site 1207 samples, ^{4}He and neon isotopes all co-vary with $^{3}He_{ET}$, confirming that extraterrestrial helium and neon dominate the helium and neon budget in these samples (Fig. 3.4). The other marine sediments measured in this study have ^{20}Ne/^{22}Ne and ^{21}Ne/^{22}Ne that require the contribution from all three mixing endmembers.

Regarding the elemental ratios, the samples that we measured have ^{3}He/^{22}Ne between 0.07 and 1.4 (Fig. 3.5). The GP16 samples have ^{3}He/^{22}Ne between

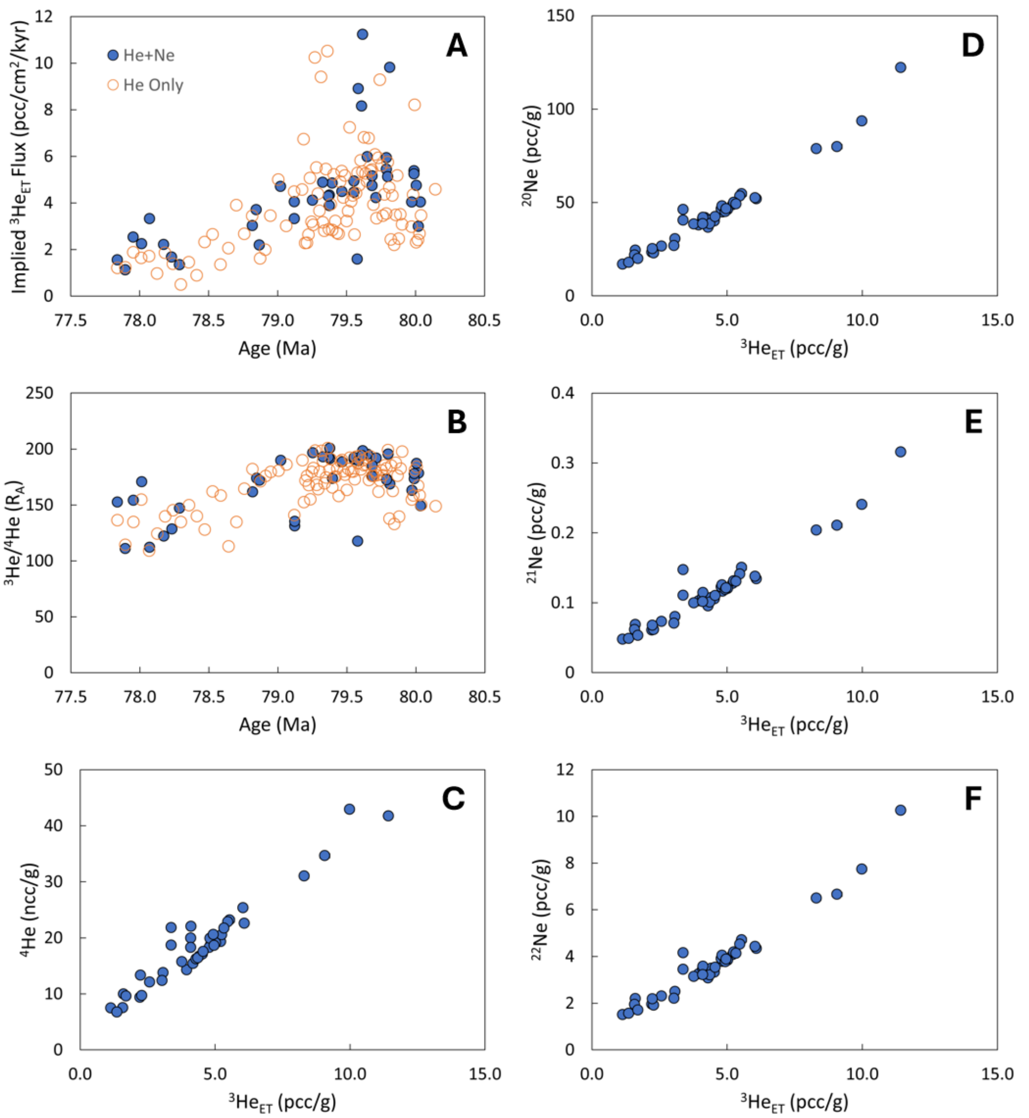

Figure 3.4: Helium and neon isotope data for Site 1207 samples. (A) Implied $^{3}He_{ET}$ flux at Site 1207. Here the implied $^{3}He_{ET}$ flux is directly proportional to the $^{3}He_{ET}$ concentration in the bulk sediment. A rapid 10-fold increase between 80 Ma and 79.6 Ma is followed by a prolonged decay over the next 1.5 Myr. The temporal profile is similar to K1 identified in Apiro (Chapter II), confirming that this is another sedimentary record of K1 outside the Umbria-Marche basin in Italy. (B) $^{3}He/^{4}He$ at Site 1207. Note the IDP-like values between 79 Ma and 80 Ma, which makes it insensitive to changes in the $^{3}He_{ET}$ flux. (C)-(F) The linear relationship between ^{4}He, ^{20}Ne, ^{21}Ne, ^{22}Ne and $^{3}He_{ET}$ indicates all of these isotopes are dominantly of extraterrestrial origin.

0.11 and 0.18, SO245 samples have $^3He/^{22}Ne$ between 0.25 and 0.42, LL-44 GPC-3 samples have $^3He/^{22}Ne$ between 0.08 and 0.34, Core 757B samples have $^3He/^{22}Ne$ between 0.28 and 0.40, Site 1207 samples have $^3He/^{22}Ne$ between 0.73 and 1.4, Site 1208 samples have $^3He/^{22}Ne$ between 0.23 and 0.66, and Site 1209 samples have $^3He/^{22}Ne$ between 0.07 and 0.23. One of our Site 1208 samples and all of our Site 1207 samples have $^3He/^{22}Ne$ higher than 0.6. These values are higher than the maximum $^3He/^{22}Ne$ of 0.52 reported in bulk marine sediments before (Fukumoto et al., 1986; Matsuda et al., 1990; Darrah et al., 2012; Chavrit et al., 2016).

3.4 Discussion

Extraterrestrial He-Ne Endmember in Marine Sediments

The three Core 757B samples we measured are consistent in He/Ne ratios with those previously reported (Chavrit et al., 2016), falling on a similar mixing line in the $^3He/^{22}Ne$–$^{20}Ne/^{22}Ne$ space (Fig. 3.5). These results confirm that the extraterrestrial He-Ne endmember in Core 757B sediments has a $^{20}Ne/^3He$ of ~3 (Fig. 3.1).

The LL-44 GPC-3 samples we measured do not agree with existing data (Darrah et al., 2012), but instead follow a trajectory similar to the Core 757B sediments in the $^3He/^{22}Ne$–$^{20}Ne/^{22}Ne$ space (Fig. 3.5). We cannot reconcile the difference between our LL-44 GPC-3 data and the previous data at present. Because uncertainties for individual measurements were not reported by Darrah et al. (2012), we cannot evaluate whether the two datasets actually agree within error. For the remainder of the discussion, we do not include data from Darrah et al. (2012).

Our Site 1209 samples agree with our Core 757B and LL-44 GPC-3 samples in both $^3He/^{22}Ne$ and $^{20}Ne/^{22}Ne$ (Fig. 3.5). The consistency among these samples indicates an apparently common composition for the extraterrestrial endmember in the marine sediments from these sites, with a $^{20}Ne/^3He$ of ~3, as constrained by the slope of the mixing line that passes through all of these samples and air/terrigenous sediments (Fig. 3.5). If the extraterrestrial He-Ne endmember has a $^{20}Ne/^{22}Ne$ of ~12.5, consistent with the implanted solar wind composition in solids (Black, 1972; Moreira, 2013), the corresponding $^3He/^{22}Ne$ is ~0.9. This composition falls within the range reported for lunar regolith ilmenite, rather than IDPs. We discuss the significance of this observation in a later section. These values are not sensitive to whether air or terrigenous sediments are chosen as the terrestrial endmember, owing to their proximity to each other in the $^3He/^{22}Ne$–$^{20}Ne/^{22}Ne$ space (Fig. 3.5).

The other marine sediment samples that we measured do not agree with samples

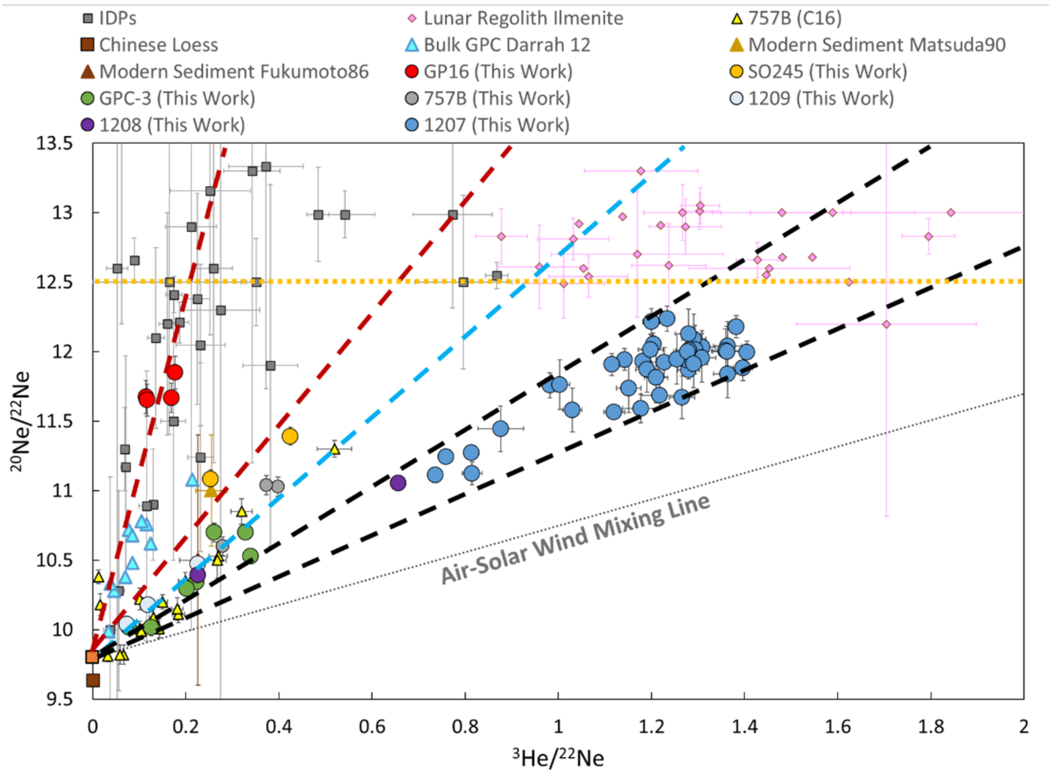

Figure 3.5: $^{3}He/^{22}Ne$-$^{20}Ne/^{22}Ne$ of bulk marine sediments measured in this study. The two red dashed lines indicate mixing lines that go through GP16 and SO245 samples, respectively. The blue dashed line is indicate the mixing line that goes through all of the Site 757B samples measured in this study and in Chavrit et al. (2016), LL-44 GPC-3 samples measured in this study, and Site 1209 samples. The black dashed lines bracket the range of mixing lines that go through Site 1207 and Site 1208 samples. All mixing lines are fixed on one end at air as the terrestrial endmember. The slope of the mixing lines is not sensitive to terrigenous sediments (represented by Chinese loess) being chosen as the terrestrial endmember. The orange dotted line extends horizontally at a $^{20}Ne/^{22}Ne$ of 12.5, which is estimated implanted solar wind neon composition in solids (Black, 1972; Moreira, 2013). The intersection points between the orange dotted line and each of the dashed mixing lines are taken as the extraterrestrial endmember for the marine sediments on the particular mixing line.

from Core 757B, LL-44 GPC-3, or Site 1209. Site 1207 and Site 1208 samples form a shallower trajectory in the ^{3}He/^{22}Ne–^{20}Ne/^{22}Ne space (Fig. 3.5). One Site 1208 sample appears more consistent with samples from Core 757B, LL-44 GPC-3, and Site 1209, but it also falls close to the mixing lines that pass through the Site 1207 samples, the other Site 1208 sample, and air/terrigenous sediments (Fig. 3.5). The slopes of these mixing lines range between 1.5 and 2, corresponding to the ^{20}Ne/^{3}He of the extraterrestrial endmember. The ^{3}He/^{22}Ne of the extraterrestrial endmember is constrained to be between 1.3 and 1.8, consistent with values measured in lunar regolith ilmenite but higher than those in IDPs (Fig. 3.5).

By contrast, mixing lines that pass through the two sets of modern sediments, GP16 and SO245, have slopes (and thus ^{20}Ne/^{3}He) greater than 3 (Fig. 3.5). The extraterrestrial He-Ne endmember in the GP16 sediments has a ^{20}Ne/^{3}He of ~13.5 and a ^{3}He/^{22}Ne of ~0.2, whereas that in the SO245 sediments has a ^{20}Ne/^{3}He of ~4.5 and a ^{3}He/^{22}Ne of ~0.6. These values agree with IDPs rather than lunar regolith ilmenite (Fig. 3.5). The modern sediment from a different location in the South Pacific (Fukumoto et al., 1986; Matsuda et al., 1990) is more consistent with the SO245 samples in ^{3}He/^{22}Ne and ^{20}Ne/^{22}Ne, indicating a similar extraterrestrial He-Ne endmember.

Heterogeneity in Extraterrestrial Endmember He/Ne

Our survey of helium and neon in marine sediments indicates at least four extraterrestrial He-Ne endmembers across locations and ages (Fig. 3.5). These include two high-^{20}Ne/^{3}He, IDP-like endmembers for modern sediments and two low-^{20}Ne/^{3}He, lunar-regolith-ilmenite–like endmembers for sediments older than ~2 Ma.

What causes the observed range in extraterrestrial endmember He/Ne? The difference in He/Ne between GP16 and SO245 sediments suggests spatial heterogeneity, since both are nominally 0 Ma in age. However, evidence for such heterogeneity is mixed. Site 1207 and Site 1208 sediments have a different extraterrestrial endmember He/Ne from Site 1209 sediments, even though they were sampled on the same oceanic plateau (the Shatsky Rise) and lie within 400 km of each other. By contrast, marine sediments from the tropical Indian Ocean (Core 757B), the northwestern Pacific (Site 1209), and the central North Pacific (LL-44 GPC-3) share a common extraterrestrial He-Ne endmember, showing no spatial heterogeneity among sites thousands of kilometers apart (Fig. 3.2).

Alternatively, the data can be organized by age. Site 1207 and Site 1208 sediments, with the lowest $^{20}Ne/^{3}He$, are older than 78 Ma. Core 757B, LL-44 GPC-3, and Site 1209 sediments, with an intermediate $^{20}Ne/^{3}He$ in the extraterrestrial He-Ne endmember, span 2–69 Ma. Modern GP16 and SO245 sediments have the highest $^{20}Ne/^{3}He$ of the four apparent extraterrestrial He-Ne endmembers, with GP16 samples falling on the steepest mixing lines. Although sediments from both cruises were collected from the upper 1–3 cm of core tops, estimated core-top ages for the four GP16 stations are 38–125 ka, younger than the estimated core-top ages of 217 and 278 ka for the two SO245 stations (Pavia et al., 2024). Thus, the range of extraterrestrial endmember He/Ne observed in marine sediments can be described as a monotonic decrease in $^{20}Ne/^{3}He$ with increasing sample age. This decrease is not continuous through time, since marine sediments between 2 Ma and 69 Ma can be explained by one specific extraterrestrial He-Ne endmember, and sediments older than ~78 Ma by another (Fig. 3.5). One sample from Site 1208 has a higher $^{20}Ne/^{3}He$ than the Site 1207 samples and the other Site 1208 sample, which appears to contradict the monotonic decrease. Additional measurements in sediments older than 85 Ma are needed to determine whether the temporal trend extends beyond the time span of this study.

An obvious hypothesis for the temporal trend is preferential loss of neon relative to helium through time. However, this contradicts measured diffusivities for helium and neon in magnetic separates of marine sediments (Matsuda et al., 1990; Hiyagon, 1994). Because neon has a lower diffusivity, it should experience less diffusive loss than helium, and $^{20}Ne/^{3}He$ in marine sediments should increase with age, which is opposite to what we observe.

Alternatively, based on helium and neon measurements in magnetic separates of marine sediments, the extraterrestrial endmember He/Ne in a sediment reflects the mixing ratio between extraterrestrial components with different $^{20}Ne/^{3}He$ (Fig. 3.1 and the Introduction to this chapter). Thus, the He/Ne of modern sediments can be explained by enrichment in the high-$^{20}Ne/^{3}He$ extraterrestrial component, whereas sediments older than ~78 Ma are more enriched in the low-$^{20}Ne/^{3}He$ component. Marine sediments between 2 Ma and 69 Ma fall in between.

Identity of Extraterrestrial Components

Since the observed extraterrestrial endmember He/Ne in marine sediments depends on the mixing ratio between different extraterrestrial components, identifying those components is crucial for understanding the mechanisms behind the observed temporal variation in the extraterrestrial endmember He/Ne.

The four GP16 samples, with the youngest estimated ages (< 125 ka), provide the best constraint on the He/Ne composition of cosmic dust deposited on Earth's surface today. These samples can be explained by mixing between a high-^{20}Ne/^{3}He, IDP-like component and air/terrigenous sediments, without requiring a low-^{20}Ne/^{3}He, lunar-regolith-ilmenite–like component (Fig. 3.5). This observation is most readily explained if IDPs are the dominant carriers of He_{ET} and Ne_{ET} in modern marine sediments, with the contribution from the low-^{20}Ne/^{3}He extraterrestrial component being negligible. Thus, we propose that IDPs constitute the high-^{20}Ne/^{3}He extraterrestrial component in modern marine sediments. If we also consider the span of He/Ne measured in magnetic separates of sediments between 19 Ma and 72 Ma, for which uncertainties were not reported (Darrah et al., 2012), IDPs can likewise serve as the high-^{20}Ne/^{3}He extraterrestrial component in ancient marine sediments (Fig. 3.5).

Is the low-^{20}Ne/^{3}He extraterrestrial component undegassed cosmic dust without preferential He loss (Darrah et al., 2012; Chavrit et al., 2016)? There are no existing He/Ne data for cosmic dust captured in space, which would most rigorously constrain the He/Ne of undegassed cosmic dust. Alternatively, minerals in lunar regolith are likely good proxies for undegassed phases in cosmic dust. As with cosmic dust, helium and neon isotope measurements reported for lunar regolith indicate that these gases are predominantly solar-wind–implanted (Curran et al., 2020). Although lunar regolith is exposed to solar wind irradiation for billions of years, whereas cosmic dust is irradiated only during its dynamic lifetime of 10^4–10^6 yr (Burns et al., 1979), a steady-state composition of implanted solar wind He/Ne is expected to be reached within a few thousand years (Moreira et al., 2016). Because lunar regolith has never experienced atmospheric entry heating, no degassing is expected. Thus, if lunar regolith exhibits a low ^{20}Ne/^{3}He ratio sufficient to explain the ^{20}Ne/^{3}He observed in some marine sediments and magnetic separates, undegassed cosmic dust is potentially the low-^{20}Ne/^{3}He extraterrestrial component.

Of the common lunar regolith minerals and phases, pyroxene, plagioclase, and agglutinates are consistent with IDPs in ^{3}He/^{22}Ne and ^{20}Ne/^{22}Ne (Fig. 3.6). Lunar ilmenite has a distinctly low ^{20}Ne/^{3}He, but this signal is muted in agglutinates and bulk lunar regolith (Fig. 3.6), both of which are aggregates of lunar regolith minerals. Bulk lunar regolith is consistent with lunar regolith silicates, indicating that silicates dominate the bulk He/Ne signature in lunar regolith. Because cosmic

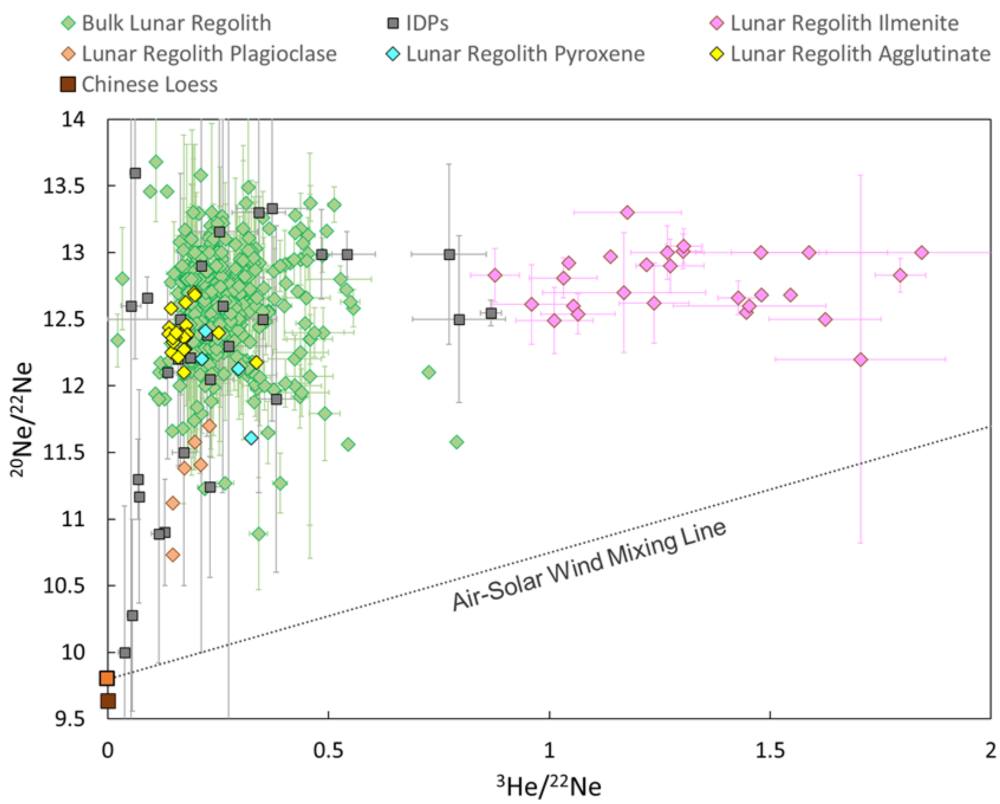

Figure 3.6: $^3He/^{22}Ne$-$^{20}Ne/^{22}Ne$ of extraterrestrial materials. $^3He/^{22}Ne$-$^{20}Ne/^{22}Ne$ of bulk lunar soil (Curran et al., 2020), non-ilmenite lunar regolith components (Curran et al., 2020), and lunar regolith ilmenite (Eberhardt et al., 1972; Huebner et al., 1975; Weber et al., 1979; Wieler et al., 1983; Becker et al., 1989; Benkert et al., 1993; Heber et al., 2003). Both the range and mean of $^3He/^{22}Ne$ of bulk lunar regolith ($0.02 < {}^3He/^{22}Ne < 0.8$, average $^3He/^{22}Ne = 0.27 \pm 0.09$ [1 σ standard deviation]) are consistent with IDPs ($0.05 < {}^3He/^{22}Ne < 0.9$, average $^3He/^{22}Ne = 0.27 \pm 0.22$; Nier et al. 1990a; Pepin et al. 2000; Kehm et al. 2006).

dust is dominated by silicate minerals, with ilmenite being a rare phase (Bradley, 2007), undegassed cosmic dust should match lunar regolith silicates and bulk lunar regolith, and thus IDPs, in He/Ne. Therefore, undegassed cosmic dust is sampled by IDPs and cannot represent the low-$^{20}Ne/^3He$ extraterrestrial component in marine sediments. We therefore argue against the previous interpretation that lunar regolith ilmenite is more representative of cosmic dust in marine sediments (Chavrit et al., 2016). Rather, IDPs and bulk lunar regolith are both representative of cosmic dust. The low-$^{20}Ne/^3He$ extraterrestrial component requires an alternative explanation.

No other mechanism or extraterrestrial material besides lunar regolith ilmenite is currently known that can account for the low $^{20}Ne/^3He$ reported in some marine sediments, especially those from Site 1207 and Site 1208 that are older than ~78 Ma (Fig. 3.5). Thus, the simplest explanation for the low-$^{20}Ne/^{3}He$ extraterrestrial component in marine sediments is ilmenite from the lunar regolith (or extraterrestrial ilmenite from other planetary bodies).

Ilmenite has been proposed as a possible carrier phase of He_{ET} in marine sediments based on acid-leaching experiments (Mukhopadhyay et al., 2006). Subsequently, ilmenite was found in pelagic red clay samples from LL-44 GPC-3 of various ages, and its extraterrestrial origin was hypothesized based on its prevalence and the low probability of a persistent terrestrial source over millions of years (Darrah et al., 2012). We therefore propose that extraterrestrial ilmenite, as represented by lunar regolith ilmenite, is the most likely low-$^{20}Ne/^{3}He$ extraterrestrial component in marine sediments.

Loss of Non-ilmenite Phases

So far, we have shown that the mixing He-Ne components in marine sediments are likely: air/terrigenous sediments, bulk cosmic dust represented by IDPs with high $^{20}Ne/^{3}He$, and extraterrestrial ilmenite with low $^{20}Ne/^{3}He$. Note that extraterrestrial ilmenite is itself a component of cosmic dust. To avoid confusion, we refer to the high-$^{20}Ne/^{3}He$ component as non-ilmenite in the following discussion and use cosmic dust as the umbrella term for all micron-sized extraterrestrial particles falling to Earth. The observed temporal trend in marine-sediment He/Ne can then be interpreted as a stronger non-ilmenite signal in younger sediments and a stronger extraterrestrial ilmenite signal in older sediments (Fig. 3.5). We can estimate the proportion of ^{3}He derived from lunar regolith ilmenite in Site 1207 and Site 1208 sediments with the lowest $^{20}Ne/^{3}He$ using:

$$^{3}\mathrm{He}_{\mathrm{ilmenite}}\% = \frac{\left(\frac{^{22}\mathrm{Ne}}{^{3}\mathrm{He}}\right)_{\mathrm{sample}} - \left(\frac{^{22}\mathrm{Ne}}{^{3}\mathrm{He}}\right)_{\mathrm{IDP}}}{\left(\frac{^{22}\mathrm{Ne}}{^{3}\mathrm{He}}\right)_{\mathrm{ilmenite}} - \left(\frac{^{22}\mathrm{Ne}}{^{3}\mathrm{He}}\right)_{\mathrm{IDP}}} \times 100 \tag{3.1}$$

We adopt a $^{3}He/^{22}Ne$ of 0.2 (the extraterrestrial endmember value in GP16 sediments) for the non-ilmenite component and a $^{3}He/^{22}Ne$ of 1.8 (the maximum extraterrestrial endmember value in Site 1207 and Site 1208) for extraterrestrial ilmenite. Thus, essentially 100 % of ^{3}He in GP16 sediments, 25 % in SO245 sediments, ~12.5 % in sediments between 2–69 Ma, and < 5% in sediments older than ~78 Ma is carried by non-ilmenite; the remainder is carried by extraterrestrial ilmenite. Using a median (rather than mean, given the strong positive skew in the distribution of ^{3}He measured in IDPs) ^{3}He concentration of ~15 μcc/g in IDPs (Nier et al., 1990a; Nier et al., 1992; Pepin et al., 2000; Kehm et al., 2006) and an average ^{3}He concentration of ~220 μcc/g in unsieved lunar regolith ilmenite (Eberhardt et al., 1972), more than 60 wt% of the He- and Ne-bearing cosmic dust in sediments older than ~78 Ma must be extraterrestrial ilmenite for its contribution to the total ^{3}He budget to exceed 95 %. Similarly, we calculate that > 70 % of ^{22}Ne in the extraterrestrial He-Ne endmember at Sites 1207 and 1208 derives from extraterrestrial ilmenite, implying a modal abundance of at least 40 wt% ilmenite in the cosmic dust fraction preserved in these sediments.

The most obvious explanation for the increasing abundance of extraterrestrial ilmenite in older sediments is an ancient astronomical source of ilmenite-rich dust. However, ilmenite occurs in meteorites only as an accessory phase, if present, with typical modal abundance $\ll$ 1 wt% (Rubin, 1997). The Moon is enriched in ilmenite, but even high-Ti lunar regolith has $\lesssim$ 10 wt% ilmenite (Papike et al., 1982). Based on existing meteorite and lunar data, no known parent body has at least ~40 wt% ilmenite to supply the required dust to Sites 1207 and 1208 (Fig. 3.5).

Although known dust sources are ilmenite-poor, ancient cosmic dust might have been secondarily fractionated to enrich ilmenite. If the average ilmenite modal abundance in source dust was ~1 wt% (likely an upper limit), a fractionation process would need to remove > 98 % of helium and neon from non-ilmenite phases to reproduce the Site 1207 and Site 1208 ^{20}Ne/^{3}He.

Fractionation could occur at several stages between the astronomical source and seafloor. Because ilmenite is harder than silicates, it may survive micrometeorite bombardment on asteroid or lunar surfaces more effectively (not expected for comets, which mainly release primary dust via sublimation). Ilmenite may also have a longer collisional lifetime during secondary dust–dust collisions in space. Such a scenario would likely require a dustier Solar System prior to 78 Ma to enhance preferential survival/ejection of ilmenite and enrich the traversing dust in ilmenite.

Alternatively, analyses of Apollo samples show that ilmenite is much more retentive of He and Ne than silicates (Baur et al., 1972; Signer et al., 1977; Benkert et al., 1993), implying different loss rates from these phases. Degassing could result from pulse heating during surface impacts on asteroids or the Moon, but the extent and direction of preferential He/Ne loss across minerals remain unconstrained. Moreover, even if silicates are preferentially degassed by primary impacts, they would be re-saturated by solar wind He and Ne within a few thousand years (Moreira et al., 2016), far shorter than a typical dynamic lifetime of 10^4–10^6 yr for cosmic dust (Burns et al., 1979).

Preferential silicate degassing might also occur during atmospheric entry heating. For micron-sized particles with the same density–size product, peak temperature is similar and heat capacity can be neglected (Love et al., 1991). Thus, a 10-µm ilmenite grain ($\rho \approx 4.8$ g/cm^3) has a thermal history equivalent to a 16-µm plagioclase grain ($\rho \approx 3.0$ g/cm^3). For fixed density, peak temperature increases with particle size (Love et al., 1991); consequently, a 10-µm ilmenite grain (equivalent to a 16-µm plagioclase grain) reaches a higher peak temperature than a 10-µm plagioclase grain. Whether ilmenite's higher retentivity can offset its higher peak temperature so that low-density silicates experience relatively greater degassing remains unclear. Phase-specific measurements of He and Ne loss rates in ilmenite and silicates are needed to address this question. Nevertheless, to increase ilmenite's contribution to the total He and Ne delivered to Earth, as implied by ancient sediments, ilmenite arriving at the top of the atmosphere may have a finer size distribution, lower entry velocities, and/or shallower entry angles than non-ilmenite (mostly silicates), lowering peak temperatures and preserving noble gases (Love et al., 1991). Mechanisms that could create such phase-specific dynamical differences remain uncertain.

Perhaps the strongest counterargument to all source/transport fractionation scenarios is that a monotonic strengthening of the ilmenite He/Ne signal with sediment age is not predicted *a priori*. By contrast, we propose that post-depositional processes can naturally produce the observed trend. Earth's aqueous, oxidizing, warm surface environment contrasts with the dry, reducing, cold conditions of space. Once deposited, cosmic dust minerals undergo weathering and alteration with differing resistance. In general, silicates are more susceptible to submarine alteration than oxides: olivine is most weatherable, followed by pyroxene, then plagioclase (Brady et al., 1997). Ilmenite, in contrast, is among the most durable minerals (White et al., 1994). Silicates also lose He and Ne more readily than ilmenite due to lower noble-gas retentivity (Signer et al., 1977; Benkert et al., 1993; Heber et al., 2003). Thus, faster alteration and/or degassing of non-ilmenite phases in cosmic dust (primarily silicates) relative to ilmenite will preferentially remove the high-^{20}Ne/^{3}He signal and strengthen the low-^{20}Ne/^{3}He signal in older sediments (Fig. 3.6), consistent with our observations (Fig. 3.5).

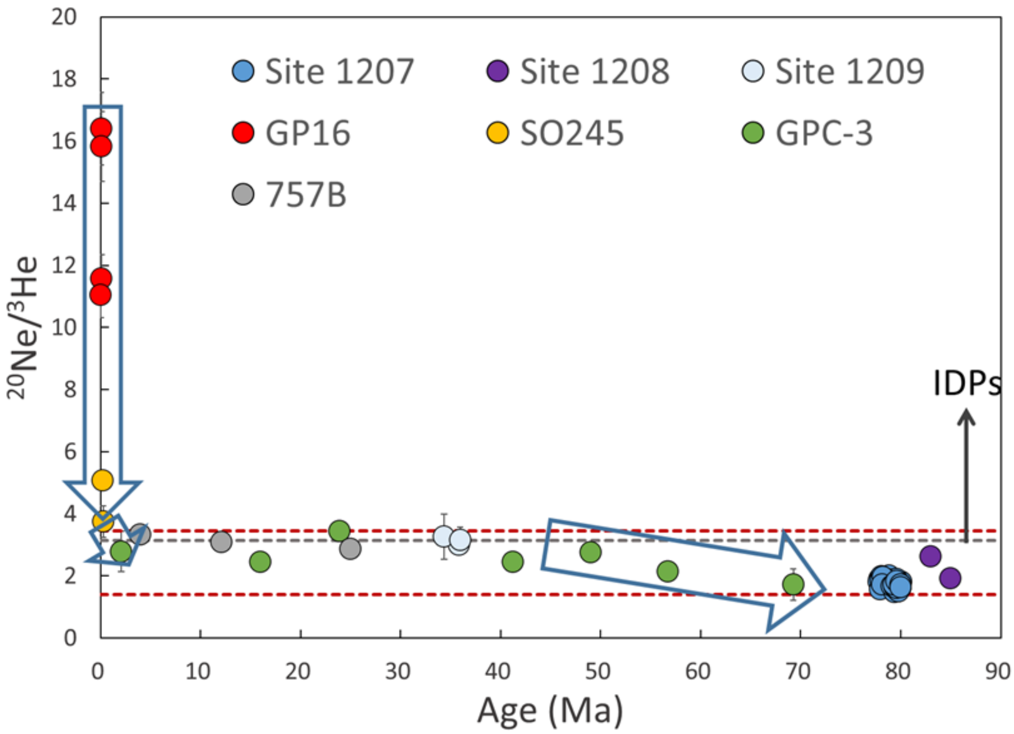

Figure 3.7: Temporal trend of marine sediment $^{20}Ne/^{3}He$. Ilmenite zone (bound by two horizontal dashed lines) is defined by measurements from Eberhardt et al. (1972), Huebner et al. (1975), Weber et al. (1979), Wieler et al. (1983), Becker et al. (1989), Benkert et al. (1993), and Heber et al. (2003). IDP zone is defined by measurements from Nier et al. (1990a), Pepin et al. (2000), and Kehm et al. (2006). Arrows show the three episodes of alteration/degassing of minerals in cosmic dust and are for visual only.

Preferential alteration/degassing of non-ilmenite can also explain the non-linear rate of decrease in $^{20}Ne/^{3}He$ through time (Fig. 3.7). Because minerals differ in weathering resistance and noble-gas retentivity, sequential alteration/degassing is expected in discrete episodes rather than continuously. We identify at least three episodes (Fig. 3.7): within ~200 ka of the present, between ~200 ka and ~2 Ma, and between 50–78 Ma. The two younger episodes likely reflect rapid alteration/degassing of distinct silicate phases; the third may reflect alteration/degassing of a more durable phase (*e.g.*, an oxide) that persists on the seafloor for > 50 Ma. Alternatively, closed-system stepped-etching experiments on lunar regolith ilmenite show elemental fractionation with implantation depth, with more deeply implanted solar wind He and Ne having lower $^{20}Ne/^{3}He$ (Heber et al., 2003). The decrease beginning near 50 Ma could therefore also correspond to the loss of more shallowly implanted He and Ne in ilmenite via alteration or diffusion.

In summary, fractionation between He and Ne in ilmenite and non-ilmenite phases at the source or during transport is neither guaranteed nor does it, *a priori*, predict the observed temporal trend in marine-sediment ^{20}Ne/^{3}He. By contrast, sequential post-depositional alteration/degassing of different phases in cosmic dust provides a simple, mechanistically plausible explanation for the monotonic decrease in ^{20}Ne/^{3}He in marine sediments through time.

Implications for ^{3}He$_{ET}$ Flux Reconstruction

Since the non-ilmenite phases in cosmic dust become altered or degassed on the seafloor over time, a correction is required when inferring the actual ^{3}He$_{ET}$ flux over geologic time from the implied ^{3}He$_{ET}$ flux reconstructed from ^{3}He$_{ET}$ concentrations measured in marine sediments. This is especially important for sediments that are millions of years old, since most ^{3}He$_{ET}$ carried by non-ilmenite has been lost. If cosmic dust contains ~1 wt% ilmenite, the implied ^{3}He$_{ET}$ flux will be lower than the actual ^{3}He$_{ET}$ flux by ~2 orders of magnitude.

The implied ^{3}He$_{ET}$ flux between 2 Ma and 85 Ma is approximately constant in our dataset, averaging 0.4 ± 0.2 pcc/cm^2/kyr (Fig. 3.8). This value was calculated with all Site 1207 samples excluded, because the implied ^{3}He$_{ET}$ flux is known to be enhanced by ~10 times during K1 (Chapter II). We also excluded the Site 1208 sample at ~85 Ma because its ^{3}He concentration is ~50× higher than its replicate (unpublished data), likely reflecting a rare ^{3}He-enriched cosmic dust particle. This “nugget effect” is not expected to bias the He/Ne of the sample, as both elements are enriched in the "nugget" (rare cosmic dust enriched in implanted solar wind ions). Only helium was measured in the replicate and including it would not change the result. Our result is consistent with reported values of implied ^{3}He$_{ET}$ flux through the Cenozoic (excluding the Quaternary) (Farley, 1995; Farley et al., 2003; Farley et al., 2006; Marcantonio et al., 2009). A similar value of 0.5 ± 0.2 pcc/cm^2/kyr has also been reported for the Late Ordovician (Patterson et al., 1998b). If a correction is applied, the actual ^{3}He$_{ET}$ flux between 2 Ma and 85 Ma, and in the Late Ordovician, is likely on the order of 40 pcc/cm^2/kyr.

This value is an order of magnitude higher than the implied ^{3}He$_{ET}$ flux in the Quaternary, which has been estimated to be ~1 pcc/cm^2/kyr from both ice cores and deep-sea sediments, and ~2–4 pcc/cm^2/kyr from IDPs captured in Earth’s stratosphere (Farley et al., 2021). We calculate an implied ^{3}He$_{ET}$ flux of ~1–2 pcc/cm^2/kyr based on GP16 samples and ~3–5 pcc/cm^2/kyr based on SO245 samples

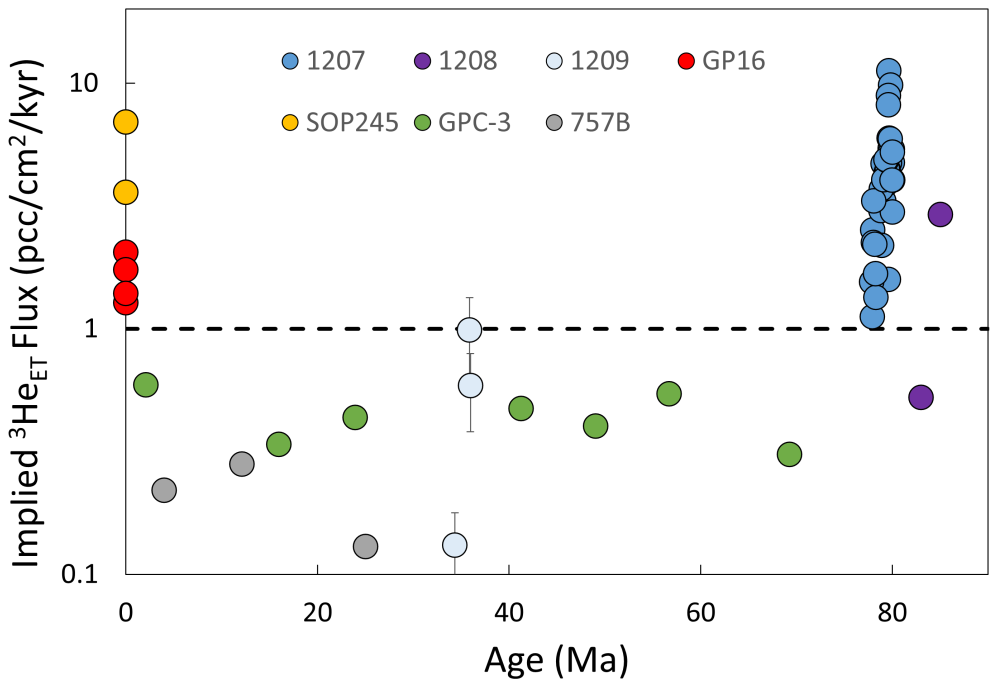

Figure 3.8: Implied $^3He_{ET}$ flux calculated for each sample in this study. Mass accumulation rates for GP16 and SO245 samples come from Pavia et al. (2024), for Site 1207, Site 1208, and Site 1209 samples come from biostratigraphy provided in Bralower et al. (2006), for Site 757B samples come from Farley et al. (2006), and for LL-44 GPC3 samples come from Farley (1995). The dashed line shows the estimated implied $^3He_{ET}$ flux of $/sim1$ pcc/cm^2/kyr for the Quaternary (Farley et al. 2021 and references therein).

(Fig. 3.8). However, there are large discrepancies between $^3He_{ET}$-derived and ^{230}Th-derived mass accumulation rates (the latter adopted here to avoid circularity) at GP16 and SO245 stations (Pavia et al., 2024), so the implied $^3He_{ET}$ flux may be inaccurate. Nevertheless, these values agree with existing data to within the same order of magnitude.

If cosmic dust flux has remained constant through time, we would also expect the actual $^3He_{ET}$ flux today to be on the order of 40 pcc/cm^2/kyr. The discrepancy between this value and the implied Quaternary $^3He_{ET}$ flux may reflect a real change in $^3He_{ET}$ flux before vs. after the Quaternary, implying a cosmic dust flux an order of magnitude higher from 2–85 Ma (and possibly back to the Late Ordovician). This scenario requires a more active Solar System sustaining high dust production for tens to hundreds of millions of years until the Quaternary. Alternatively, the actual $^3He_{ET}$ flux today may indeed be ~40 pcc/cm^2/kyr, and the reported Quaternary value of ~1 pcc/cm^2/kyr could result from rapid alteration/degassing of non-ilmenite phases on Earth's surface. If so, removal of ~98 % of total $^{3}He_{ET}$ would be so rapid that neither ice cores nor surface marine sediments measured to date are "modern" enough to capture the true $^{3}He_{ET}$ flux (Farley et al. 2021 and references therein). Indeed, a ~98 % loss of ^{3}He carried by non-ilmenite is already implied in SO245 sediments based on their $^{3}He/^{22}Ne$, assuming GP16 samples represent sediments without any post-depositional ^{3}He loss. However, in this case the general agreement in the implied $^{3}He_{ET}$ flux measured at both GP16 and SO245 (Fig. 3.8) would indicate that the mass accumulation rates estimated for GP16 samples are low by roughly an order of magnitude (Pavia et al., 2024). We do not yet have sufficient constraints to discriminate among these scenarios.

Source of Extraterrestrial Ilmenite and Its Importance

Despite being only a minor component of cosmic dust, extraterrestrial ilmenite ultimately becomes the most important phase enabling reconstruction of past $^{3}He_{ET}$ flux and cosmic dust flux. Using a ^{3}He concentration of 220 µcc/g measured in unsieved lunar regolith ilmenite (Eberhardt et al., 1972) and assuming no helium loss from extraterrestrial ilmenite on the seafloor, an average implied $^{3}He_{ET}$ flux of 0.4 pcc/cm^{2}/kyr in ancient marine sediments indicates an extraterrestrial ilmenite flux of ~9 t/yr. It is therefore important to understand the astronomical source of the continuous delivery of extraterrestrial ilmenite through geologic time.

As noted in the previous subsection, ilmenite occurs only as an accessory phase ($\ll$ 1 wt%) in most meteorites (Rubin, 1997) and is known to exist at weight-percent levels only on the Moon (Papike et al., 1982). By contrast, lunar dust is only a tiny fraction of the total cosmic dust flux. Present-day cosmic dust flux to Earth has been estimated, using various techniques, to lie between 2 and 100 kt/yr (Plane, 2012), the majority sourced from comets and asteroids (Nesvorný et al., 2010). Recently, a mass flux of 3.5 kt/yr was estimated for cosmic dust smaller than 100 µm (Fénisse et al., 2025), which is perhaps the best estimate for the fine-grained, helium- and neon-carrying dust. In comparison, secondary lunar dust flux to Earth has been modeled as ~7 t/yr (Yang et al., 2022; Yang et al., 2024).

If 10 wt% of lunar regolith is ilmenite, and assuming no fractionation during secondary lunar dust ejection and transport, ~0.7 t of lunar ilmenite would reach Earth's surface annually. This is likely an overestimate because 10 wt% is the maximum, not the average, modal abundance observed in lunar regolith (Papike et al., 1982). This indicates that more than 90 % of the extraterrestrial ilmenite flux

(~9 t/yr) needed to supply the ^{3}He in ancient marine sediments has to come from elsewhere other than the Moon. If the rest of the extraterrestrial ilmenite comes from a non-lunar source, a modal abundance of ~0.2 wt% (~8 t/yr out of ~3.5 kt/yr) is expected for the ilmenite in non-lunar cosmic dust <100 µm (Fénisse et al., 2025) . This is comparable to the fact that ilmenite is only observed as an accessory phase in most meteorites (Rubin, 1997), and indicates that the majority of extraterrestrial ilmenite flux on Earth comes from a non-lunar source (asteroids and/or comets).

However, Yang et al. (2022) have stated that the uncertainty in the estimated secondary lunar dust flux on Earth (~7 t/yr) is around one order of magnitude due to the uncertainty in the production rate of secondary lunar dust. In addition, we note that the estimated secondary lunar dust flux depends on the primary cosmic dust flux on the Moon, which has been scaled down from a primary cosmic dust of ~43 t/day (~16 t/yr; Carrillo-Sánchez et al. 2016) on Earth (Pokorný et al., 2019). Considering the large uncertainty in estimated cosmic dust flux on Earth (2–100 kt/yr; Plane 2012), the secondary lunar dust flux on Earth could be more than one order of magnitude higher than 7 t/yr and the Moon is potentially capable of supplying the majority of extraterrestrial ilmenite on Earth. This would require the ilmenite abundance in non-lunar cosmic dust <100 µm to be much lower than 0.2 wt%, which still makes it an accessory phase. Because of the large uncertainty in estimated secondary lunar dust flux and the loose constraints we have in ilmenite abundance in the non-lunar cosmic dust, we tentatively conclude that comets, asteroids, and the Moon are all sources of extraterrestrial ilmenite on Earth.

During the K1 $^3He_{ET}$ enhancement event recorded in our Site 1207 samples where He_{ET} and Ne_{ET} are carried exclusively by extraterrestrial ilmenite (Fig. 3.5), the increase in $^3He_{ET}$ flux through the main event essentially tracks the increased delivery of extraterrestrial ilmenite to Earth's surface (Fig. 3.4). We attributed the rise in $^3He_{ET}$ flux during K1 to excess dust production from a comet shower (Chapter II). Thus, part of the excess extraterrestrial ilmenite delivered during K1 may have a cometary origin, if ilmenite is present in cometary dust. However, even if cometary dust lacks ilmenite, primary cometary particles bombarding asteroid and lunar surfaces will eject secondary dust that likely includes ilmenite. The same mechanism may operate in other $^3He_{ET}$ enhancement events regardless of the primary dust source (Farley et al., 1998; Farley et al., 2006; Farley et al., 2012), with the surfaces of asteroids and the Moon activated by primary dust impacts. The ejected secondary dust will contribute to the extraterrestrial ilmenite flux wherever the parent body contains ilmenite. In this sense, asteroids and the Moon act as amplifiers of the cosmic dust signal, converting part of the primary dust into extraterrestrial ilmenite, which is a much more stable recorder that retains He_{ET} and Ne_{ET} for at least tens of millions of years after deposition on Earth.

The Moon acting as a cosmic dust amplifier may also help resolve a long-standing puzzle about the Late Miocene $^{3}He_{ET}$ enhancement event (Farley et al., 2006), which has been linked to the Veritas asteroid family disruption at ~8 Ma (Farley et al., 2006; Nesvorny et al., 2006). As discussed in Chapter II, cosmic dust subject to the Poynting–Robertson effect undergoes size sorting, with smaller grains' orbits decaying more rapidly (Burns et al., 1979). Asteroidal dust smaller than ~50 µm spirals sunward from the main belt within 10^4–10^5 yr, whereas a 200-µm particle can have a dynamic lifetime of up to 1.5 Myr (Burns et al., 1979). Because most He_{ET} in marine sediments is carried by dust <~50 µm (Farley et al., 1997b; Mukhopadhyay et al., 2006; Brook et al., 2009; McGee et al., 2010), there is an apparent conundrum: the dynamic lifetimes of 50-µm cosmic dust particles are far shorter than the 2-Myr duration of the event. To address this, a "collision-cascade" model has been invoked to continuously comminute asteroid fragments and replenish fine dust (Farley et al., 2006).

We note that although dust >~50 µm is more likely degassed during atmospheric entry and thus does not deliver He_{ET} to Earth's surface (Farley et al., 1997a; Mukhopadhyay et al., 2006; Brook et al., 2009; McGee et al., 2010), such particles impacting the lunar surface can eject secondary lunar dust <~50 µm (Horányi et al., 2015). It has been estimated that each 1 g of primary impactors on the Moon can generate ~10 g of secondary dust (Pokorný et al., 2019; Szalay et al., 2019), of which ~6 % can escape lunar gravity and ~0.12 % may eventually be accreted by Earth (Yang et al., 2022; Yang et al., 2024). More than 80 % of secondary lunar dust accreted by Earth is estimated to be smaller than 20 µm (Yang et al., 2024), compatible with observations that most He_{ET} in marine sediments is carried by dust <~50 µm (Farley et al., 1997b; Mukhopadhyay et al., 2006; Brook et al., 2009; McGee et al., 2010). Thus, such secondary lunar dust could sustain Earth's accretion of excess $^{3}He_{ET}$– and Ne_{ET}– bearing particles after primary asteroidal dust <~50 µm is depleted by the Poynting–Robertson effect.

In other words, Earth's accretion of excess He_{ET}– and Ne_{ET}– bearing cosmic dust after an asteroid-collision event may proceed in two phases. Phase 1: primary asteroidal dust from the disrupted asteroid and secondary asteroidal dust ejected from asteroids in the main asteroidal belt that are <~50 µm arrive at Earth simultaneously and deliver He_{ET} and Ne_{ET} intact; secondary lunar dust ejected from the lunar surface is also accreted with He_{ET} and Ne_{ET}. Phase 2: primary and secondary asteroidal dust >~50 µm arrive at Earth but are preferentially degassed during atmospheric entry heating. However, secondary lunar dust ejected by both primary and secondary asteroidal particles >~50 µm when they reach 1 AU remains a persistent source of He_{ET}– and Ne_{ET}– bearing particles in Phase 2. This reservoir can prolong the supply of $^3He_{ET}$–bearing dust to Earth.

Asteroidal dust with diameters of ~300 µm is expected to reach Earth and the Moon in ~2.5 Myr after release from the main belt (Burns et al., 1979). Thus, asteroidal dust in the ~50–300 µm range, despite being unable to deliver He_{ET} to Earth intact, has dynamic lifetimes sufficient to sustain secondary lunar dust production for > 2 Myr, matching the duration of the Late Miocene $^3He_{ET}$ enhancement without invoking a collision cascade. This requires that 300-µm primary and secondary asteroidal dust are still capable of ejecting excess secondary lunar regolith ilmenite that is resolvable above the background extraterrestrial ilmenite flux. Consequently, the event's duration also constrains the size distribution of dust produced in the Veritas breakup.

Although our discussion focuses on K1 and the Late Miocene $^3He_{ET}$ enhancement, asteroids and the Moon acting as amplifiers of the cosmic dust signal is likely common to similar production events (*i.e.*, comet showers and asteroid collisions). We note that our conclusions in Chapter II are unchanged by this mechanism: during a comet shower, the temporal trend of $^3He_{ET}$ flux tracks the number of active comets, as does the flux of secondary asteroidal and lunar dust ejected by primary cometary particles.

3.5 Conclusion

We conducted a comprehensive survey of global marine sediments (0–85 Ma) for their helium and neon isotopes. We find a monotonic decrease in $^{20}Ne/^3He$ with sediment age, which we attribute to preferential alteration/degassing of the high-$^{20}Ne/^3He$ non-ilmenite phases in cosmic dust on the seafloor. We interpret the low-$^{20}Ne/^3He$ component in ancient marine sediments to be extraterrestrial ilmenite, rather than undegassed cosmic dust. Extraterrestrial ilmenite is therefore crucial for reconstructing the $^3He_{ET}$ flux through geologic time, as it becomes the sole carrier phase for He_{ET} and Ne_{ET} in sediments older than ~78 Ma.

To sustain a continuous supply of extraterrestrial ilmenite, comets, asteroids, and the Moon are all plausible sources. Asteroids and the Moon are especially important: excess primary cosmic dust released during asteroid collisions or comet showers can eject secondary dust from asteroidal and lunar surfaces. In this process, part of the primary dust is converted into secondary ilmenite derived from asteroids and the Moon, which is more durable and more retentive of He_{ET} and Ne_{ET} than silicates on Earth's surface. Asteroids and the Moon thus act as amplifiers of the primary cosmic dust signal, providing a universal explanation for the observed temporal behavior of $^3He_{ET}$ enhancement events, regardless of whether their ultimate origin is asteroidal or cometary.

References

Amari, Sachiko and Minoru Ozima (1985). "Search for the Origin of Exotic Helium in Deep-Sea Sediments". In: *Nature* 317.6037, pp. 520–522. ISSN: 1476-4687. DOI: 10.1038/317520a0.

– (1988). "Extra-Terrestrial Noble Gases in Deep Sea Sediments". In: *Geochimica et Cosmochimica Acta* 52.5, pp. 1087–1095. ISSN: 0016-7037. DOI: 10.1016/0016-7037(88)90263-3.

Baur, H., U. Frick, H. Funk, L. Schultz, and P. Signer (1972). "Thermal Release of Helium, Neon, and Argon from Lunar Fines and Minerals". In: *Lunar and Planetary Science Conference Proceedings* 3, p. 1947.

Becker, Richard H and Robert O. Pepin (1989). "Long-Term Changes in Solar Wind Elemental and Isotopic Ratios: A Comparison of Two Lunar Ilmenites of Different Antiquities". In: *Geochimica et Cosmochimica Acta* 53.5, pp. 1135–1146. ISSN: 0016-7037. DOI: 10.1016/0016-7037(89)90219-6.

Benkert, Jean-Paul, Heinrich Baur, Peter Signer, and Rainer Wieler (1993). "He, Ne, and Ar from the Solar Wind and Solar Energetic Particles in Lunar Ilmenites and Pyroxenes". In: *Journal of Geophysical Research: Planets* 98.E7, pp. 13147–13162. ISSN: 2156-2202. DOI: 10.1029/93JE01460.

Black, David C. (1972). "On the Origins of Trapped Helium, Neon and Argon Isotopic Variations in Meteorites—II. Carbonaceous Meteorites". In: *Geochimica et Cosmochimica Acta* 36.3, pp. 377–394. ISSN: 0016-7037. DOI: 10.1016/0016-7037(72)90029-4.

Bradley, J. P. (2007). "1.26 - Interplanetary Dust Particles". In: *Treatise on Geochemistry*. Ed. by Heinrich D. Holland and Karl K. Turekian. Oxford: Pergamon, pp. 1–24. ISBN: 978-0-08-043751-4. DOI: 10.1016/B0-08-043751-6/01152-X.

Brady, Patrick V. and Sigurdur R. Gíslason (1997). “Seafloor weathering controls on atmospheric CO2 and global climate”. en. In: *Geochimica et Cosmochimica Acta* 61.5, pp. 965–973. ISSN: 00167037. DOI: 10.1016/S0016-7037(96)00385-7.

Bralower, T.J., I. Premoli Silva, and M.J. Malone, eds. (2006). *Proceedings of the Ocean Drilling Program, 198 Scientific Results*. Vol. 198. Proceedings of the Ocean Drilling Program. Ocean Drilling Program. DOI: 10.2973/odp.proc.sr.198.2006.

Brook, Edward J., Mark D. Kurz, and Joshua Curtice (2009). “Flux and Size Fractionation of 3He in Interplanetary Dust from Antarctic Ice Core Samples”. In: *Earth and Planetary Science Letters* 286.3, pp. 565–569. ISSN: 0012-821X. DOI: 10.1016/j.epsl.2009.07.024.

Brownlee, Donald E. (1985). “Cosmic Dust: Collection and Research”. In: *Annual Review of Earth and Planetary Sciences* 13.1, pp. 147–173. DOI: 10.1146/annurev.ea.13.050185.001051.

Burns, Joseph A., Philippe L. Lamy, and Steven Soter (1979). “Radiation Forces on Small Particles in the Solar System”. In: *Icarus* 40.1, pp. 1–48. ISSN: 0019-1035. DOI: 10.1016/0019-1035(79)90050-2.

Carrillo-Sánchez, J. D., D. Nesvorný, P. Pokorný, D. Janches, and J. M. C. Plane (2016). “Sources of Cosmic Dust in the Earth’s Atmosphere”. In: *Geophysical Research Letters* 43.23, pp. 11, 979–11, 986. ISSN: 1944-8007. DOI: 10.1002/2016GL071697.

Chavrit, Déborah, Manuel Moreira, and Frédéric Moynier (2016). “Estimation of the Extraterrestrial 3He and 20Ne Fluxes on Earth from He and Ne Systematics in Marine Sediments”. In: *Earth and Planetary Science Letters* 436, pp. 10–18. ISSN: 0012-821X. DOI: 10.1016/j.epsl.2015.12.030.

Curran, N. M., M. Nottingham, L. Alexander, I. A. Crawford, E. Füri, and K. H. Joy (2020). “A Database of Noble Gases in Lunar Samples in Preparation for Mass Spectrometry on the Moon”. In: *Planetary and Space Science* 182, p. 104823. ISSN: 0032-0633. DOI: 10.1016/j.pss.2019.104823.

Darrah, Thomas H. and Robert J. Poreda (2012). “Evaluating the Accretion of Meteoritic Debris and Interplanetary Dust Particles in the GPC-3 Sediment Core Using Noble Gas and Mineralogical Tracers”. In: *Geochimica et Cosmochimica Acta* 84, pp. 329–352. ISSN: 0016-7037. DOI: 10.1016/j.gca.2012.01.030.

Eberhardt, P., J. Geiss, H. Graf, N. Grögler, M. D. Mendia, M. Mörgeli, H. Schwaller, and A. Stettler (1972). “Trapped Solar-Wind Noble Gases in Apollo 12 Lunar Fines 12001 and Apollo 11 Breccia 10046”. In: *Third Lunar Science Conf., Geochim. Cosmochim. Acta Suppl* Vol. 2, pp. 1821–1856.

Farley, Kenneth A. (1995). “Cenozoic variations in the flux of interplanetary dust recorded by3He in a deep-sea sediment”. en. In: *Nature* 376.6536, pp. 153–156. ISSN: 0028-0836, 1476-4687. DOI: 10.1038/376153a0.

Farley, Kenneth A. (2001). “Extraterrestrial Helium in Seafloor Sediments: Identification, Characteristics, and Accretion Rate Over Geologic Time”. In: *Accretion of Extraterrestrial Matter Throughout Earth’s History*. Boston, MA: Springer US, pp. 179–204. DOI: 10.1007/978-1-4419-8694-8_11.

Farley, Kenneth A. and S. F. Eltgroth (2003). “An alternative age model for the Paleocene–Eocene thermal maximum using extraterrestrial 3He”. en. In: *Earth and Planetary Science Letters* 208.3–4, pp. 135–148. ISSN: 0012821X. DOI: 10.1016/S0012-821X(03)00017-7.

Farley, Kenneth A., S. G. Love, and Desmond B. Patterson (1997a). “Atmospheric Entry Heating and Helium Retentivity of Interplanetary Dust Particles”. In: *Geochimica et Cosmochimica Acta* 61.11, pp. 2309–2316. ISSN: 0016-7037. DOI: 10.1016/S0016-7037(97)00068-9.

– (1997b). “Atmospheric entry heating and helium retentivity of interplanetary dust particles”. en. In: *Geochimica et Cosmochimica Acta* 61.11, pp. 2309–2316. ISSN: 00167037. DOI: 10.1016/S0016-7037(97)00068-9.

Farley, Kenneth A., Alessandro Montanari, and Rodolfo Coccioni (2012). “A record of the extraterrestrial 3He flux through the Late Cretaceous”. en. In: *Geochimica et Cosmochimica Acta* 84, pp. 314–328. ISSN: 00167037. DOI: 10.1016/j.gca.2012.01.015.

Farley, Kenneth A., Alessandro Montanari, E. M. Shoemaker, and C. S. Shoemaker (1998). “Geochemical Evidence for a Comet Shower in the Late Eocene”. en. In: *Science* 280.5367, pp. 1250–1253. ISSN: 0036-8075, 1095-9203. DOI: 10.1126/science.280.5367.1250.

Farley, Kenneth A., Susan Taylor, Jonathan Treffkorn, James H. Lever, and Anthony L. Gow (2021). “3 He flux obtained from South Pole air and snow-ice and its connection to interplanetary dust particles”. en. In: *Meteoritics & Planetary Science* 56.11, pp. 1988–2001. ISSN: 1086-9379, 1945-5100. DOI: 10.1111/maps.13759.

Farley, Kenneth A., David Vokrouhlický, William F. Bottke, and David Nesvorný (2006). “A late Miocene dust shower from the break-up of an asteroid in the main belt”. en. In: *Nature* 439.7074, pp. 295–297. ISSN: 0028-0836, 1476-4687. DOI: 10.1038/nature04391.

Fénisse, G., D. V. Bekaert, P. -H. Blard, J. Duprat, I. Mattia, M. Genge, M. D. Suttle, O. Barres, C. Engrand, and Y. Marrocchi (2025). “The Extraterrestrial Dust Accretion Rate on Earth at Dome C, Antarctica: A Fresh Look with 3He”. In: *Earth and Planetary Science Letters* 663, p. 119396. ISSN: 0012-821X. DOI: 10.1016/j.epsl.2025.119396.

Fukumoto, Hirotoshi, Keisuke Nagao, and Jun-ichi Matsuda (1986). “Noble Gas Studies on the Host Phase of High 3He4He Ratios in Deep-Sea Sediments”. In: *Geochimica et Cosmochimica Acta* 50.10, pp. 2245–2253. ISSN: 0016-7037. DOI: 10.1016/0016-7037(86)90079-7.

Heber, Veronika S., Heinrich Baur, and Rainer Wieler (2003). "Helium in Lunar Samples Analyzed by High-Resolution Stepwise Etching: Implications for the Temporal Constancy of Solar Wind Isotopic Composition". In: *The Astrophysical Journal* 597.1, p. 602. ISSN: 0004-637X. DOI: 10.1086/378402.

Heber, Veronika S., Rainer Wieler, Heinrich Baur, Chad Olinger, Tom A. Friedmann, and Donald S. Burnett (2009). "Noble Gas Composition of the Solar Wind as Collected by the Genesis Mission". In: *Geochimica et Cosmochimica Acta* 73.24, pp. 7414–7432. ISSN: 0016-7037. DOI: 10.1016/j.gca.2009.09.013.

Hiyagon, Hajime (1994). "Retention of Solar Helium and Neon in IDPs in Deep Sea Sediment". In: *Science* 263.5151, pp. 1257–1259. DOI: 10.1126/science.263.5151.1257.

Horányi, M., J. R. Szalay, S. Kempf, J. Schmidt, Eberhard Grün, R. Srama, and Z. Sternovsky (2015). "A Permanent, Asymmetric Dust Cloud around the Moon". In: *Nature* 522.7556, pp. 324–326. ISSN: 1476-4687. DOI: 10.1038/nature14479.

Hudson, B., G. J. Flynn, P. Fraundorf, C. M. Hohenberg, and J. Shirck (1981). "Noble Gases in Stratospheric Dust Particles: Confirmation of Extraterrestrial Origin". en. In: *Science* 211.4480, pp. 383–386. ISSN: 0036-8075, 1095-9203. DOI: 10.1126/science.211.4480.383.

Huebner, W., T. Kirsten, and J. Kiko (1975). "Rare Gases in Apollo 17 Soils with Emphasis on Analysis of Size and Mineral Fractions of Soil 74241." In: *Lunar and Planetary Science Conference Proceedings* 2, pp. 2009–2026.

Kehm, Karl, S. Crowther, J. D. Gilmour, R. K. Mohapatra, and C. M. Hohenberg (2009). "Upper limit concentrations of trapped xenon in individual interplanetary dust particles from the stratosphere". en. In: *Meteoritics & Planetary Science* 44.2, pp. 249–259. ISSN: 1086-9379, 1945-5100. DOI: 10.1111/j.1945-5100.2009.tb00732.x.

Kehm, Karl, George J. Flynn, and Charles M. Hohenberg (2006). "Noble Gas Space Exposure Ages of Individual Interplanetary Dust Particles". In: *Meteoritics & Planetary Science* 41.8, pp. 1199–1217. ISSN: 1945-5100. DOI: 10.1111/j.1945-5100.2006.tb00516.x.

Krylov, A. Ya, B. A. Mamyrin, Yu. I. Silin, and L. V. Khabarin (1973). "Helium Isotopes in Ocean Sediments". In: *Geochem. Int.* 10, pp. 202–205.

Love, S. G. and Donald E. Brownlee (1991). "Heating and Thermal Transformation of Micrometeoroids Entering the Earth's Atmosphere". In: *Icarus* 89.1, pp. 26–43. ISSN: 0019-1035. DOI: 10.1016/0019-1035(91)90085-8.

Marcantonio, Franco, Sean Higgins, Robert F. Anderson, Martin Stute, Peter Schlosser, and E. Troy Rasbury (1998). "Terrigenous Helium in Deep-Sea Sediments". In: *Geochimica et Cosmochimica Acta* 62.9, pp. 1535–1543. ISSN: 0016-7037. DOI: 10.1016/S0016-7037(98)00091-X.

Marcantonio, Franco, Deborah J. Thomas, Stella Woodard, David McGee, and Gisela Winckler (2009). "Extraterrestrial 3He in Paleocene Sediments from Shatsky Rise: Constraints on Sedimentation Rate Variability". In: *Earth and Planetary Science Letters* 287.1, pp. 24–30. ISSN: 0012-821X. DOI: 10.1016/j.epsl.2009.07.029.

Matsuda, Jun-ichi, Miho Murota, and Keisuke Nagao (1990). "He and Ne Isotopic Studies on the Extraterrestrial Material in Deep-Sea Sediments". In: *Journal of Geophysical Research: Solid Earth* 95.B5, pp. 7111–7117. ISSN: 2156-2202. DOI: 10.1029/JB095iB05p07111.

McGee, David, Franco Marcantonio, Jerry F. McManus, and Gisela Winckler (2010). "The Response of Excess 230Th and Extraterrestrial 3He to Sediment Redistribution at the Blake Ridge, Western North Atlantic". In: *Earth and Planetary Science Letters* 299.1-2, pp. 138–149. ISSN: 0012821X. DOI: 10.1016/j.epsl.2010.08.029.

Merrihue, Craig (1964). "Rare Gas Evidence for Cosmic Dust in Modern Pacific Red Clay". In: *Annals of the New York Academy of Sciences* 119.1, pp. 351–367. ISSN: 1749-6632. DOI: 10.1111/j.1749-6632.1965.tb47445.x.

Montanari, Alessandro, Kenneth A. Farley, Rodolfo Coccioni, N. Sabatino, D. Bice, M. Yesko, M. Sinnesael, and N. de Winter (2023). "Cosmogenic 3He Anomaly K1 vs. the Early Campanian Isotopic Event (ECE) as Recorded in Pelagic Limestones of the Umbria-Marche Succession (Italy)". In: *GSA Bulletin* 136.3-4, pp. 1753–1767. ISSN: 0016-7606. DOI: 10.1130/B36952.1.

Moreira, Manuel (2013). "Noble Gas Constraints on the Origin and Evolution of Earth's Volatiles". In: *Geochemical Perspectives* 2.2, pp. 229–230. ISSN: 2223-7755.

Moreira, Manuel and Sébastien Charnoz (2016). "The Origin of the Neon Isotopes in Chondrites and on Earth". In: *Earth and Planetary Science Letters* 433, pp. 249–256. ISSN: 0012-821X. DOI: 10.1016/j.epsl.2015.11.002.

Mukhopadhyay, Sujoy and Kenneth A. Farley (2006). "New Insights into the Carrier Phase(s) of Extraterrestrial 3He in Geologically Old Sediments". In: *Geochimica et Cosmochimica Acta* 70.19, pp. 5061–5073. ISSN: 0016-7037. DOI: 10.1016/j.gca.2006.06.1566.

Nesvorny, D, D Vokrouhlicky, W Bottke, and M Sykes (2006). "Physical properties of asteroid dust bands and their sources". en. In: *Icarus* 181.1, pp. 107–144. ISSN: 00191035. DOI: 10.1016/j.icarus.2005.10.022.

Nesvorný, David, Peter Jenniskens, Harold F. Levison, William F. Bottke, David Vokrouhlický, and Matthieu Gounelle (2010). "COMETARY ORIGIN OF THE ZODIACAL CLOUD AND CARBONACEOUS MICROMETEORITES. IMPLICATIONS FOR HOT DEBRIS DISKS". In: *The Astrophysical Journal* 713.2, p. 816. ISSN: 0004-637X. DOI: 10.1088/0004-637X/713/2/816.

Nier, Alfred O. and Dennis J. Schlutter (1990a). "Helium and neon isotopes in stratospheric particles". en. In: *Meteoritics* 25.4, pp. 263–267. ISSN: 0026-1114. DOI: 10.1111/j.1945-5100.1990.tb00710.x.

– (1992). "Extraction of Helium from Individual Interplanetary Dust Particles by Step-Heating". In: *Meteoritics* 27.2, pp. 166–173. ISSN: 1945-5100. DOI: 10.1111/j.1945-5100.1992.tb00744.x.

Nier, Alfred O., Dennis J. Schlutter, and Donald E. Brownlee (1990b). "Helium and Neon Isotopes in Deep Pacific Ocean Sediments". In: *Geochimica et Cosmochimica Acta* 54.1, pp. 173–182. ISSN: 0016-7037. DOI: 10.1016/0016-7037(90)90205-Y.

Ozima, Minoru, M. Takayanagi, S. Zashu, and Sachiko Amari (1984). "High 3He/4He Ratio in Ocean Sediments". In: *Nature* 311.5985, pp. 448–450. ISSN: 1476-4687. DOI: 10.1038/311448a0.

Papike, J. J., S. B. Simon, and J. C. Laul (1982). "The Lunar Regolith: Chemistry, Mineralogy, and Petrology". In: *Reviews of Geophysics* 20.4, pp. 761–826. ISSN: 1944-9208. DOI: 10.1029/RG020i004p00761.

Patterson, Desmond B. and Kenneth A. Farley (1998a). "Extraterrestrial 3He in Seafloor Sediments: Evidence for Correlated 100 Kyr Periodicity in the Accretion Rate of Interplanetary Dust, Orbital Parameters, and Quaternary Climate". In: *Geochimica et Cosmochimica Acta* 62.23, pp. 3669–3682. ISSN: 0016-7037. DOI: 10.1016/S0016-7037(98)00263-4.

Patterson, Desmond B., Kenneth A. Farley, and Birger Schmitz (1998b). "Preservation of Extraterrestrial 3He in 480-Ma-old Marine Limestones". In: *Earth and Planetary Science Letters* 163.1, pp. 315–325. ISSN: 0012-821X. DOI: 10.1016/S0012-821X(98)00197-6.

Pavia, Frank J., Jordan T. Abell, Jennifer L. Middleton, Annie Leal, Sebastian M. Vivancos, Martin Q. Fleisher, Gisela Winckler, and Robert F. Anderson (2024). "Discrepant Mass Accumulation Rates of Sediments in the South Pacific Ocean from 230Th and 3He Measurements". In: *Geochimica et Cosmochimica Acta* 365, pp. 215–228. ISSN: 0016-7037. DOI: 10.1016/j.gca.2023.11.019.

Pepin, Robert O., R. L. Palma, and Dennis J. Schlutter (2000). "Noble Gases in Interplanetary Dust Particles, I: The Excess Helium-3 Problem and Estimates of the Relative Fluxes of Solar Wind and Solar Energetic Particles in Interplanetary Space". In: *Meteoritics & Planetary Science* 35.3, pp. 495–504. ISSN: 1945-5100. DOI: 10.1111/j.1945-5100.2000.tb01431.x.

Pepin, Robert O., Dennis J. Schlutter, Richard H. Becker, and Daniel B. Reisenfeld (2012). "Helium, Neon, and Argon Composition of the Solar Wind as Recorded in Gold and Other Genesis Collector Materials". In: *Geochimica et Cosmochimica Acta* 89, pp. 62–80. ISSN: 0016-7037. DOI: 10.1016/j.gca.2012.04.024.

Peucker-Ehrenbrink, B., Greg Ravizza, and Gisela Winckler (2016). "Geochemical Tracers of Extraterrestrial Matter in Sediments". en. In: *Elements* 12.3, pp. 191–196. ISSN: 1811-5209, 1811-5217. DOI: 10.2113/gselements.12.3.191.

Plane, John M. C. (2012). "Cosmic Dust in the Earth's Atmosphere". In: *Chemical Society Reviews* 41.19, pp. 6507–6518. DOI: 10.1039/C2CS35132C.

Pokorný, Petr, Diego Janches, Menelaos Sarantos, Jamey R. Szalay, Mihály Horányi, David Nesvorný, and Marc J. Kuchner (2019). "Meteoroids at the Moon: Orbital Properties, Surface Vaporization, and Impact Ejecta Production". In: *Journal of Geophysical Research: Planets* 124.3, pp. 752–778. ISSN: 2169-9100. DOI: 10.1029/2018JE005912.

Rubin, Alan E. (1997). "Mineralogy of meteorite groups". en. In: *Meteoritics & Planetary Science* 32.2, pp. 231–247. ISSN: 1086-9379, 1945-5100. DOI: 10.1111/j.1945-5100.1997.tb01262.x.

Sano, Yuji, Bernard Marty, and Pete Burnard (2013). "Noble Gases in the Atmosphere". In: *The Noble Gases as Geochemical Tracers*. Ed. by Pete Burnard. Berlin, Heidelberg: Springer, pp. 17–31. ISBN: 978-3-642-28836-4. DOI: 10.1007/978-3-642-28836-4_2.

Signer, P., H. Baur, U. Derksen, P. Etique, H. Funk, P. Horn, and R. Wieler (1977). "Helium, Neon, and Argon Records of Lunar Soil Evolution." In: *Lunar and Planetary Science Conference Proceedings* 3, pp. 3657–3683.

Szalay, J. R., P. Pokorný, Z. Sternovsky, Z. Kupihar, A. R. Poppe, and M. Horányi (2019). "Impact Ejecta and Gardening in the Lunar Polar Regions". In: *Journal of Geophysical Research: Planets* 124.1, pp. 143–154. ISSN: 2169-9100. DOI: 10.1029/2018JE005756.

Takayanagi, M. and Minoru Ozima (1987). "Temporal Variation of 3He/4He Ratio Recorded in Deep-Sea Sediment Cores". In: *Journal of Geophysical Research: Solid Earth* 92.B12, pp. 12531–12538. ISSN: 2156-2202.

Weber, H. W. and L. Schultz (1979). "On the Fractionation of Heavy Noble Gases during the Agglutination Process". In: *Lunar and Planetary Science Conference*, pp. 1322–1324.

White, Art F, Maria L Peterson, and Michael F Hochella (1994). "Electrochemistry and dissolution kinetics of magnetite and ilmenite". en. In: *Geochimica et Cosmochimica Acta* 58.8, pp. 1859–1875. ISSN: 00167037. DOI: 10.1016/0016-7037(94)90420-0.

Wieler, R. and P. Signer (1983). "Noble Gas Release by On-Line Etching of Lunar Soil Mineral Separates." In: *Meteoritics* 18, pp. 420–421. ISSN: 0026-1114.

Yang, Kun, Yu Jiang, Youpeng Liang, and Xiaodong Liu (2024). "Investigation of Lunar Ejecta Dynamics: Particles Reaching the near-Earth Space and Their Effect on Earth-based Observation". In: *Astronomy & Astrophysics* 692, A185. ISSN: 0004-6361, 1432-0746. DOI: 10.1051/0004-6361/202348697.

Yang, Kun, Jürgen Schmidt, Weiming Feng, and Xiaodong Liu (2022). "Distribution of Dust Ejected from the Lunar Surface into the Earth-Moon System". In: *Astronomy & Astrophysics* 659, A120. ISSN: 0004-6361, 1432-0746. DOI: 10.1051/0004-6361/202140810.

Yatsevich, Igor and Masahiko Honda (1997). "Production of Nucleogenic Neon in the Earth from Natural Radioactive Decay". In: *Journal of Geophysical Research: Solid Earth* 102.B5, pp. 10291–10298. ISSN: 2156-2202. DOI: 10.1029/97JB00395.

Chapter 4

THE EARTH: DOES CLIMATE FEEL COSMIC DUST?

4.1 Introduction

The Late Eocene witnessed some of the most significant changes in Earth's climate in the last 66 Myr. The cooling trend that began with the Early Eocene Climate Optimum at ~47 Ma reached a tipping point at the Eocene-Oligocene Boundary (EOB) at ~34 Ma (Westerhold et al., 2020), when the Earth experienced a rapid warmhouse-icehouse transition. This is manifested by a sharp positive shift in the global marine δ^{18}O record (Zachos et al., 2001; Zachos et al., 2008; Cramer et al., 2009; Miller et al., 2020) and the initiation of Antarctic glaciation (Lear et al., 2000).

Simultaneously, the Solar System was unusually active. Multiple bolide impacts occurred within this era (Koeberl, 2009; Schmieder et al., 2020), including the two largest craters in the Cenozoic: Popigai (~100 km in diameter) and Cheasapeake Bay (40–85 km in diameter). There was also a 2-Myr enhancement in the flux of cosmic dust (*i.e.*, sub-millimeter extraterrestrial dust particles from asteroids or comets) between ~34 Ma and ~36 Ma, based on ^{3}He records in marine sediments (known as the Late Eocene ^{3}He enhancement event; Farley 1995; Farley et al. 1998). Extraterrestrial ^{3}He (^{3}He$_{ET}$) in marine sediments and limestone has been routinely analyzed to track changes in cosmic dust flux due to the distinctively high ^{3}He/^{4}He in cosmic dust (~10^{-4}; *e.g.*, Nier et al. 1990) compared to terrestrial components in marine sediments (10^{-8}–10^{-6}; *e.g.*, Merrihue 1964; Takayanagi et al. 1987). Larger meteorites and micrometeorites (a subset of cosmic dust between a few hundreds of µm and ~2000 µm) more readily lose He during atmospheric entry heating, which makes ^{3}He$_{ET}$ uniquely a tracer of fine cosmic dust particles smaller than a few tens of µm (Farley et al., 1997; McGee et al., 2010).

Was Late Eocene climate sensitive to the enhanced flux of extraterrestrial material? Several previous studies assessed the climatic and environmental effects of the bolide impacts. These studies analyzed δ^{18}O and δ^{13}C across the impact horizons in marine sediments, or assessed the variations in nannofossil assemblages, but yielded inconsistent results. Some reported a cooling pulse at the impact horizons (Coccioni et al., 2000; Vonhof et al., 2000; Spezzaferri et al., 2002; Śliwińska et al., 2019), while others reported warming pulses instead (Bodiselitsch et al., 2004), or no change in Earth's sea surface temperature (Pusz et al., 2009; Wade et al., 2024). Similarly, both an enhanced (Vonhof et al., 2000) and a decreased marine primary productivity (Pusz et al., 2009) were suggested. These conflicting results potentially reflect spatial heterogeneity in the climatic and environmental responses to the impacts. Alternatively, since climatic responses to impacts were estimated to only last a few decades (Vellekoop et al., 2014; Artemieva et al., 2017; Brugger et al., 2017; Tabor et al., 2020; Morgan et al., 2022; Senel et al., 2023), these inconsistencies could also result from undersampling of the transient climatic responses due to sampling resolutions typically longer than ~5 kyr (Vonhof et al., 2000; Bodiselitsch et al., 2004; Pusz et al., 2009; Śliwińska et al., 2019; Wade et al., 2024).

In contrast, the climatic and environmental consequences of the ~2-Myr enhancement in cosmic dust flux during the Late Eocene (Farley et al., 1998) remain poorly constrained. The modern cosmic dust accretion rate is estimated to range from 5 to 270 tons/day, depending on the method of estimation (Plane, 2012). Assuming that the pre-event accretion rate in the Late Eocene was comparable to the present-day value, we calculated that a total of ~10^{15}–10^{17} g of excess cosmic dust was deposited on Earth by integration across the entire duration of the Late Eocene ^{3}He enhancement event (Fig. 4.1). For comparison, the Chicxulub impact at the Cretaceous–Paleogene boundary injected approximately 10^{16}–10^{19} g of micron- to submicron-sized silicate dust from target rocks into the atmosphere (Toon et al., 2016), which encircled the Earth within 4–5 hours (Morgan et al., 2022). The residence time of such fine dust particles in the atmosphere is estimated to range from several months to ~10 years (Tabor et al., 2020; Senel et al., 2023), long enough to reduce solar radiation and trigger an "impact winter" (Vellekoop et al., 2014; Artemieva et al., 2017; Brugger et al., 2017; Tabor et al., 2020; Morgan et al., 2022; Senel et al., 2023). The Late Eocene ^{3}He enhancement event represents a comparable total mass of dust injection, albeit over a much longer timescale, yet its potential climatic and environmental effects have not previously been evaluated.

The ^{3}He record (Farley et al., 1998) and stable isotope records (Bodiselitsch et al., 2004; Jovane et al., 2007) from the Massignano section provide some hints of a possible climatic or environmental sigificance of the Late Eocene ^{3}He event. Although the peak of the ^{3}He enhancement predates the EOB by ~2 Myr, its gradual decline appears to extend into the boundary interval (Fig. 4.1). This raises the question of whether the 2-Myr enhancement in cosmic dust flux could have

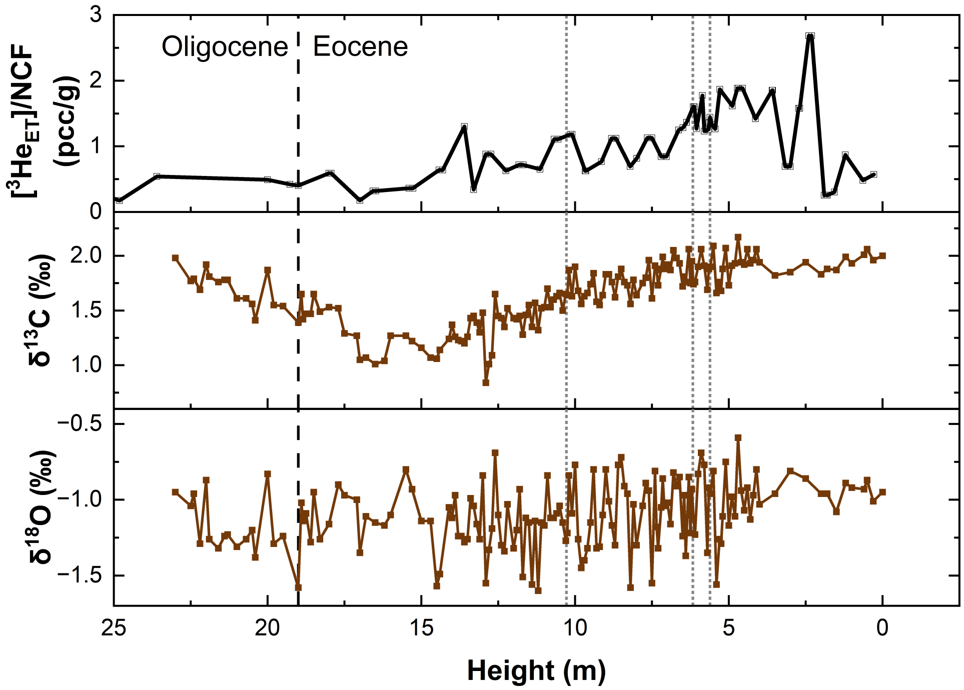

Figure 4.1: [$^3He_{ET}$]/NCF (Farley et al., 1998) and bulk carbonate stable isotopes (Bodiselitsch et al., 2004) measured in the pelagic limestone from Massignano, Italy. [$^3He_{ET}$]/NCF (extraterrestrial ^{3}He normalized to the non-carbonate fraction of limestone) tracks changes in cosmic dust flux, and is binned with a bin size of 20 cm to better reveal the long-term trends. Dashed vertical line at 19 m is the global stratotype section and point (GSSP) for the Eocene-Oligocene boundary (EOB) fixed in Massignano (Silva et al., 1993). Dotted vertical lines at 5.61 m, 6.17 m, and 10.28 m are identified Ir anomalies and impact ejecta layers at Massignano (Montanari et al., 1993; Clymer et al., 1996; Bodiselitsch et al., 2004; Glass et al., 2004), likely resulting from bolide impacting events in the Late Eocene.(Montanari et al., 2023)

contributed to the warmhouse–icehouse transition at the EOB. Bodiselitsch et al. (2004) compared the ^{3}He record (Farley et al., 1998) with their stable isotope data, both from the Massignano section, but their discussion focused on bolide impacts rather than sustained cosmic dust input. Although the bulk carbonate δ^{18}O record shows no clear trend, both bulk δ^{13}C and [$^3He_{ET}$]/NCF (the $^3He_{ET}$ concentration in the non-carbonate fraction, a proxy for cosmic dust flux) decrease between ~5 and ~17 msl (Fig. 4.1). This decline in δ^{13}C was later confirmed by Jovane et al. (2007) using analyses of Agrenocythere ostracods from the same section, effectively ruling out the effect of diagenetic alteration on δ^{13}C. The observed co-variation between δ^{13}C and cosmic dust flux could, in principle, reflect changes in global ocean primary productivity driven by enhanced cosmic dust input.

However, comparisons between the Massignano records and open-ocean records suggest that the Massignano $\delta^{13}C$ variations may reflect a localized Tethyan signal rather than a global one, due to the progressive isolation of the Tethys region from the open ocean circulation (Jovane et al., 2007). Although the ostracod $\delta^{18}O$ record is less noisy than the bulk carbonate record and captures some short-term excursions seen in global datasets, it lacks the characteristic ~1‰ positive shift in $\delta^{18}O$ at the EOB (Jovane et al., 2007). These discrepancies imply that the Massignano $\delta^{18}O$ records may reflect regional conditions or have been affected by diagenesis (Bodiselitsch et al., 2004; Jovane et al., 2007). Therefore, the global climatic and environmental response to the Late Eocene ^3He event cannot be reliably inferred from the Massignano stable isotope and ^3He data alone. A sedimentary archive from an open-ocean setting preserving both stable isotope and ^3He records is needed to assess the global signal.

On a theoretical level, could a factor-of-five increase in cosmic dust flux during the Late Eocene ^3He event have had any climatic or environmental impact? The modern cosmic dust flux of 5–270 tons/day (Plane, 2012) is minuscule compared to the present-day atmospheric dust loading of ~26 million tons (Kok et al., 2023). However, unlike terrestrial dust sourced from deserts, cosmic dust is injected directly into the upper atmosphere. Given their sub-millimeter sizes, such particles can persist in the atmosphere for much longer, potentially on the order of $\sim 10^1$ years (Jasper Kok, personal communication). Under present-day conditions, this corresponds to a steady-state cosmic dust loading of ~0.02–1 million tons. If similar residence times applied in the Late Eocene, the enhanced cosmic dust flux during the ^3He event could have increased the total atmospheric dust burden by 0.4–20 % (Fig. 4.2), thereby altering Earth's radiative balance (Kok et al., 2023). Such an increase could have affected surface temperature, potentially similar to post-impact cooling after Chicxulub (Vellekoop et al., 2014; Artemieva et al., 2017; Brugger et al., 2017; Tabor et al., 2020; Morgan et al., 2022; Senel et al., 2023) and could have left a signature in global ocean $\delta^{18}O$ records.

At the same time, the enhanced cosmic dust flux during the Late Eocene ^3He event could have increased the delivery of bioavailable iron to the oceans. Assuming a modern cosmic-dust-derived bioavailable Fe flux of ~0.35 µmol/m^2/yr (Reiners et al., 2018), a fivefold increase in dust flux would raise this to ~1.8 µmol/m^2/yr. If the total global ocean Fe input was, as today, dominated by eolian sources on the order of

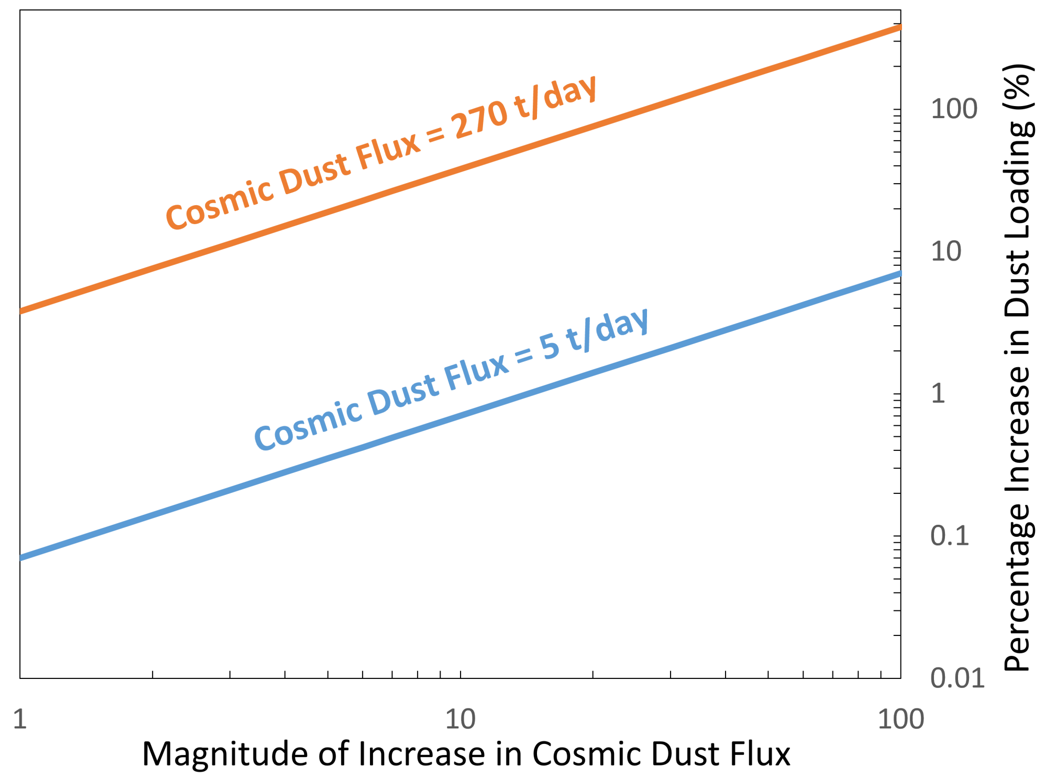

Figure 4.2: Extent of expected perturbation of cosmic dust flux to total atmospheric dust loading. The two lines show the upper and lower limit of estimated cosmic dust flux on Earth today, estimated with different methods (Plane, 2012). Total atmospheric dust loading is assumed to be 26 million tons (Kok et al., 2023). A residence time of 10 years for cosmic dust have been used for the calculations.

50–100 μmol/m^2/yr, the global bioavailable Fe flux would have increased by roughly 2–4 % (Reiners et al., 2018). Using the full present-day range of 5–270 tons day^{-1} for cosmic dust flux (Plane, 2012), the increase in bioavailable Fe flux could range from 0.1–10 %. If marine primary productivity responded positively to this additional Fe input, the global ocean δ^{13}C record would be expected to shift toward heavier values (Johnson, 2001; Reiners et al., 2018). This predicted trend is opposite in direction to the observed decline in δ^{13}C at Massignano, though, as noted above, the Massignano signal may be regional rather than global.

Although several ^{3}He records (Farley et al., 2006) and stable isotope records (*e.g.*, Cramer et al. 2009 and references therein) from open-ocean settings are already available, uncertainties in their age models make it difficult to align these datasets directly, as they were obtained from different sediment cores. To overcome this limitation, we constructed a parallel sedimentary record containing both ^{3}He and stable isotope measurements from the same open-ocean drill core from ODP

Site 1209 to directly assess of the relationship between $^{3}He_{ET}$ flux and stable isotope variations. We chose this site because these sediments were deposited in the northwest Pacific Ocean and should have recorded an open-ocean signal. Furthermore, since these sediments were unconsolidated, we expected them to be less subject to diagenic isotopic modifications. As we will show later in the Discussion, this site turns out to be much more complicated in its sedimentary environment than expected, which made it difficult for age model construction and interpreting both helium and stable isotope records we obtained. Nevertheless, with a more complete deep-sea sediment record of the Late Eocene, we assessed Earth's climatic and environmental response to enhanced cosmic dust based on our new stable isotope and helium isotope data.

4.2 Materials and Methods

Samples

Site 1209 is located on Shatsky Rise, a large igneous province in the northwest Pacific (Bralower et al., 2002). Shatsky Rise consists of three bathymetric highs from north to south, with Site 1209 being close to the center of the most elevated southern high (the Tamu massif) at 2387 m water depth (Bralower et al., 2002). Three holes were drilled at this site, recovering a total of ~300 m of nannofossil ooze and nannofossil ooze with clay from present to lower Maastrichtian (Late Cretaceous; Bralower et al., 2002). Shatsky Rise has been distant from continental margins since its formation in the Equatorial Pacific in the Late Jurassic/Early Cretaceous and during its subsequent northward migration (Nakanishi et al., 1999), which makes it an ideal site to study an open-ocean sedimentary record in the Paleogene.

An apparently complete sediment sequence across the EOB was recovered at Site 1209, with an evident but gradual sediment color transition from light brown/tan in the upper Eocene to light gray/white in the lower Oligocene. This transition was interpreted to arise from deepening of the lysocline across the EOB (Bralower et al., 2002), which has been reported across the tropical Pacific (Coxall et al., 2005). Sediments in this interval have relatively high carbonate contents (> 60 wt%), showing that this site was well-above the carbonate compensation depth (CCD).

However, recent geochemistry and biostratigraphy studies of Site 1209 have reported intervals of intense carbonate dissolution (Bhattacharya et al., 2020; Viganò et al., 2023), which may reflect the temporary shoaling of the lysocline. Due to these carbonate dissolution horizons, the preservation status of calcareous nannofossils is poor to very poor and multiple biohorizons were identified with conflicts (Table 4.1). Nevertheless, the Top of *Ericsonia formosa* (32.92 Ma; Agnini et al, 2014) identified at 132.83 ± 0.08 adj. rmcd[1] (Viganò et al., 2023) and the Base of *Reticulofenestra umbilicus* (42.67 Ma; Agnini et al, 2014) identified between 155.615 ± 0.240 m (Bralower et al., 2006) bracket the Late Eocene ^{3}He enhancement event that lasted from 34 Ma to 36 Ma. As a result, we analyzed a total of 44 samples from ODP Site 1209, Hole C, Core 4H, between 139.72 m and 145.51 m.

Table 4.1: Biohorizons identified close to our studied section at Site 1209 and their ages.

Biohorizons	**Adj. rmcd (m)**	**Age (Ma)**
LO *Ericsonia formosa*[1]	132.83 ± 0.08	32.92[3]
LO *Chiasmolithus grandis*[2]	137.730 ± 1.275	37.77[3]
LO *Discoaster saipanensis*[1]	139.73 ± 0.13	34.62[4]
LO *Discoaster barbadiensis*[1]	139.73 ± 0.13	34.77[3]
Bc *Clausicoccus subdistichus*[1]	140.23 ± 0.13	33.88[3]
LO *Hantkenina* spp.[2]	140.055 ± 0.475	33.90[5] or 34.09[4]
FO *Dictyococcites bisectus*[2]	148.076 ± 0.273	40.34[3]
FO *Sphenolithus obtusus*[2]	154.625 ± 0.750	39.31–40.13[6,7]
FO *Reticulofenestra umbilicus*[2]	155.615 ± 0.240	42.67[3]

References: 1. Viganò et al. (2023); 2. Bralower et al. (2006); 3. Agnini et al. (2014); 4. Sahy et al. (2017); 5. Hutchinson et al. (2021); 6. Fornaciari et al. (2010); 7. (Toffanin et al., 2013)

Helium Isotopes

Samples for helium isotope measurements were prepared in the same way described in Chapter II & III. Around 2–5 g of bulk sediments were freeze-dried, weighed, then leached with 10 v/v% acetic acid to remove carbonate. The insoluble residue was rinsed with deionized water three times, then freeze-dried and collected. The mass fraction of the insoluble residue was recorded as the NCF (non-carbonate fraction) of each bulk sediment sample. Around 30–100 mg of each residue sample was subsampled and wrapped in tin foil, before loaded into the auto-sampler of the mass spectrometer. Helium extraction, purification, and measurement followed the same protocol described in Chapter II.

The sensitivity and pressure nonlinearity of the mass spectometer was calibrated with a synthetic helium gas standard with a ^{3}He/^{4}He ratio of 2.05 R_A. Based on

[1]adj. rmcd: adjusted revised meter composite depth (Bralower et al., 2005). For simplicity, "adj. rmcd" is written as "m" in the rest of the chapter.

replicate measurements on gas standards with similar ^{4}He partial pressures to each sample gas, the analytical precision was determined to be better than 1 % for both ^{3}He and ^{4}He. The blank levels for both ^{3}He and ^{4}He were < 0.5 %, and no blank correction was performed.

We have observed a few measurements with abnormally high ^{3}He concentrations and ^{3}He/^{4}He than their replicates. These measurements likely resulted from the inclusion of rare ^{3}He-rich cosmic dust particles dominating the ^{3}He budget of a sample (the "nugget effect"; *e.g.*, Patterson et al. 1998. We have defined a measurement biased by "nuggets" as a one that is more than 40 % higher in [^{3}He] (bulk sediment ^{3}He concentration) than the average of the replicated measurements (Patterson et al., 1998). In this way, we have identified and rejected 5 measurements in the total of 80 measurements.

Stable Isotopes

Bulk sediment stable isotope ratios were measured at the Stable Isotope Laboratory, University of California, Santa Cruz, on a Thermo Scientific MAT 253 Isotope Ratio Mass Spectrometer coupled to a Thermo Scientific Kiel IV autocarbonate device. The results were calibrated to Vienna PeeDee Belemnite ‰ (vPDB ‰) using NBS-18 and CM-12 as standards. The analytical precision was better than 0.02 ‰ for δ^{13}C and better than 0.13 ‰ for δ^{18}O based on reproducibility of standards.

4.3 Results

Bulk carbonate δ^{13}C varies between 1.07 ‰ (VPDB) and 2.43 ‰ (Fig. 4.3). It is relatively constant between 142.12 m and 145.51 m, with a mean of 2.17 ± 0.14 ‰. A negative shift of ~0.5 ‰ occurs between 144.12 m and 144.22 m. A much more substantial negative shift occurs from 142.12 m to 141.12 m, where δ^{13}C decreases by ~1.2 ‰.

Bulk carbonate δ^{18}O ranges between –0.83 ‰ and 0.68 ‰ (Fig. 4.3). It gradually increases from ~0.0 ‰ (145.51 m) to ~0.4 ‰ (142.30 m). It then decreases to ~–0.8 ‰ (141.92 m), nearly coincident with δ^{13}C, and stays relatively constant through the rest of the studied section.

We report helium results as the average of replicate measurements ("nugget"-corrected; Fig. 4.3). [^{3}He] (bulk sediment ^{3}He concentration) ranges from 0.50 pcc/g (pcc: 10^{-12} cm^3 at standard temperature and pressure) to 7.2 pcc/g. [^{4}He] ranges from 8.1 ncc/g (ncc: 10^{-9} cm^3 at standard temperature and pressure) and

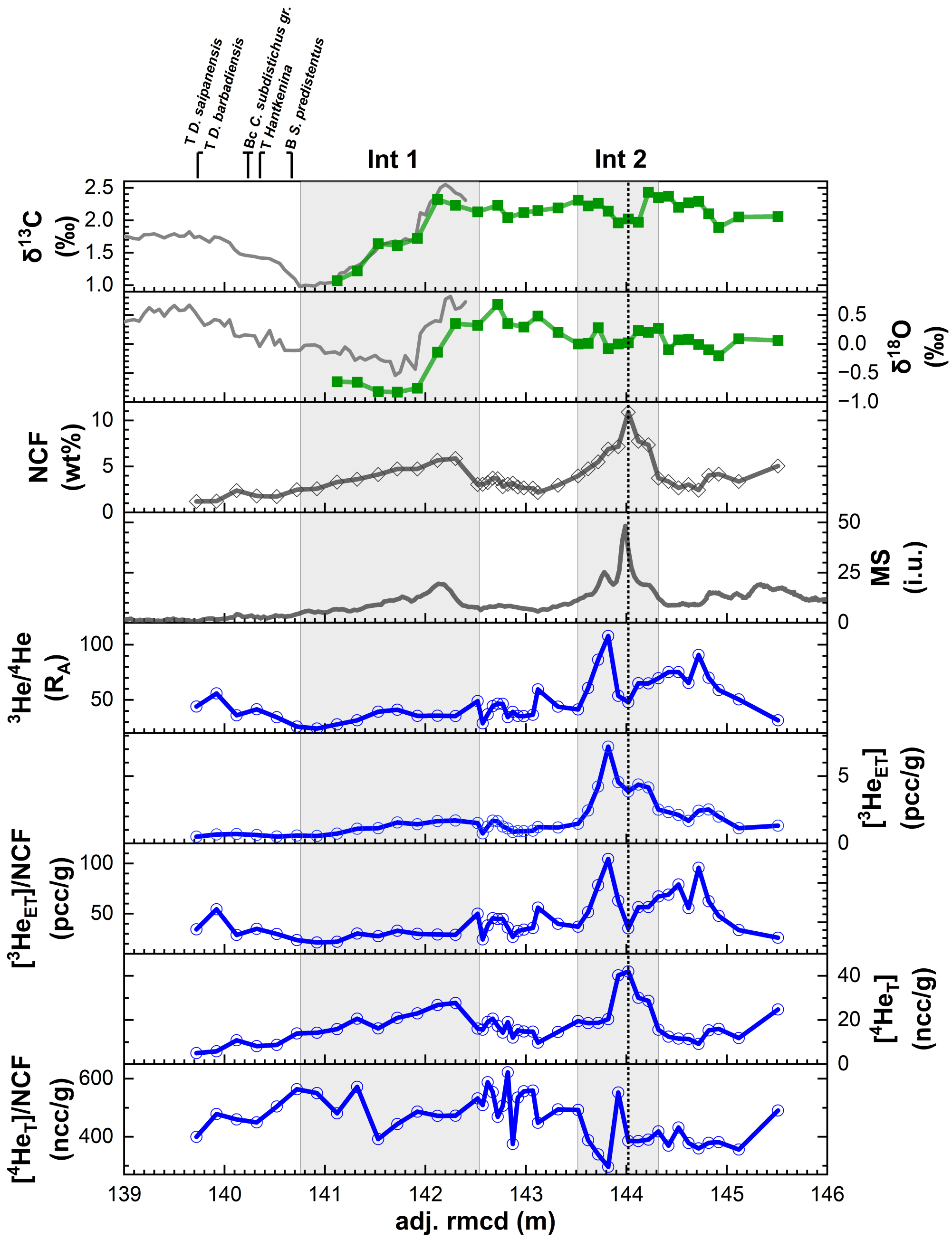

73 ncc/g. ^{3}He/^{4}He ranges between 24 R_A (1 R_A = 1.382 × 10^{-6}, which is the atmospheric ^{3}He/^{4}He; Sano et al. (2013)) and 91 R_A. It increases from 31 R_A at 145.51 m to 91 R_A at 144.72 m, then gradually decreases to 48 R_A at 144.02 m, above which it starts to increase again. A second peak of 108 R_A occurs at 143.82 m.

Figure 4.3: Bulk carbonate stable isotope ratios, helium isotope data, non-carbonate fraction (NCF), and magnetic susceptibility (MS) depth profile in our studied section. The green curves in the stable isotope records are from this study, while the grey curves are previous data on bulk sediments from Site 1209, Hole C (Viganò et al., 2023). MS data covering our studied section comes from Shipboard measurements (Bralower et al., 2002). NCF and helium isotope data are average values of replicate measurements, excluding those that experience "nugget effects". Shaded areas indicate two intervals (Int 1, Int 2) of increasing NCF. The vertical dotted line shows the location of the highest NCF in our studied section. Identified biohorizons within our studied section (Viganò et al., 2023) are shown on the top.

Helium in marine sediments is as a mixture of two sources: terrigenous sediments and fine cosmic dust particles. With a terrigenous endmember $^3He/^4He$ of 0.01–0.03 R_A (Takayanagi et al., 1987; Marcantonio et al., 1998; Patterson et al., 1998) and an extraterrestrial endmember $^3He/^4He$ of ~200 R_A (Nier et al., 1990), the relative contribution of the two mixing sources can be mathematically deconvolved (Takayanagi et al., 1987; Patterson et al., 1998). In our studied section, more than 99.9 ‰ of ^3He is extraterrestrial ($^3He_{ET}$), and 48–86 ‰ of ^4He is terrigenous (^4He_T). The range of [$^3He_{ET}$] is the same as [^3He] within the reported precision. An interval with elevated [$^3He_{ET}$] occurs between 143.5 m and 145.4 m, with a peak of 7.2 pcc/g at 143.8 m. [^4He_T] ranges between 5.8 ncc/g and 43 ncc/g. Two elevated intervals occur between 143 m and 144.5 m and above 142.5 m.

We also report [$^3He_{ET}$] and [^4He_T] normalized to NCF. NCF is not identical to the the absolute carbonate content determined with coulometry, for example, but it tracks the relative variations in carbonate contents in the sediments. In our studied interval, NCF ranges from 1.2 wt‰ in the uppermost samples to 11 wt‰ at 144.02 m (Fig. 4.3). Two intervals of elevated NCF are observed between 143.1 m to 144.5 m and between 141.0 m and 142.5 m. Such variations could result from changes in the non-carbonate flux (terrigenous and authigenic minerals), or changes in the carbonate production rate/preservation efficiency, or both (see Discussion).

We found [$^3He_{ET}$]/NCF to range between 21 pcc/g and 104 pcc/g. It has a similar depth profile to $^3He/^4He$, with two peaks, at 144.7 m and 143.8 m. [^4He_T]/NCF ranges between 329 ncc/g and 619 ncc/g.

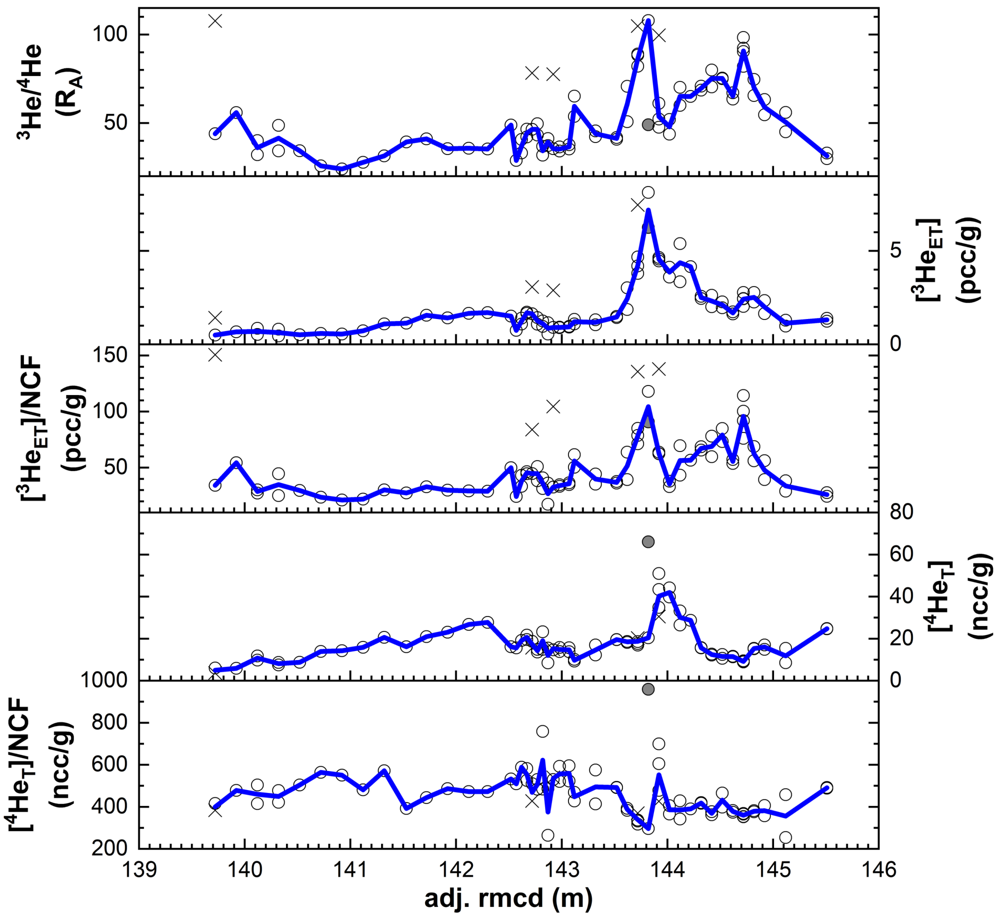

Figure 4.4: The complete dataset of helium isotope measurements. Open circles are data points used to calculate the mean of replicate measurements of each sample. Crosses are measurements that show anomalously high ^{3}He concentrations than their replicates ("nugget effect"). We excluded their ^{3}He measurements from calculations and discussions, but kept their ^{4}He measurements since they agree with replicates. The grey circle has anomalously high ^{4}He concentration, which could result from sampling of a rare ^{4}He-enriched phase (*e.g.*, a zircon). Since its ^{3}He is close to the replicate, we only excluded its ^{4}He from calculations and discussions. The blue curve connects the mean values of replicate measurements of each sample.

4.4 Discussion

Variations in NCF

To interpret the ^{3}He and stable isotope records we obtained, we must first discuss the syn-sedimentary and post-sedimentary processes at Site 1209. [$^3He_{ET}$] in our samples is not only controlled by the $^3He_{ET}$ flux, but also dependent on the mass accumulation rate (assuming helium retentivity in the sediments does not change during the interval of interest; Eqn. 1.1). Either an increase in $^3He_{ET}$ flux or a decrease in mass accumulation rate can result in an apparent increase in measured [$^3He_{ET}$]. Since carbonates dominate the marines sediments in Late Eocene sediments at Site 1209 (Bhattacharya et al., 2020; Viganò et al., 2023), the mass accumulation rate is expected to be modulated by the carbonate accumulation rate. Therefore, if the noncarbonate flux into the ocean is constant, NCF can be used to track variations in the carbonate accumulation rate, and essentially the mass accumulation rate. On the other hand, while bulk carbonate δ^{13}C and δ^{18}O depend on the carbon and oxygen isotope ratios in the seawater at the time of sedimentation, they could be later altered in diagenetic processes (Bodiselitsch et al., 2004; Bhattacharya et al., 2020). If such processes involve carbonate dissolution, an apparent decrease in carbonate accumulation rate is expected and will be displayed as an increase in NCF. Therefore, NCF in our samples can provide information regarding the sedimentation environment that concerns both [$^3He_{ET}$] and stable isotope ratios.

In our studied section, the sediment mass accumulation rate is dominated by the carbonate accumulation rate because NCF never exceeds 11 wt%. However, we have also observed large variations in NCF in our studied section, especially within Int 1 and Int 2 (Fig. 4.3). We first attempt to interpret if these variations result from a change in the net carbonate accumulation rate, or a change in the non-carbonate flux to the sea floor.

NCF, [^4He_T], and sediment magnetic susceptibility (MS) from the IODP shipboard report (Bralower et al., 2002) show apparent covariations (Fig. 4.3). Intervals with low carbonate content (*i.e.*, increases in NCF) and peaks in MS have been attributed to carbonate dissolution horizons (*e.g.*, Bhattacharya et al. 2020). However, such covariations can also be explained by changes in detrital sediment flux to the seafloor, which contributes to both NCF and MS, while keeping carbonate accumulation rate constant. Indeed, NCF includes a mixture of detrital, authigenic (*e.g.*, phosphates, sulfates) and extraterrestrial minerals, while MS reflects the concentration of magnetic minerals from different sources (detrital, biogenic, authigenic, volcanic, extraterrestrial, etc.; Roberts et al. 2013). Thus, the covariation between NCF and MS alone is not sufficient to distinguish between a constant non-carbonate flux or a constant carbonate accumulation rate, or any scenario in between.

This ambiguity also applies to interpreting the covariations between [^4He_T] and NCF, and [^4He_T] and MS, because ^4He_T in deep-sea sediments is carried exclusively by detrital minerals. But since we have measured both [^4He_T] and NCF in each sample, we can use their ratio ([^4He_T]/NCF) to track the variations in the mixing ratio between detrital minerals and other phases in the NCF, or the variation in the ^4He concentration of detrital minerals transported to Site 1209. Nevertheless, if [^4He_T]/NCF is constant, the variations in NCF are most easily explained by a constant flux of all the minerals in the NCF but a changing carbonate accumulation rate. Indeed, the peaks in NCF are more muted in the [^4He_T]/NCF record within Int 1 and Int 2 (Fig. 4.3). Variations still exist in [^4He_T]/NCF within Int 1 and Int 2, but the max-to-min ratios of 1.5 (Int 1) and 1.9 (Int 2) are smaller than those in NCF (2.4 for Int 1, 2.9 for Int 2), and similar to the max-to-min ratio [^4He_T]/NCF of 1.7 outside the two intervals. Values of [^4He_T]/NCF within Int 1 and Int 2 almost all fall within the range of [^4He_T]/NCF outside these two intervals, except the two data points at 143.72 m and 143.82 m (Fig. 4.3). Thus, we ran a Kolmogorov–Smirnov test to evaluate if there is a difference between the distributions of [^4He_T]/NCF within Int 1+Int 2 and outside, assuming the latter reflects the natural variability in [^4He_T]/NCF. The p value of the Kolmogorov–Smirnov test result is 0.41, and thus we cannot reject the null hypothesis that the two distributions are statistically the same at 95 % confidence interval. This suggests that the mixing ratio between detrital minerals and other phases in the NCF can be assumed to be the same within our studied section, and the variations in NCF are most easily explained by changes in the carbonate accumulation rate. If so, normalizing [$^3He_{ET}$] to NCF will effectively correct for variations caused by changes in the sediment mass accumulation rate (dominated by carbonate accumulation rate).

Indeed, a detailed scanning electron microscope (SEM) study on Int 1 found calcareous nannofossils to be visibly degraded, which clearly indicates carbonate dissolution (Viganò et al., 2023). Such carbonate dissolution events are equivalent to decreases in the carbonate accumulation rate. There has been no SEM study on Int 2, which would have helped assess our assumption of a constant NCF. In the following discussions, we will tentatively use NCF as a constant flux proxy and

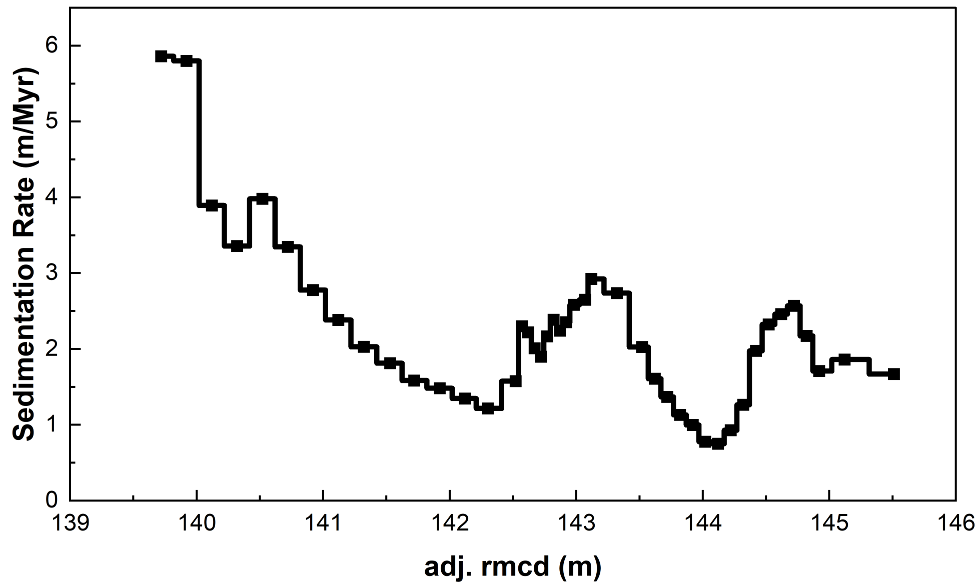

Figure 4.5: Sedimentation rate model based on average sedimentation rate of 1.8 m/Myr between the Top of *Hantkenina* spp. and the Base of *Reticulofenestra umbilicus* . NCF is used as a constant flux proxy to correct for variations in carbonate accumulation rate/preservation efficiency.

interpret changes in $^3He_{ET}$ flux based on [$^3He_{ET}$]/NCF record instead of [$^3He_{ET}$], but acknowledge that this could be an oversimplification of the sedimentation conditions at Site 1209. We note that using [^4He_T] as a constant flux proxy will yield the same conclusions.

Enhanced Cosmic Dust Flux

[$^3He_{ET}$]/NCF in the interval between 142.5 m and 145.5 m shows enhanced values as high as ~100 pcc/g, compared to the upper section with relatively constant values around 25 pcc/g (Fig. 4.3). Two peaks occur at ~143.8 m and ~144.7 m, respectively. Assuming a constant NCF through our studied section, this interval with enhanced and varying [$^3He_{ET}$]/NCF reflect actual changes in extraterrestrial ^3He flux (Farley et al., 1997; Mukhopadhyay et al., 2006; McGee et al., 2010).

There is no existing age model that covers the interval studied in this work (Bhattacharya et al., 2020; Viganò et al., 2023). To compare our record at Site 1209 to other sedimentary $^3He_{ET}$ records in the Late Eocene, we constructed an age model for our studied section based on biohorizons identified without age conflicts (Bralower et al., 2006; Viganò et al., 2023) and using NCF as a constant flux proxy.

We first derived the global mean sedimentation rate of 1.8 m/Myr using the Top of *Hantkenina* spp. and the Base of *R. umbilicus* (Table 4.1). We then normalized the average NCF of each two adjacent samples to the global mean NCF of 3.9 wt% in our studied section. The sedimentation rate between each two adjacent samples was constrained by scaling the global mean sedimentation rate to the normalized NCF. Since the Base of *R. umbilicus* is beyond the studied section where we have NCF data, we assumed the NCF between our deepest sample and the Base of *R. umbilicus* to be constant and equal to the average NCF of our studied section. We acknowledge that this assumption is potentially an important source of error because the interval with assumed constant NCF is almost twice as long as our studied interval (Table 4.1). Finally, we calculated the age of each sample by anchoring our age model to the Top of *Hantkenina* spp.

Due to the large variations in NCF, sedimentation rate within our studied interval varies by a factor of six between ~1 m/Myr and ~6 m/Myr (Fig. 4.5). The two low intervals around 144 m and 142.5 m are associated with Int 1 and Int 2, and have been tentatively interpreted as intervals with carbonate dissolution. The continuous increase in sedimentation rate above 142.5 m is consistent with the observed decrease in NCF (Fig. 4.3 and a transition in sediment color from brown/tan to gray/white (Materials and Methods). We interpret this increase in sedimentation rate to reflect the deepening of the CCD at the end of the Eocene, which has been reported extensively in other marine sedimentary records as well (Coxall et al., 2005; Lear et al., 2004).

The apparent large variations in the sedimentation rate make it difficult to directly interpret the [$^3He_{ET}$] record. Since we have made the assumption that NCF can be used as a constant flux proxy, we will use [$^3He_{ET}$]/NCF as a tracer for the $^3He_{ET}$ flux in the following discussions. Based on our age model, the interval of enhanced [$^3He_{ET}$]/NCF at Site 1209 overlaps with the Late Eocene ^3He enhancement event identified at Massignano, Italy (Farley et al., 1998) and ODP Site 757 (Farley et al., 2006) (Fig. 4.6). We note that the age model for Site 757 samples also has large uncertainties (Farley et al., 2006), and thus the alignment of the three ^3He records in Fig. 4.6 should not be taken as being accurate. Nevertheless, despite the uncertainties in the age models for both Site 1209 samples and Site 757 samples, the broader peak in [$^3He_{ET}$]/NCF at ~143.8 m in depth scale in our studied section agrees both in age and magnitude with the peaks in [$^3He_{ET}$]/NCF at Massignano and Site 757, indicating a ~5-fold increase in cosmic dust flux at ~36 Ma observed

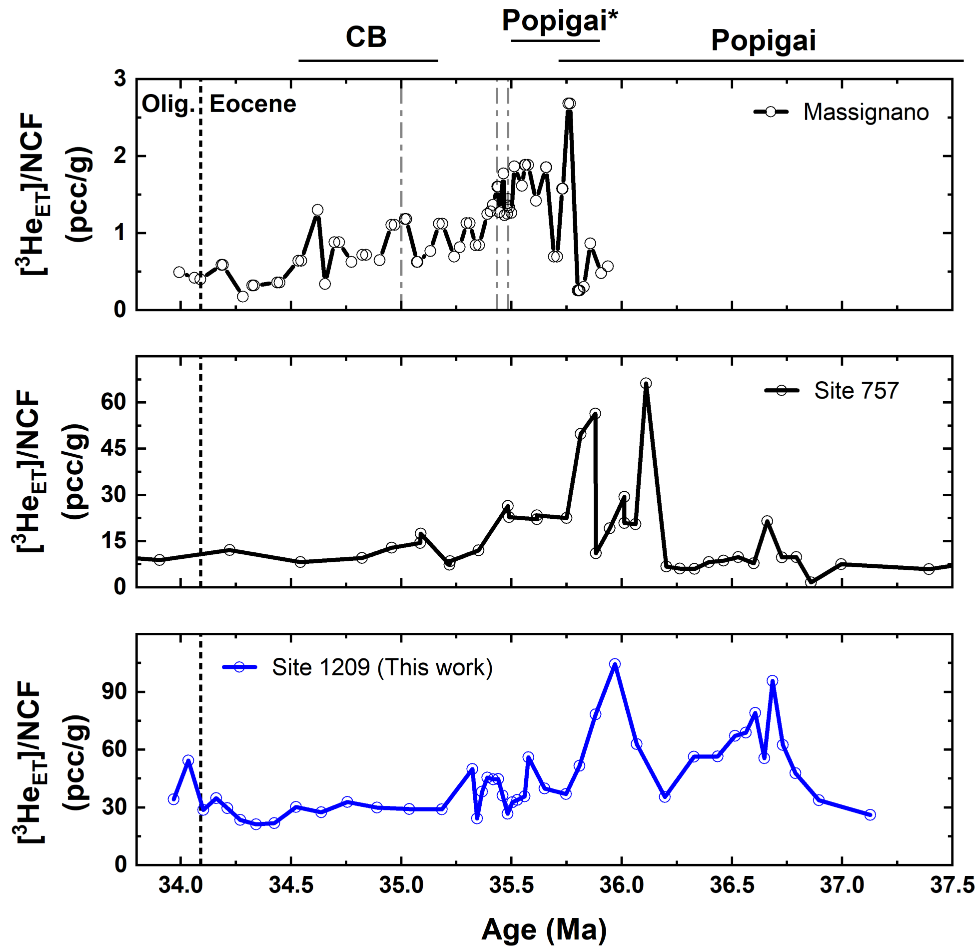

Figure 4.6: Records of the Late Eocene ^{3}He enhancement event reported at different locations. (Upper) The Massignano record plotted against the most recent age model with U-Pb ages (Sahy et al., 2017). The ages of the two large impact craters (Popigai and Chesapeake Bay, or CB) in the Late Eocene are shown on the top (Schmieder et al., 2020). "Popigai*" indicates the originally proposed age of the crater (Bottomley et al., 1997), while "Popigai" indicates the conservatively revised age (Schmieder et al., 2020). Dash-dot lines are ages of the Ir anomalies at Massignano, likely results of bolide impacts. (Middle) Record from ODP Site 757 plotted against an age model based on a linear sedimentation rate model interpolated between the Top of *R. umbilicus*, the Top of *D. saipanensis*, and the Top of *C. gigas* at this site (Peirce et al., 1989). (Lower) Our record from Site 1209.

in global marine sediment records.

The Massignano record does not have older samples to confirm the deeper peak in our record (Farley et al., 1998), but there is also a double-peak in [$^3He_{ET}$]/NCF at Site 757 (Farley et al., 2006), suggesting that the enhancement in cosmic dust flux could have started earlier than ~37 Ma. Alternatively, an actual decrease in non-carbonate flux with a constant carbonate accumulation rate will also create an apparent increase in [$^3He_{ET}$]/NCF and $^3He/^4He$, but has no effect on [$^3He_{ET}$]. Since [$^3He_{ET}$] is muted at ~144.7 m (Fig. 4.3) when both [$^3He_{ET}$]/NCF and $^3He/^4He$ show a local maximum, it is possible that the deeper (*i.e.*, older) peak in [$^3He_{ET}$]/NCF at Site 1209 is due to a decrease in NCF rather than an increase in the $^3He_{ET}$ flux. If this is true, [$^3He_{ET}$] will instead better capture the actual change in $^3He_{ET}$ flux between ~144.3 m and ~145.5 m (Fig. 4.3), which shows a gradual increase towards the peak at ~143.8 m (36 Ma).

Nevertheless, the interval between 142.5 m and 145.5 m at Site 1209 with enhanced [$^3He_{ET}$]/NCF and [$^3He_{ET}$] (Fig. 4.3) is identified as the Late Eocene ^3He enhancement event based on our age model. The double-peak feature in [$^3He_{ET}$]/NCF is yet to be confirmed with another sedimentary record with smaller variations in NCF. The potential mechanisms of creating multiple peaks in cosmic dust flux are beyond the scope of this paper and will not be discussed here.

Climatic/Environmental Responses

Our study provides another sedimentary record of $^3He_{ET}$ and stable isotope ratios in tandem to compare with the previous work at Massignano (Farley et al., 1998; Bodiselitsch et al., 2004) (Fig. 4.8). It also completes the sampling gap of previous work in Site 1209 (Bhattacharya et al., 2020; Viganò et al., 2023), allowing us to assess the long-term variations in $\delta^{13}C$ and $\delta^{18}O$ through the end of the Eocene (Fig. 4.9).

The bulk carbonate $\delta^{13}C$ records from our study and Massignano both show a negative shift of 1–1.2 ‰ from the Late Eocene towards the EOB, reaching a minimum of 1 ‰ at 34.3 Ma (Fig. 4.8). A similar negative shift has also been found in $\delta^{13}C$ measured in ostracods from the same section in Massignano (Jovane et al., 2007). The decrease in $\delta^{13}C$ in our record is at ~35.1 Ma, which is similar to other bulk carbonate $\delta^{13}C$ records from the north Pacific (Westerhold et al. 2020; Taylor et al. 2023; Fig. 4.7) but 0.2 Myr later than the decrease in $\delta^{13}C$ in the Massignano record. Thus, the negative shift in bulk carbonate $\delta^{13}C$ is likely a global pattern at the

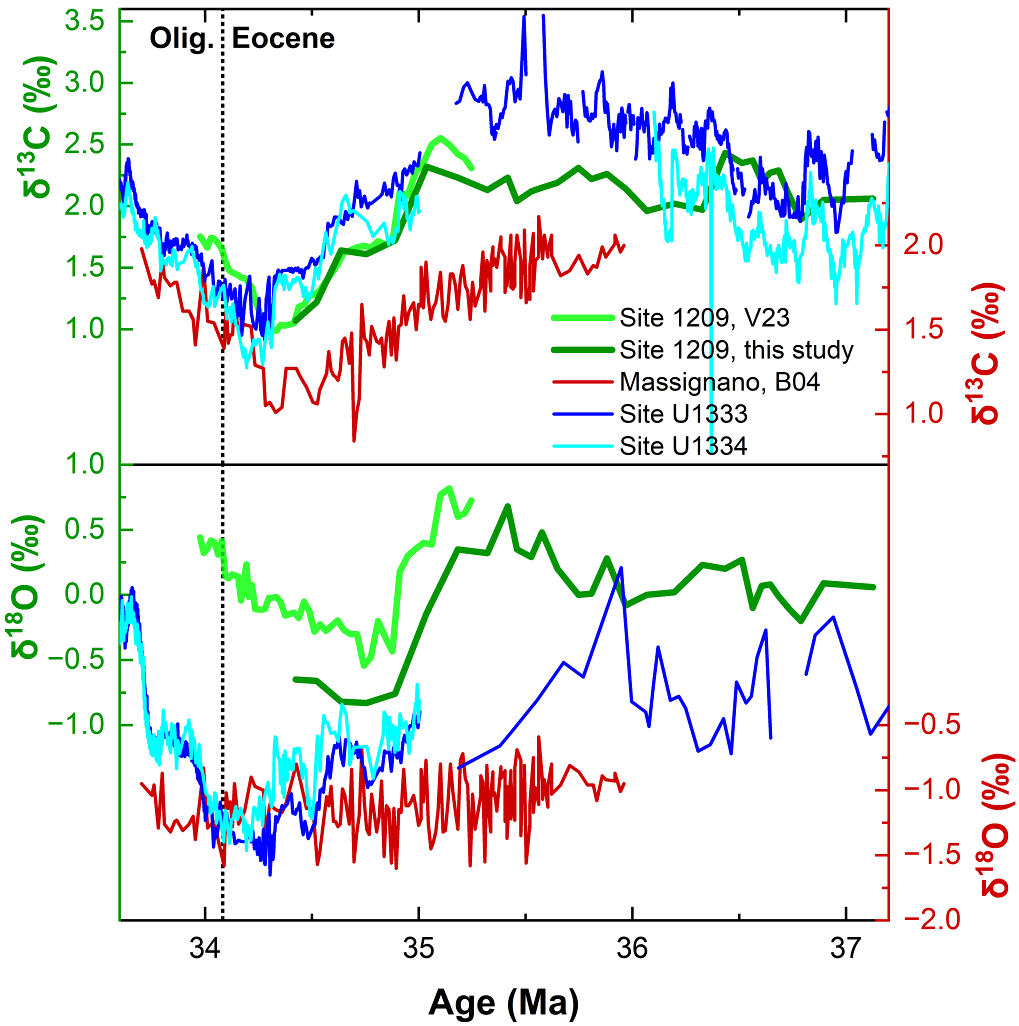

Figure 4.7: Compiled marine carbonate $\delta^{13}C$ and $\delta^{18}O$ records in north Pacific (Site 1209, U1333, and U1334) and Massignano. All of north Pacific records are plotted on the left y-axis. V23: Viganò et al. (2023). B04: Bodiselitsch et al. (2004). Site U1333 and U1334 data are from Westerhold et al. (2020) and Taylor et al. (2023)

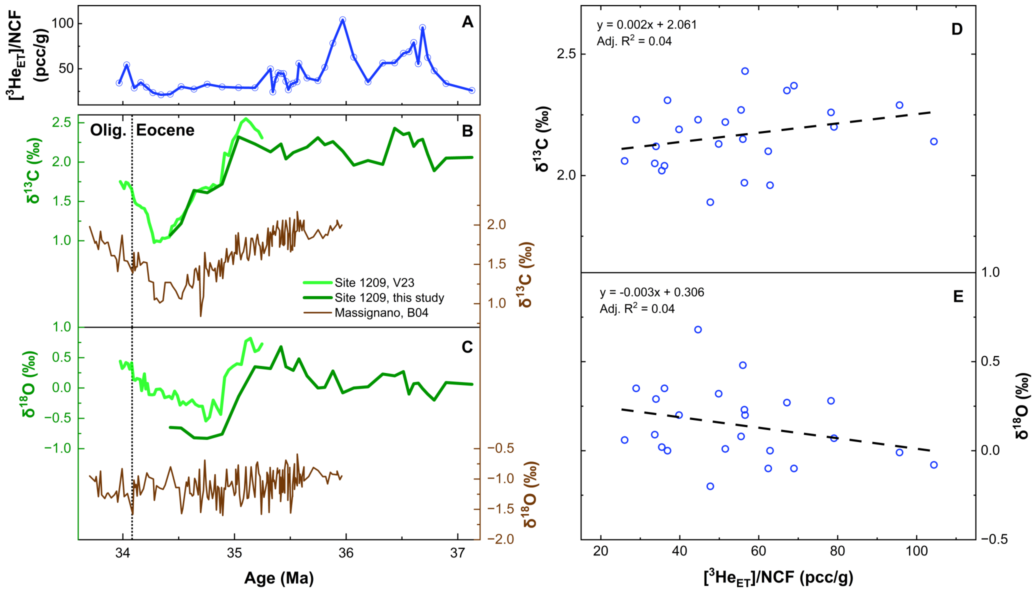

Figure 4.8: [$^3He_{ET}$]/NCF record (Panel A), bulk carbonate stable isotope ratio records (Panel B, C) from Site 1209 and Massginano, and correlation between stable isotope ratios and [$^3He_{ET}$]/NCF within the Late Eocene ^{3}He enhancement event (Panel D, E). Site 1209 stable isotope data are plotted against the left y-axis, while the Massignano data are plotted against the right one. Vertical dotted line in B and C shows the age of the EOB at 34.09 Ma (Sahy et al., 2017). V23: Viganò et al. (2023). B04: Bodiselitsch et al. (2004). Dashed lines in D and E are best linear fits to data.

end of Eocene, with regional differences in the time of its initiation. Alternatively, the apparent delay of the decline in δ^{13}C at Site 1209 might result from unrecognized errors in our age model.

Prior to 35.2 Ma, when most variations in cosmic dust flux (tracked by [$^3He_{ET}$]/NCF) occurs, δ^{13}C stays relatively constant around 2.1 ‰ in our record (Fig. 4.8). There are two 0.4-‰ positive shifts in δ^{13}C at ~36.95 Ma and ~36.75 Ma, that apparently coincide with the two [$^3He_{ET}$]/NCF peaks (Fig. 4.8). These positive shifts may reflect responses of the primary productivity in the oceans to enhanced cosmic dust flux (Johnson, 2001; Reiners et al., 2018). On the other hand, there is a negative shift of –0.5 ‰ between 35.88 Ma and 36.43 Ma (144.22–144.72 m), which corresponds to the increase in NCF in Int 2 rather than an increase in [$^3He_{ET}$]/NCF (Fig. 4.3). We believe this negative shift is more likely a result of a carbonate dissolution event, which is usually accompanied by a negative excursion in δ^{13}C in the Late Eocene in the north Pacific (*e.g.*, Bhattacharya et al. 2020).

For data within the span of the Late Eocene ^{3}He enhancement event, δ^{13}C and [^{3}He$_{ET}$]/NCF shows a very weak positive correlation with an adjusted R^2 of only 0.04 (Fig. 4.8). When compared with the longer δ^{13}C record in the Late Eocene at Site 1209, our δ^{13}C record between 35.2 Ma and 37.1 Ma agrees well the long-term trend (Fig. 4.9). Multiple δ^{13}C excursions and shifts on the order of 0.5 ‰ exist on top of the relatively constant long-term δ^{13}C record (Fig. 4.9), suggesting that the ~0.4-‰ positive excursions coinciding with the two [^{3}He$_{ET}$]/NCF peaks may be independent of enhanced cosmic dust flux, alternatively. In summary, our record does not support a strong correlation between δ^{13}C and [^{3}He$_{ET}$]/NCF, suggesting an insensitive response of carbon productivity in the north Pacific to the 5-fold increase in cosmic dust flux during the Late Eocene ^{3}He enhancement event.

We use bulk carbonate δ^{18}O as a proxy for sea surface temperature in our studied section. We note that there is a systematic shift of ~–0.3 ‰ in our δ^{18}O record compared to other records reported at Site 1209 (Fig. 4.8). This discrepancy is currently unresolved. Nevertheless, our δ^{18}O record documents the relative changes and overlaps with the other Site 1209 records when shifted positively by 0.3 ‰ (Fig. 4.9). Comparing to other bulk carbonate δ^{18}O records from the north Pacific, our δ^{18}O record is positively shifted by > 0.6 ‰ but agrees in trend in general (Fig. 4.7). Part of the discrepancies may be explained by δ^{18}O signal altered by carbonate dissolution and digenesis at Site 1209, which has been observed within Int 1 (Fig. 4.3; 140.5-142.8 m). In contrast, both our record and other north Pacific records differ substantially from the Massignano record (Fig. 4.8). δ^{18}O at Massignano stays relatively constant around –1.25 ‰ from the Late Eocene through the EOB, which is likely a diagenetically altered signal inherited during Massignano limestone formation (Bodiselitsch et al., 2004).

The interval with potentially diagenetically altered δ^{18}O is younger and beyond the Late Eocene ^{3}He enhancement event within our studied section, which allows us to assess the responses of sea surface temperature in the north Pacific to excess cosmic dust flux during the Late Eocene ^{3}He enhancement event. Bulk carbonate δ^{18}O within the Late Eocene ^{3}He enhancement event shows a very weak correlation with [^{3}He$_{ET}$]/NCF with an adjusted R^2 of 0.04 (Fig. 4.8). The long-term δ^{18}O record at Site 1209 shows a gradual increase from –0.5 ‰ at ~154 m to 0.5 ‰ at ~145 m, then continues to increase through the interval with enhanced cosmic dust, until it reaches 0.8 ‰ at ~142 m (Fig. 4.9). This corresponds to a timespan of ~5 Myr (~35 Ma to ~40 Ma, based on calcareous nannofossils at Site 1209; Bralower

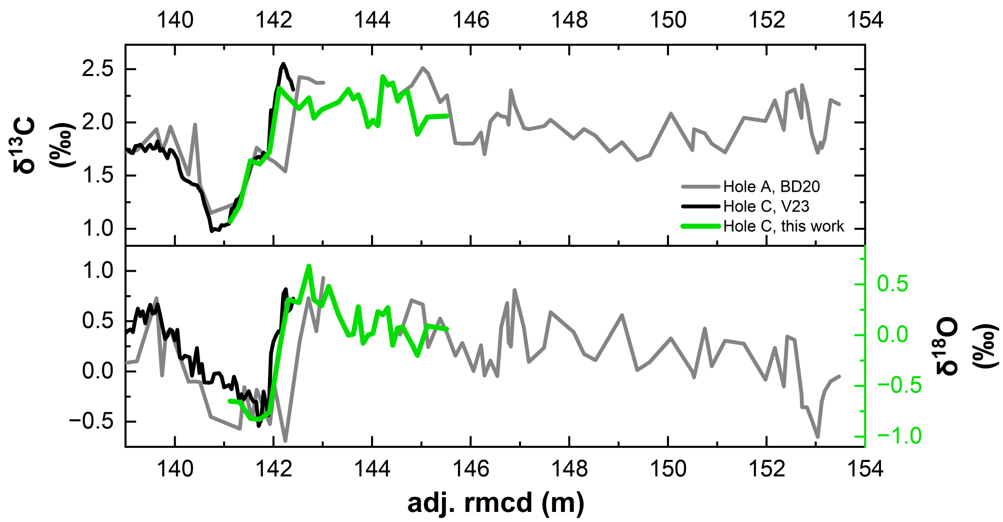

Figure 4.9: Bulk carbonate stable isotope ratio records from Site 1209. Our δ^{18}O is plotted on the right axis to visually correct for the systematic difference to the other two records. Shaded area indicates the span of the Late Eocene ^{3}He enhancement event with enhanced [$^3He_{ET}$]/NCF. BD20: Bhattacharya et al. (2020). V23: Viganò et al. (2023)

et al. 2002), recording a continuous long-term cooling trend in the sea surface temperature towards the EOB that is typical in marine carbonate δ^{18}O during this time (*e.g.*, Westerhold et al. 2020; Taylor et al. 2023). Similar to δ^{13}C, our record does not support a sensitive response of δ^{18}O (and sea surface temperature in the north Pacific) to enhanced cosmic dust flux during the Late Eocene ^{3}He enhancement event.

The absence of climatic or environmental responses to variation in cosmic dust flux could be due to the slow injection rate of excess cosmic dust into the atmosphere. Although the total amount of excess cosmic dust in the atmosphere during the Late Eocene ^{3}He enhancement event is similar in magnitude to the amount of silicate dust injected into the atmosphere immediately after the Chicxulub impacting event, the former completed within a time interval of ~2 Myr. It suggests that our simple dust-loading-perturbation calculation may have overestimated the climatic effect of cosmic dust (Fig. 4.2), and a more refined climatic model, potentially including atmospheric circulations and cloud formations, is desired.

4.5 Conclusion

We provide the first marine drill core record of both helium isotopes and stable isotopes across the Late Eocene ^{3}He enhancement event, based on which we have only found very weak correlation between ^{3}He and stable isotopes during the Late Eocene ^{3}He enhancement event in the north Pacific. This suggests that both Earth's climate and environment were not sensitive to the slow injection of cosmic dust that was 5 times above the background flux into the atmosphere over the course of 2 Myr. Marine drill core records from other oceans will help assess whether there were regional differences in Earth's climatic and environmental responses to the Late Eocene ^{3}He enhancement event. An important implication of our conclusion is that the 100-kyr period in cosmic dust accretion rate in the last 700 kyr was unlikely to have any climatic significance.

We note that the climatic and environmental significance of cosmic dust has also been hypothesized for other intervals in the geological history. For instance, ^{3}He$_{ET}$ flux showed a 100-kyr period that correlated with the 100-kyr cycle in δ^{18}O in marine carbonate sediments for the last 700 kyr (Farley et al., 1995; Patterson et al., 1998), which reconciled with the hypothesis that a periodic change in cosmic dust flux was the driving force of the 100-kyr periodicity observed in the global seawater δ^{18}O trend (Muller et al., 1995; Muller et al., 1997). Furthermore, a ~1.5-Myr enhancement in ^{3}He$_{ET}$ flux after the L-chondrite parent body breakup event in the Ordovician coincided with the Mid-Ordovician ice age, with the dust from the L-chondrite parent body hypothesized to be the trigger of the latter (Schmitz et al., 2019). As discussed in Chapter II, the K1 ^{3}He enhancement event in the Late Cretaceous also coincided with a moderate excursion in δ^{13}C, known as the Early Campanian Event (ECE; Montanari et al. 2023).

Therefore, since we have reported that a 5-fold increase in cosmic dust flux during the Late Eocene ^{3}He enhancement event was not large enough to generate observable climatic or environmental perturbations in marine carbonate δ^{13}C or δ^{18}O records, we might be able to provide new constraints for the likelihood of the hypotheses above. This implies that Earth's climate system is unlikely to be sensitive to the observed 100-kyr period in cosmic dust accretion rate, which varies by only 2–3 times (Farley et al., 1995; Patterson et al., 1998). On the other hand, both the ~10-fold increase in ^{3}He$_{ET}$ flux during K1 and the ~200-fold increase in cosmic dust during the Ordovician L-chondrite parent body breakup event are larger in magnitude than the Late Eocene ^{3}He enhancement event, and may still have nontrivial climatic/environmental effects.

Of course, the sensitivity of Earth's climate and environment to external perturbations does not necessarily scale linearly with the atmospheric dust loading, but various factors need to be considered. This is the limitation of our approach, which only explored the linear, direct responses of Earth's climate/environment to cosmic dust flux. In practice, micron-sized dust particles in Earth's atmosphere not only change its optical properties, but can also influence cloud formations and atmosphere chemistry (Ogurtsov et al., 2011; Plane et al., 2017). When coupled with astronomical cycles that perturbs Earth's climate periodically, these interactions could potentially be further enhanced. Within our studied time interval, Earth's climate system was also approaching the major tipping point at the EOB, with increasing fluctuations between a deterministic state and a stochastic state and a potentially decreasing ability to correct for small climatic perturbations (Dakos et al., 2008; Scheffer et al., 2009; Westerhold et al., 2020). Myr-interactions between dust and climate in the Late Eocene have not been explored with complex climate models like the General Circulation Models (GCMs), which could be informative in evaluating the complicated interactions between enhanced cosmic dust flux and Earth's climate and environment.

References

Agnini, Claudia, Eliana Fornaciari, Isabella Raffi, Rita Catanzariti, Heiko Pälike, Jan Backman, and Domenico Rio (2014). "Biozonation and Biochronology of Paleogene Calcareous Nannofossils from Low and Middle Latitudes". In: *Newsletters on Stratigraphy*, pp. 131–181. ISSN: , DOI: `10.1127/0078-0421/2014/0042`.

Artemieva, Natalia, Joanna Morgan, and Expedition 364 Science Party (2017). "Quantifying the Release of Climate-Active Gases by Large Meteorite Impacts With a Case Study of Chicxulub". In: *Geophysical Research Letters* 44.20, pp. 10, 180–10, 188. ISSN: 1944-8007. DOI: `10.1002/2017GL074879`.

Bhattacharya, Joyeeta and Gerald R. Dickens (2020). "Eocene Carbonate Accumulation in the North-Central Pacific Ocean: New Insights from Ocean Drilling Program Site 1209, Shatsky Rise". In: *Sedimentary Geology* 405, p. 105705. ISSN: 0037-0738. DOI: `10.1016/j.sedgeo.2020.105705`.

Bodiselitsch, Bernd, Alessandro Montanari, Christian Koeberl, and Rodolfo Coccioni (2004). "Delayed Climate Cooling in the Late Eocene Caused by Multiple Impacts: High-Resolution Geochemical Studies at Massignano, Italy". In: *Earth and Planetary Science Letters* 223.3, pp. 283–302. ISSN: 0012-821X. DOI: `10.1016/j.epsl.2004.04.028`.

Bottomley, Richard, Richard Grieve, Derek York, and Victor Masaitis (1997). “The Age of the Popigai Impact Event and Its Relation to Events at the Eocene/Oligocene Boundary”. In: *Nature* 388.6640, pp. 365–368. ISSN: 1476-4687. DOI: 10.1038/41073.

Bralower, T.J., I Premoli Silva, and M.J. Malone (2005). “15. DATA REPORT: REVISED COMPOSITE DEPTH RECORDS FOR SHATSKY RISE SITES 1209, 1210, AND 1211”. In.

Bralower, T.J., I Premoli Silva, M.J. Malone, M.A. Arthur, K. Averyt, and P.R. Bown (2002). “Site 1209”. In: *Proceedings of the Ocean Drilling Program, Initial Reports*. Vol. 198, pp. 1–102.

Bralower, T.J., I. Premoli Silva, and M.J. Malone, eds. (2006). *Proceedings of the Ocean Drilling Program, 198 Scientific Results*. Vol. 198. Proceedings of the Ocean Drilling Program. Ocean Drilling Program. DOI: 10.2973/odp.proc.sr.198.2006.

Brugger, Julia, Georg Feulner, and Stefan Petri (2017). “Baby, It’s Cold Outside: Climate Model Simulations of the Effects of the Asteroid Impact at the End of the Cretaceous”. In: *Geophysical Research Letters* 44.1, pp. 419–427. ISSN: 1944-8007. DOI: 10.1002/2016GL072241.

Clymer, Aron K., David M. Bice, and Alessandro Montanari (1996). “Shocked Quartz from the Late Eocene: Impact Evidence from Massignano, Italy”. In: *Geology* 24.6, pp. 483–486. ISSN: 0091-7613. DOI: 10.1130/0091-7613(1996)024<0483:SQFTLE>2.3.CO;2.

Coccioni, Rodolfo, D. Basso, H. Brinkhuis, S. Galeotti, S. Gardin, S. Monechi, and S. Spezzaferri (2000). “Marine Biotic Signals across a Late Eocene Impact Layer at Massignano, Italy: Evidence for Long-Term Environmental Perturbations?” In: *Terra Nova* 12.6, pp. 258–263. ISSN: 1365-3121. DOI: 10.1046/j.1365-3121.2000.00305.x.

Coxall, Helen K., Paul A. Wilson, Heiko Pälike, Caroline H. Lear, and Jan Backman (2005). “Rapid Stepwise Onset of Antarctic Glaciation and Deeper Calcite Compensation in the Pacific Ocean”. In: *Nature* 433.7021, pp. 53–57. ISSN: 1476-4687. DOI: 10.1038/nature03135.

Cramer, B. S., J. R. Toggweiler, J. D. Wright, M. E. Katz, and K. G. Miller (2009). “Ocean Overturning since the Late Cretaceous: Inferences from a New Benthic Foraminiferal Isotope Compilation”. In: *Paleoceanography* 24.4. ISSN: 1944-9186. DOI: 10.1029/2008PA001683.

Dakos, Vasilis, Marten Scheffer, Egbert H. van Nes, Victor Brovkin, Vladimir Petoukhov, and Hermann Held (2008). “Slowing down as an Early Warning Signal for Abrupt Climate Change”. In: *Proceedings of the National Academy of Sciences* 105.38, pp. 14308–14312. DOI: 10.1073/pnas.0802430105.

Farley, Kenneth A. (1995). "Cenozoic variations in the flux of interplanetary dust recorded by3He in a deep-sea sediment". en. In: *Nature* 376.6536, pp. 153–156. ISSN: 0028-0836, 1476-4687. DOI: 10.1038/376153a0.

Farley, Kenneth A., S. G. Love, and Desmond B. Patterson (1997). "Atmospheric Entry Heating and Helium Retentivity of Interplanetary Dust Particles". In: *Geochimica et Cosmochimica Acta* 61.11, pp. 2309–2316. ISSN: 0016-7037. DOI: 10.1016/S0016-7037(97)00068-9.

Farley, Kenneth A., Alessandro Montanari, E. M. Shoemaker, and C. S. Shoemaker (1998). "Geochemical Evidence for a Comet Shower in the Late Eocene". en. In: *Science* 280.5367, pp. 1250–1253. ISSN: 0036-8075, 1095-9203. DOI: 10.1126/science.280.5367.1250.

Farley, Kenneth A. and Desmond B. Patterson (1995). "A 100-Kyr Periodicity in the Flux of Extraterrestrial 3He to the Sea Floor". In: *Nature* 378.6557, pp. 600–603. ISSN: 1476-4687. DOI: 10.1038/378600a0.

Farley, Kenneth A., David Vokrouhlický, William F. Bottke, and David Nesvorný (2006). "A late Miocene dust shower from the break-up of an asteroid in the main belt". en. In: *Nature* 439.7074, pp. 295–297. ISSN: 0028-0836, 1476-4687. DOI: 10.1038/nature04391.

Fornaciari, Eliana, Claudia Agnini, R. Catanzariti, Domenico Rio, M. E. Bolla, and E. Valvasoni (2010). "Mid-Latitude Calcareous Nannofossil Biostratigraphy and Biochronology across the Middle to Late Eocene Transition". In.

Glass, Billy P., Shaobin Liu, and Alessandro Montanari (2004). "Impact Ejecta in Upper Eocene Deposits at Massignano, Italy". In: *Meteoritics & Planetary Science* 39.4, pp. 589–597. ISSN: 1945-5100. DOI: 10.1111/j.1945-5100.2004.tb00921.x.

Hutchinson, David K., Helen K. Coxall, Daniel J. Lunt, Margret Steinthorsdottir, Agatha M. de Boer, Michiel Baatsen, Anna von der Heydt, Matthew Huber, Alan T. Kennedy-Asser, Lutz Kunzmann, Jean-Baptiste Ladant, Caroline H. Lear, Karolin Moraweck, Paul N. Pearson, Emanuela Piga, Matthew J. Pound, Ulrich Salzmann, Howie D. Scher, Willem P. Sijp, Kasia K. Śliwińska, Paul A. Wilson, and Zhongshi Zhang (2021). "The Eocene–Oligocene Transition: A Review of Marine and Terrestrial Proxy Data, Models and Model–Data Comparisons". In: *Climate of the Past* 17.1, pp. 269–315. ISSN: 1814-9324. DOI: 10.5194/cp-17-269-2021.

Johnson, Kenneth. S. (2001). "Iron supply and demand in the upper ocean: Is extraterrestrial dust a significant source of bioavailable iron?" en. In: *Global Biogeochemical Cycles* 15.1, pp. 61–63. ISSN: 0886-6236, 1944-9224. DOI: 10.1029/2000GB001295.

Jovane, Luigi, Mario Sprovieri, Fabio Florindo, Gary Acton, Rodolfo Coccioni, Barbara Dall'Antonia, and Jaume Dinarès-Turell (2007). "Eocene-Oligocene Paleoceanographic Changes in the Stratotype Section, Massignano, Italy: Clues from

Rock Magnetism and Stable Isotopes". In: *Journal of Geophysical Research: Solid Earth* 112.B11. ISSN: 2156-2202. DOI: 10.1029/2007JB004963.

Koeberl, Christian (2009). "Late Eocene Impact Craters and Impactoclastic Layers—An Overview". In: *The Late Eocene Earth—Hothouse, Icehouse, and Impacts*. Ed. by Christian Koeberl and Alessandro Montanari. Geological Society of America. ISBN: 978-0-8137-2452-2. DOI: 10.1130/2009.2452(02).

Kok, Jasper F., Trude Storelvmo, Vlassis A. Karydis, Adeyemi A. Adebiyi, Natalie M. Mahowald, Amato T. Evan, Cenlin He, and Danny M. Leung (2023). "Mineral Dust Aerosol Impacts on Global Climate and Climate Change". In: *Nature Reviews Earth & Environment* 4.2, pp. 71–86. ISSN: 2662-138X. DOI: 10.1038/s43017-022-00379-5.

Lear, C. H., H. Elderfield, and P. A. Wilson (2000). "Cenozoic Deep-Sea Temperatures and Global Ice Volumes from Mg/Ca in Benthic Foraminiferal Calcite". In: *Science* 287.5451, pp. 269–272. DOI: 10.1126/science.287.5451.269.

Lear, C. H., Y. Rosenthal, H. K. Coxall, and P. A. Wilson (2004). "Late Eocene to Early Miocene Ice Sheet Dynamics and the Global Carbon Cycle". In: *Paleoceanography* 19.4. ISSN: 1944-9186. DOI: 10.1029/2004PA001039.

Marcantonio, Franco, Sean Higgins, Robert F. Anderson, Martin Stute, Peter Schlosser, and E. Troy Rasbury (1998). "Terrigenous Helium in Deep-Sea Sediments". In: *Geochimica et Cosmochimica Acta* 62.9, pp. 1535–1543. ISSN: 0016-7037. DOI: 10.1016/S0016-7037(98)00091-X.

McGee, David, Franco Marcantonio, Jerry F. McManus, and Gisela Winckler (2010). "The Response of Excess 230Th and Extraterrestrial 3He to Sediment Redistribution at the Blake Ridge, Western North Atlantic". In: *Earth and Planetary Science Letters* 299.1-2, pp. 138–149. ISSN: 0012821X. DOI: 10.1016/j.epsl.2010.08.029.

Merrihue, Craig (1964). "Rare Gas Evidence for Cosmic Dust in Modern Pacific Red Clay". In: *Annals of the New York Academy of Sciences* 119.1, pp. 351–367. ISSN: 1749-6632. DOI: 10.1111/j.1749-6632.1965.tb47445.x.

Miller, Kenneth G., James V. Browning, W. John Schmelz, Robert E. Kopp, Gregory S. Mountain, and James D. Wright (2020). "Cenozoic Sea-Level and Cryospheric Evolution from Deep-Sea Geochemical and Continental Margin Records". In: *Science Advances* 6.20, eaaz1346. DOI: 10.1126/sciadv.aaz1346.

Montanari, Alessandro, Frank Asaro, Helen V. Michel, and James P. Kennett (1993). "Iridium Anomalies of Late Eocene Age at Massignano (Italy), and ODP Site 689B (Maud Rise, Antarctic)". In: *PALAIOS* 8.5, pp. 420–437. ISSN: 0883-1351. DOI: 10.2307/3515017. JSTOR: 3515017.

Montanari, Alessandro, Kenneth A. Farley, Rodolfo Coccioni, N. Sabatino, D. Bice, M. Yesko, M. Sinnesael, and N. De Winter (2023). "Cosmogenic 3He anomaly K1 vs. the early Campanian isotopic event (ECE) as recorded in pelagic limestones of the Umbria-Marche succession (Italy)". en. In: *Geological Society of America Bulletin*. ISSN: 0016-7606, 1943-2674. DOI: 10.1130/B36952.1.

Morgan, Joanna V., Timothy J. Bralower, Julia Brugger, and Kai Wünnemann (2022). "The Chicxulub Impact and Its Environmental Consequences". In: *Nature Reviews Earth & Environment* 3.5, pp. 338–354. ISSN: 2662-138X. DOI: 10.1038/s43017-022-00283-y.

Mukhopadhyay, Sujoy and Kenneth A. Farley (2006). "New Insights into the Carrier Phase(s) of Extraterrestrial 3He in Geologically Old Sediments". In: *Geochimica et Cosmochimica Acta* 70.19, pp. 5061–5073. ISSN: 0016-7037. DOI: 10.1016/j.gca.2006.06.1566.

Muller, Richard A. and Gordon J. MacDonald (1995). "Glacial Cycles and Orbital Inclination". In: *Nature* 377.6545, pp. 107–108. ISSN: 1476-4687. DOI: 10.1038/377107b0.

– (1997). "Glacial Cycles and Astronomical Forcing". In: *Science* 277.5323, pp. 215–218. DOI: 10.1126/science.277.5323.215.

Nakanishi, Masao, William W. Sager, and Adam Klaus (1999). "Magnetic Lineations within Shatsky Rise, Northwest Pacific Ocean: Implications for Hot Spot-Triple Junction Interaction and Oceanic Plateau Formation". In: *Journal of Geophysical Research: Solid Earth* 104.B4, pp. 7539–7556. ISSN: 2156-2202. DOI: 10.1029/1999JB900002.

Nier, Alfred O. and Dennis J. Schlutter (1990). "Helium and neon isotopes in stratospheric particles". en. In: *Meteoritics* 25.4, pp. 263–267. ISSN: 0026-1114. DOI: 10.1111/j.1945-5100.1990.tb00710.x.

Ogurtsov, M. G. and O. M. Raspopov (2011). "Possible Impact of Interplanetary and Interstellar Dust Fluxes on the Earth's Climate". In: *Geomagnetism and Aeronomy* 51.2, pp. 275–283. ISSN: 1555-645X. DOI: 10.1134/S0016793211020137.

Patterson, Desmond B. and Kenneth A. Farley (1998). "Extraterrestrial 3He in Seafloor Sediments: Evidence for Correlated 100 Kyr Periodicity in the Accretion Rate of Interplanetary Dust, Orbital Parameters, and Quaternary Climate". In: *Geochimica et Cosmochimica Acta* 62.23, pp. 3669–3682. ISSN: 0016-7037. DOI: 10.1016/S0016-7037(98)00263-4.

Peirce, J., J. Weissel, and et al., eds. (1989). *Proceedings of the Ocean Drilling Program, 121 Initial Reports*. Vol. 121. Proceedings of the Ocean Drilling Program. Ocean Drilling Program. DOI: 10.2973/odp.proc.ir.121.1989.

Plane, John M. C. (2012). "Cosmic Dust in the Earth's Atmosphere". In: *Chemical Society Reviews* 41.19, pp. 6507–6518. DOI: 10.1039/C2CS35132C.

Plane, John M. C., George J. Flynn, Anni Määttänen, John E. Moores, Andrew R. Poppe, Juan Diego Carrillo-Sanchez, and Constantino Listowski (2017). "Impacts of Cosmic Dust on Planetary Atmospheres and Surfaces". In: *Space Science Reviews* 214.1, p. 23. ISSN: 1572-9672. DOI: 10.1007/s11214-017-0458-1.

Pusz, Aimee E., Kenneth G. Miller, James D. Wright, Miriam E. Katz, Benjamin S. Cramer, and Dennis V. Kent (2009). "Stable Isotopic Response to Late Eocene Extraterrestrial Impacts". In: pp. 83–95. DOI: 10.7916/D8W66W40.

Reiners, Peter W. and Alexandra V. Turchyn (2018). "Extraterrestrial dust, the marine lithologic record, and global biogeochemical cycles". en. In: *Geology* 46.10, pp. 863–866. ISSN: 0091-7613. DOI: 10.1130/G45040.1.

Roberts, Andrew P., Fabio Florindo, Liao Chang, David Heslop, Luigi Jovane, and Juan C. Larrasoaña (2013). "Magnetic Properties of Pelagic Marine Carbonates". In: *Earth-Science Reviews* 127, pp. 111–139. ISSN: 0012-8252. DOI: 10.1016/j.earscirev.2013.09.009.

Sahy, Diana, Daniel J. Condon, Frederik J. Hilgen, and Klaudia F. Kuiper (2017). "Reducing Disparity in Radio-Isotopic and Astrochronology-Based Time Scales of the Late Eocene and Oligocene". In: *Paleoceanography* 32.10, pp. 1018–1035. ISSN: 1944-9186. DOI: 10.1002/2017PA003197.

Sano, Yuji, Bernard Marty, and Pete Burnard (2013). "Noble Gases in the Atmosphere". In: *The Noble Gases as Geochemical Tracers*. Ed. by Pete Burnard. Berlin, Heidelberg: Springer, pp. 17–31. ISBN: 978-3-642-28836-4. DOI: 10.1007/978-3-642-28836-4_2.

Scheffer, Marten, Jordi Bascompte, William A. Brock, Victor Brovkin, Stephen R. Carpenter, Vasilis Dakos, Hermann Held, Egbert H. van Nes, Max Rietkerk, and George Sugihara (2009). "Early-Warning Signals for Critical Transitions". In: *Nature* 461.7260, pp. 53–59. ISSN: 1476-4687. DOI: 10.1038/nature08227.

Schmieder, Martin and David A. Kring (2020). "Earth's Impact Events Through Geologic Time: A List of Recommended Ages for Terrestrial Impact Structures and Deposits". In: *Astrobiology* 20.1, pp. 91–141. ISSN: 1531-1074. DOI: 10.1089/ast.2019.2085.

Schmitz, Birger, Kenneth A. Farley, Steven Goderis, Philipp R. Heck, Stig M. Bergström, Samuele Boschi, Philippe Claeys, Vinciane Debaille, Andrei Dronov, Matthias van Ginneken, David A.T. Harper, Faisal Iqbal, Johan Friberg, Shiyong Liao, Ellinor Martin, Matthias M. M. Meier, Bernhard Peucker-Ehrenbrink, Bastien Soens, Rainer Wieler, and Fredrik Terfelt (2019). "An Extraterrestrial Trigger for the Mid-Ordovician Ice Age: Dust from the Breakup of the L-chondrite Parent Body". In: *Science Advances* 5.9, eaax4184. DOI: 10.1126/sciadv.aax4184.

Senel, Cem Berk, Pim Kaskes, Orkun Temel, Johan Vellekoop, Steven Goderis, Robert DePalma, Maarten A. Prins, Philippe Claeys, and Özgür Karatekin (2023). "Chicxulub Impact Winter Sustained by Fine Silicate Dust". In: *Nature Geoscience* 16.11, pp. 1033–1040. ISSN: 1752-0908. DOI: 10.1038/s41561-023-01290-4.

Silva, Isabella Premoli and D. Graham Jenkins (1993). "Decision on the Eocene-Oligocene Boundary Stratotype". In: *Episodes Journal of International Geoscience* 16.3, pp. 379–382. DOI: 10.18814/epiiugs/1993/v16i3/002.

Śliwińska, Kasia K., Erik Thomsen, Stefan Schouten, Petra L. Schoon, and Claus Heilmann-Clausen (2019). "Climate- and Gateway-Driven Cooling of Late Eocene to Earliest Oligocene Sea Surface Temperatures in the North Sea Basin". In: *Scientific Reports* 9.1, p. 4458. ISSN: 2045-2322. DOI: 10.1038/s41598-019-41013-7.

Spezzaferri, Silvia, Daniela Basso, and Rodolfo Coccioni (2002). "LATE EOCENE PLANKTONIC FORAMINIFERAL RESPONSE TO AN EXTRATERRESTRIAL IMPACT AT MASSIGNANO GSSP (NORTHEASTERN APPENNINES, ITALY)". In: *Journal of Foraminiferal Research* 32.2, pp. 188–199. ISSN: 0096-1191. DOI: 10.2113/0320188.

Tabor, Clay R., Charles G. Bardeen, Bette L. Otto-Bliesner, Rolando R. Garcia, and Owen B. Toon (2020). "Causes and Climatic Consequences of the Impact Winter at the Cretaceous-Paleogene Boundary". In: *Geophysical Research Letters* 47.3, e60121. ISSN: 1944-8007. DOI: 10.1029/2019GL085572.

Takayanagi, M. and Minoru Ozima (1987). "Temporal Variation of 3He/4He Ratio Recorded in Deep-Sea Sediment Cores". In: *Journal of Geophysical Research: Solid Earth* 92.B12, pp. 12531–12538. ISSN: 2156-2202.

Taylor, V. E., T. Westerhold, S. M. Bohaty, J. Backman, T. Dunkley Jones, K. M. Edgar, K. E. Egan, M. Lyle, H. Pälike, U. Röhl, J. Zachos, and P. A. Wilson (2023). "Transient Shoaling, Over-Deepening and Settling of the Calcite Compensation Depth at the Eocene-Oligocene Transition". In: *Paleoceanography and Paleoclimatology* 38.6, e2022PA004493. ISSN: 2572-4525. DOI: 10.1029/2022PA004493.

Toffanin, Federica, Claudia Agnini, Domenico Rio, Gary Acton, and Thomas Westerhold (2013). "Middle Eocene to Early Oligocene Calcareous Nannofossil Biostratigraphy at IODP Site U1333 (Equatorial Pacific)". In: *Micropaleontology* 59.1, pp. 69–82. ISSN: 0026-2803. JSTOR: 24413317.

Toon, Owen B., Charles Bardeen, and Rolando Garcia (2016). "Designing Global Climate and Atmospheric Chemistry Simulations for 1 and 10 Km Diameter Asteroid Impacts Using the Properties of Ejecta from the K-Pg Impact". In: *Atmospheric Chemistry and Physics* 16.20, pp. 13185–13212. ISSN: 1680-7316. DOI: 10.5194/acp-16-13185-2016.

Vellekoop, Johan, Appy Sluijs, Jan Smit, Stefan Schouten, Johan W. H. Weijers, Jaap S. Sinninghe Damsté, and Henk Brinkhuis (2014). "Rapid Short-Term Cooling Following the Chicxulub Impact at the Cretaceous–Paleogene Boundary". In: *Proceedings of the National Academy of Sciences* 111.21, pp. 7537–7541. DOI: 10.1073/pnas.1319253111.

Viganò, Allyson, Thomas Westerhold, Paul R. Bown, Tom Dunkley Jones, and Claudia Agnini (2023). “Calcareous Nannofossils across the Eocene-Oligocene Transition: Preservation Signals and Biostratigraphic Remarks from ODP Site 1209 (NW Pacific, Shatsky Rise) and IODP Hole U1411B (NW Atlantic Ocean, Newfoundland Ridge)”. In: *Palaeogeography, Palaeoclimatology, Palaeoecology* 629, p. 111778. ISSN: 0031-0182. DOI: 10.1016/j.palaeo.2023.111778.

Vonhof, Hubert B., Jan Smit, Henk Brinkhuis, Alessandro Montanari, and Alexandra J. Nederbragt (2000). “Global Cooling Accelerated by Early Late Eocene Impacts?” In: *Geology* 28.8, pp. 687–690. ISSN: 0091-7613. DOI: 10.1130/0091-7613(2000)28<687:GCABEL>2.0.CO;2.

Wade, Bridget S. and Natalie K. Y. Cheng (2024). “No Paleoclimatic Anomalies Are Associated with the Late Eocene Extraterrestrial Impact Events”. In: *Communications Earth & Environment* 5.1, pp. 1–7. ISSN: 2662-4435. DOI: 10.1038/s43247-024-01874-x.

Westerhold, Thomas, Norbert Marwan, Anna Joy Drury, Diederik Liebrand, Claudia Agnini, Eleni Anagnostou, James S. K. Barnet, Steven M. Bohaty, David De Vleeschouwer, Fabio Florindo, Thomas Frederichs, David A. Hodell, Ann E. Holbourn, Dick Kroon, Vittoria Lauretano, Kate Littler, Lucas J. Lourens, Mitchell Lyle, Heiko Pälike, Ursula Röhl, Jun Tian, Roy H. Wilkens, Paul A. Wilson, and James C. Zachos (2020). “An Astronomically Dated Record of Earth’s Climate and Its Predictability over the Last 66 Million Years”. In: *Science* 369.6509, pp. 1383–1387. DOI: 10.1126/science.aba6853.

Zachos, James, Gerald R. Dickens, and Richard E. Zeebe (2008). “An Early Cenozoic Perspective on Greenhouse Warming and Carbon-Cycle Dynamics”. In: *Nature* 451.7176, pp. 279–283. ISSN: 1476-4687. DOI: 10.1038/nature06588.

Zachos, James, Mark Pagani, Lisa Sloan, Ellen Thomas, and Katharina Billups (2001). “Trends, Rhythms, and Aberrations in Global Climate 65 Ma to Present”. In: *Science* 292.5517, pp. 686–693. DOI: 10.1126/science.1059412.